Load induced cracking and failure of concrete deck slabs in girder-slab type bridges

Kaiser Kareem

Civil Engineering

January 1989

Abstract

An experimental study was conducted on three different groups of girder-slab type, reinforced concrete deck panels, to investigate the pattern of crack formation, crack growth and overall failure mode. Areas of study included (i) the influence of distribution steel on crack pattern and crack growth under a simulated moving wheel load; (ii) critical orientation and nucleation of cracks in panels weakened by a flaw in the form of conical inserts; and (iii) mode of failure and ultimate capacity of deck panels with varying amounts of reinforcement steel and different load areas.

The study indicate that with higher amount of distribution steel, finer cracks spread over a larger area are produced. The flexural capacity of a deck slab of girder-slab type bridge is enhanced to an appreciable degree due to support restraints. No significant advantage is achieved by increasing the amount of steel. A hypothesis has been advanced that impairment of punching capacity occurs only when (i) the cracks developed join to form a closed envelop (a flawed zone); (ii) the crack surface geometry bears a critical orientation with regard to wheel load and has reached a critical height through the slab thickness; and (iii) the closed boundary of this flawed zone at the bottom of the slab is greater than that of the weel print. All reinforced panels failed in punching shear type failure.

Load Induced Cracking and Failure of Concrete Deck Slabs in Girder-Slab Type Bridges

by

Kaiser Kareem

A Thesis Presented to the

FACULTY OF THE COLLEGE OF GRADUATE STUDIES

KING FAHD UNIVERSITY OF PETROLEUM & MINERALS

DHAHRAN, SAUDI ARABIA

In Partial Fulfillment of the
Requirements for the Degree of

MASTER OF SCIENCE

In

CIVIL ENGINEERING

January, 1989

INFORMATION TO USERS

This manuscript has been reproduced from the microfilm master. UMI films the text directly from the original or copy submitted. Thus, some thesis and dissertation copies are in typewriter face, while others may be from any type of computer printer.

The quality of this reproduction is dependent upon the quality of the copy submitted. Broken or indistinct print, colored or poor quality illustrations and photographs, print bleedthrough, substandard margins, and improper alignment can adversely affect reproduction.

In the unlikely event that the author did not send UMI a complete manuscript and there are missing pages, these will be noted. Also, if unauthorized copyright material had to be removed, a note will indicate the deletion.

Oversize materials (e.g., maps, drawings, charts) are reproduced by sectioning the original, beginning at the upper left-hand corner and continuing from left to right in equal sections with small overlaps. Each original is also photographed in one exposure and is included in reduced form at the back of the book.

Photographs included in the original manuscript have been reproduced xerographically in this copy. Higher quality 6" x 9" black and white photographic prints are available for any photographs or illustrations appearing in this copy for an additional charge. Contact UMI directly to order.

UMI

A Bell & Howell Information Company
300 North Zeeb Road, Ann Arbor MI 48106-1346 USA
313/761-4700 800/521-0600

LOAD INDUCED CRACKING AND FAILURE OF CONCRETE DECK SLABS IN GIRDER-SLAB TYPE BRIDGES

BY

KAISER KAREEM

A Thesis Presented to the

FACULTY OF THE COLLEGE OF GRADUATE STUDIES

KING FAHD UNIVERSITY OF PETROLEUM & MINERALS

DHAHRAN, SAUDI ARABIA

In Partial Fulfillment of the
Requirements for the Degree of

MASTER OF SCIENCE
In
CIVIL ENGINEERING

JANUARY, 1989

KING FAHD UNIVERSITY OF PETROLEUM & MINERALS

DHAHRAN, SAUDI ARABIA

This thesis, written by

KAISER KAREEM

under the direction of his thesis committee, and approved by all the members, has been presented to and accepted by the Dean, College of Graduate Studies, in partial fulfillment of the requirements for the degree of

MASTER OF SCIENCE IN CIVIL ENGINEERING

Thesis Committee

Chairman (Dr. A. K. Azad)

Co-chairman (Dr. M. H. Baluch)

Member (Dr. M. Y. Al-Mandil)

Dr. R.I. Allayla
Department Chairman

Dr. Abdullah S. Al-Zakri
Dean College of Graduate Studies

Date : 23/5/89

بِسْمِ اللّٰهِ الرَّحْمٰنِ الرَّحِيْمِ

In the name of Allah, most beneficient, most merciful.

In the name of Allah, most beneficient, most merciful.

Have not those who disbelieve known that the heavens and the earth
were joined together as one united piece, then We parted them ?
And We have made from water every living thing,
will they not then believe ?
(Al-Qur'an, surah 21, verse 30)

And Allah has made the earth (wide spread) as a carpet.
That you may go about therein, in broad roads.
(Al-Qur'an, surah 71, verse 19-20)

He who has made for you the earth like a bed (spread out) and
has enabled you to go about therein by roads.
(Al-Qur'an, surah 20, verse 53)

Dedicated

To

My Mother and to the Memories of My Father

ACKNOWLEDGEMENT

Praise and gratitude be to Allah, the Creator and the Sustainer of the universe, and peace be upon his prophet Muhammad. Acknowledgement is due to the King Fahd University of Petroleum and Minerals for extending facilities to complete this work. The financial support for this work provided under the National Project "A Study of Cracking of Concrete Bridge Decks in Saudi Arabia," by the King Abdulaziz City for Science and Technology (KACST), is greatfully acknowledged.

I would like to offer my indebtedness and sincere appreciation to my thesis committee chairman, Dr. A. K. Azad, for his help and guidance throughout this work. I gratefully acknowledge the invaluable suggestions and advises offered by committee co-chairman, Dr. M. H. Baluch. I am also thankful to committee member, Dr. M. Y. Al-Mandil, for his help and encouragement.

I would like to express my thanks to Mr. Yasin and laboratory technicians Mr. Omer and Mr. Zaini, for their assistance in various aspects of this experimental work. Thanks are due to brothers Khalid, Saleem, Misbahuddin and Muqtar for their co-operation during this thesis work.

I owe my family and my uncles an expression of gratitude for their patience, understanding and encouragement which made this work possible. Lastly, I am thankful to all my colleagues and friends who made my stay at the university a memorable and valuable experience.

TABLE OF CONTENTS

Chapter *Page*

LIST OF TABLES

LIST OF FIGURES

LIST OF PLATES

خلاصة الرسالة

اسم الطالب : قيصر كريم

عنوان الدراسة : التشققات والفشل في أسطح الجسور الخرسانية بسبب الأحمال

التخصص : هندسة انشائية

تاريخ الدرجة : يناير ١٩٨٩م

لقد تم عمل تجارب مخبرية على ثلاثة مجموعات من البلاطات الخرسانية لمحاكاة بلاطات الجسور ذات الكمرات الخرسانية المسلحة . وتهدف الدراسة الى معرفة واستقصاء بداية التشقق وأنتشار التشققات وأنواع الفشل الكلي الذي يصيب هذه البلاطات . وقد تم دراسة تأثير المتغيرات التالية : ١) تأثير كمية الحديد المستعمل في الاتجاه الثانوي للبلاطة . ٢) تأثير التشققات المبدئية (انشائية ولا انشائية) على مقدار الفشل الموضعي للبلاطات . ٣) نماذج الفشل والطاقة التحميلية لبلاطات ذات كميات متفاوتة في حديد التسليح الرئيسي ومحملة على مساحات متفاوتة .

أفادت هذه الدراسة بأن زيادة كميات الحديد الثانوي تسبب في توزيع التشققات على مساحات أكبر من سطح البلاطة . كما أن التدعيم لجوانب البلاطات يزيد من قوتها في مقاومة جهود الانحناء . وقد تم تقديم نظرية حول تدني مقادير الاحمال المسببة للفشل الموضعي (فشل القص) ، وذلك للاسباب التالية : (أ) ترابط التشققات ببعضها لتشكل منطقة أختلال معزولة عن باقي البلاطة . (ب) شكل المنطقة المعزولة يكون خطيرا عندما يتشابه مع المساحة المشغولة بعجلات المركبات وخصوصا عندما تصل هذه التشققات الى منسوب مرتفع في سماكة البلاطة . (ج) يكون سطح المنطقة المعزولة بالتشققات في أسفل البلاطة أكبر من المساحة المشغولة بعجلات المركبات على سطح البلاطة . وأخيرا فان جميع هذه البلاطات قد فشلت بسبب اجهاد القص الموضعي .

درجة الماجستير في العلوم

جامعة الملك فهد للبترول والمعادن
الظهران – المملكة العربية السعودية

يناير ١٩٨٩م

THESIS ABSTRACT

NAME OF STUDENT : KAISER KAREEM

TITLE OF STUDY : LOAD INDUCED CRACKING AND FAILURE OF CONCRETE DECK SLABS IN GIRDER-SLAB TYPE BRIDGES

MAJOR FIELD : STRUCTURAL ENGINEERING

DATE OF DEGREE : JANUARY, 1989

An experimental study was conducted on three different groups of girder-slab type, reinforced concrete deck panels, to investigate the pattern of crack formation, crack growth and overall failure mode. Areas of study included (i) the influence of distribution steel on crack pattern and crack growth under a simulated moving wheel load; (ii) critical orientation and nucleation of cracks in panels weakened by a flaw in the form of conical inserts; and (iii) mode of failure and ultimate capacity of deck panels with varying amounts of reinforcement steel and different load areas.

The study indicate that with higher amount of distribution steel, finer cracks spread over a larger area are produced. The flexural capacity of a deck slab of girder-slab type bridge is enhanced to an appreciable degree due to support restraints. No significant advantage is achieved by increasing the amount of steel. A hypothesis has been advanced that impairment of punching capacity occurs only when (i) the cracks developed join to form a closed envelop (a flawed zone); (ii) the crack surface geometry bears a critical orientation with regard to wheel load and has reached a critical height through the slab thickness; and (iii) the closed boundary of this flawed zone at the bottom of the slab is greater than that of the wheel print. All reinforced panels failed in punching shear type failure.

MASTER OF SCIENCE DEGREE
KING FAHD UNIVERSITY OF PETROLEUM & MINERALS
Dhahran, Saudi Arabia.

Chapter 1

INTRODUCTION

1.1 DETERIORATION OF BRIDGE DECKS

A number of concrete bridge decks, built in the early stages of the rapid development of Saudi Arabia, suffered premature damages in the form of severe cracking of deck slabs (Plate 1.1). Many slab-in-girder type bridges encountered pot-hole type failure. A typical view of such a failure is shown in Plate 1.2. Several interactive factors have collectively contributed to such cracking in longitudinal and transverse directions and in the development of eventual pot-hole type failures. The most dominant factor has been identified as the effect of heavy vehicular loadings, which were widely used in the past.

A deck slab which carries the applied load directly before transmitting to the supporting beams or girders may fail in two ways. One is punching shear type failure, in which the load penetrates through the slab, causing a localized failure in the form of pot holes. This usually occurs when a heavy wheel load is applied on a thin slab. Although punching capacity is enhanced to a certain degree by reinforcing steel, concrete capacity for punching shear is generally considered in the design as the controlling factor. The other mode of failure is the typical flexure failure in which the slabs fail in bending caused by the applied load.

Plate 1.1: View of Severe Cracking of Concrete Bridge Decks in Saudi Arabia.

Plate 1.2: View of Typical Pot-Hole Type Bridge Failure in Saudi Arabia.

The load carrying capacity of a slab which is allowed to move laterally i.e., edges are simply supported or unrestrained, is lower than the slab whose edges are laterally restrained. The restrained slabs are known to carry higher loads than those predicted by the Yield line method [1]. This is due to the in-plane compressive forces induced by support restraints, which enhances the moment carrying capacity of the slab. This behavior is often referred to as arching action or compressive membrane action. Although it has been claimed that this membrane effect also enhances the punching capacity of a deck slab to a certain extent, the flexural capacity enhancement is generally much more pronounced.

Generally, stress induced cracking in any particular direction of the slab would depend mainly on the amount of steel present in the direction perpendicular to it. Cracking parallel to main transverse tension steel may depend on the amount of distribution (longitudinal) steel. More number of small diameter bars are known to distribute the cracks better than a few large diameter bars for the same amount of steel.

The study of cracking and failure of concrete bridge deck slabs has drawn attention as past studies [13,14] have indicated that the ultimate flexure capacity of a deck slab of a normal girder-slab type deck is substantially larger than the ultimate strength predicted by ordinary flexure theory, because of the arching effect in decks. Also the current specifications of American Association of State Highway and Transportion Officials (AASHTO [2]) for bridge design are conservative, resulting in unnecessary high amount of steel reinforcement.

Most bridge design codes, such as those of AASHTO provide procedures, by prescribing simplified formulas for the design of deck slab for a girder-slab type bridge deck. AASHTO also provides empirical formula for the amount of distribution steel. In view of the evidence of existence of the favourable influence of membrane forces both from in-situ tests and some small scale tests, Ontario Bridge Design Code [3] has introduced an empirical design method using 0.3% isotropic steel at both top and bottom faces of the slab. When a deck slab is subjected repeatedly to a high load level, the crack propagation and nucleation may lead to progressive fracture and eventual failure at a subcritical load level. The fatigue life of a deck slab depends among others, on the maximum stress level, and is reduced sharply as the stress level approaches closer to the level of maximum static load capacity. Fatigue may become therefore critical if the deck slab is likely to be subjected to repetitive overloading.

As a part of the National project "A Study of the Cracking of Concrete Bridge Decks in Saudi Arabia," financed by the King Abdulaziz City for Science and Technology, a study was carried out to investigate the pattern of crack formation and crack growth under subcritical load level to document modes of failure and to suggest, based on the findings, recommendations which may avert damages due to cracking and failures of deck slabs. This work is essentially the core of this thesis. Attempt has been made in this work to better explain the formation of the pot holes due to punching and to suggest measures to avoid such failures under occasional overloading.

1.2 LITERATURE REVIEW

The ability of deck slabs in girder-slab bridges to hold loads larger than the designed loads, even in some what deteriorated condition cannot be explained by the Westergaard's flexure theory, upon which the AASHTO design provisions are based. Tests performed by Okleston [4,5] in 1956, showed that collapse loads were three to four times the load carrying capacity predicted by the yield line theory. This enhanced ultimate strength was attributed to the arch action or to the influence of inplane compressive membrane forces resulting from support restraint. Other studies [6,7] have shown that the compressive membrane action enhances both flexural and shear capacities of the slabs resulting in failure at higher loads than those predicted by yield line theory. In view of the improved flexure capacity, a deck slab of normal design when subjected to a heavy wheel load may fail in punching shear rather than in bending.

Attempts had been made in the past to study the punching capacity of a reinforced concrete slab. Many of the earlier studies were done on specimens representing a portion of flat plate system or on column footings [28,29]. Elstner and Hognested [30] tested thirty nine, six feet square slabs, loading to failure through a centrally located column stud. The tests included a number of variables such as concrete strength, percentage of tension and compression reinforcement steel etc. Of the thirty nine slabs tested, thirty four failed by the column punching through the slab. They derived expression for the ultimate shearing stress of slabs and identified a number of major factors determining the

strength of siab.

In 1960, Kinnunen and Nylander [8] studied the punching capacity of simply supported circular slabs with radial and circumferential reinforcement and circular load area. Based on the experimental observations and findings, they developed an idealized model, in which, the outer portion of the slab bounded by the shear and radial cracks, is supposed to be carried by a compressed conical shell that develops from the loaded area to the bottom of the shear crack. This was later extended by Kinnunen [9] for slabs with two way reinforcement.

Yitzhaki [31] tested a number of specimens representing flat slabs and derived expression for the prediction of the punching strength which gave some recognition to the flexural strength. Gesund and Dikshit [32] examined the slab column interaction of uniformly loaded flat plate by use of the yield line theory. They developed expressions for the bending punching strength of flat plates when supported on column located in the interior or at near the boundaries. By comparing the expressions developed with the experimental data available in the literature, they concluded that bending punching is possible around all columns.

Herzog [33] derived simpler formulas from the test results available in the literature, for the prediction of strength in punching shear of footings and slabs. Long [34] developed a two phase formula for predicting the punching capacity of slabs at interior columns, by simplifying previously reported analytic procedures, which take into consideration the interaction of flexural and shear effects. Jiang and Shen [27] recently proposed a theoretical solution similar to

Braestrup and Nielsen [26], for the punching shear strength of concrete slabs, based on plasticity approach in which problem is treated as axisymmetrical and a second degree parabola curve is used for Coulomb-Mohr yield envelop.

Taylor and Hayes [10] have shown that the punching shear strength of concrete slabs is greatly enhanced when the edges are restrained against movement. This enhancement is more for slabs with high strength concrete or low reinforcement ratio. Enhanced punching strength for restrained slabs is also shown by Hewitt [12]. In view of the fact that it is difficult, if not impossible, to prescribe exactly the degree of support restraint, no universal approach has been developed for the design of restrained slabs. Empirical approaches to this problem have been found to be more fruitful.

Hewitt and Batchelor [13] developed a model for punching load of a slab with known boundary restraints. An empirical factor, which could be deduced from tests, was proposed for use in predicting the punching strength of slabs whose boundary restraints are not exactly known. The model involves incorporation of boundary restraining forces and moments into the idealized model of failure proposed by Kinnunen and Nylander [8] for a simply supported slab.

Studies performed in Canada [14] on I-beam bridge slabs of 1/8th scale direct models of 80 ft span four beam bridges showed the conservative nature of the AASHTO specifications. The panels failed in punching shear type of failure. The conclusion was that the isotropic reinforcement of 0.3% satisfies both the serviceability and ultimate limit states considerations. Beal [15], investigated

the ultimate load capacity of bridge decks by conducting tests on one slab reinforced with AASHTO specifications and three others with varying amounts of isotropic reinforcement under simulated wheel loads. Results showed with either reinforcement pattern, service load bending moments were from 40% to 65% of those predicted by flexure theory. Failures were by punching and were at loads atleast six times greater than the design loads. A 59% reduction in total reinforcement had no effect on failure mode and did not reduce the strength below a safe level. Fang [16] who conducted full scale tests on concrete bridge decks designed by the new Ontario Bridge design concept, subjecting to static and pulsating concentrated loads, concluded that isotropic steel reinforcement pattern given by the OHBDC [3] results in adequate safety.

The fatigue strength of the reinforced concrete structure will be governed either by fatigue life of the concrete or by the fatigue life of the reinforcement. Limited tests have been conducted on the effects of repeated loading on bridge slabs. Deck slabs designed by the current design methods have high reserves of strength against failure, as the actual static failure load is higher than predicted by ordinary theories. Batchelor and Hewitt [22] conducted tests on 1/8th scale direct model of 80 ft single span four beam composite steel concrete bridge. The panels failed by punching in a sudden and explosive manner when tested to failure under fatigue loading.

Deck slabs designed by the current design methods have unnecessary high reserves of strength against fatigue failure. Limited fatigue tests on small scale models have also demonstrated that maximum load under the fatigue cycle to

cause failure in number of cycles exceeding one million was also greater than the design loads [14].

Limited research has been conducted on the fatigue life of reinforced concrete slabs, under concentrated loads. Okada, Okamura and Sonoda [23] investigated the behavior of concrete slabs under repetitive loading by testing seven slabs with full scale dimensions, to clarify the fatigue mechanism of reinforced concrete slabs under moving loads.

Sonoda and Horikawa [17] simulated the effects of a traffic wheel-load by applying a stepwise moving pulsating load on 1/3 scale model decks. They concluded that the fatigue life of deck slabs was remarkably reduced under the stepwise moving load compared to that under a pulsating load applied at a fixed point.

Recently Perdikaris and Bein [18] conducted tests on 1/6.6 scale reinforced concrete bridge deck slab under static load, pulsating load applied at a fixed point, and moving constant wheel load. Both orthotropic and isotropic reinforcing arrangements were considered. The failure mode for all reinforced model decks was that of punching shear. The crack pattern due to the moving wheel-load was more segmental and extensive than that due to fixed pulsating load, indicating an entirely different fracture process. They concluded that the AASHTO design approach is overconservative and that steel reinforcement content could be reduced significantly and satisfy both serviceability and strength requirements.

The Research [24,25] carried out at KFUPM, under the national project "A Study of Cracking of Concrete Bridge deck in Saudi Arabia," on the investigation of static and fatigue life of restrained and unrestrained concrete deck slab models under a simulated wheel load, concluded that the punching capacity is impaired by the presence of initial non-structural cracks and that it is enhanced to a certain degree by edge restraint and increase in tension steel. Fatigue life of a restrained deck slab can be approximated by a bi-linear relationship between non-dimensionalized load parameter and the number of cycles to failure, independent of the type of concrete, its construction and strength.

1.3 SCOPE AND OBJECTIVES

In the proposed research, the study of static and fatigue failure of restrained slabs of a typical bridge deck would be supplemented by undertaking a series of tests on small scale deck models. The failure mode of the deck slab would be highlighted. The loaded area will be varied in static tests to record the transition of mode of failure from punching shear to that of flexure or edge shear, if any, within the range of loaded areas considered in this study.

The Influence of distribution steel on the density and the pattern of stress induced cracks at the bottom of slab will be observed. The aim would be to note the amount of cracking in relation to the amount of distribution steel and the latter's influence on the crack size and crack distribution. Comparison of the crack patterns will be made for different panels to show the significance of

the distribution steel on flexural cracking.

For a better understanding of the punching failure and the detrimental influence of the random crack propagation and nucleation which may form a weakened zone on the punching capacity, a series of slabs cast with initial flaws in the form of conical frustums will be tested. In this manner, the critical depth and orientation of the nucleated cracks can be observed.

The primary objectives of the proposed research are as follows:

1) to observe the crack pattern under subcritical load level for a deck slab with varying amount of distribution steel i.e., the influence of the distribution steel on the crack pattern will be observed,

2) to study the detrimental influence of cracks, if any, on the punching capacity of slabs, by undertaking tests on panels with simulated flaw expected from crack nucleation of randomly oriented and propagated cracks,

3) to determine the failure load of deck slabs with varying amounts of main steel and different load areas, when subjected to the static action of a simulated wheel load,

4) to conduct fatigue tests at the maximum load level of 50-60% of static failure load capacity, to indicate threshold value of failure in fatigue due to the repetitive action of a wheel load, and

5) to suggest procedure to inhibit punching and flexural failure.

Essentially, the study focusses on three major items: (i) crack pattern and density of cracking in relation to the distribution steel, if any, (ii) Static and fatigue tests on simulated deck panels, and (iii) on impairment of punching capacity due to possible weakness rendered by critical orientation and nucleation of cracks.

A series of tests were conducted on girder-slab bridge deck models to gather test data. The test panels were designed by considering the testing and handling facilities available and were not proportioned by following any particular prototype. Slab thickness and the span however were kept within the range used in practice.

Chapter 2

EXPERIMENTAL PROGRAM

2.1 EXPERIMENTAL DESIGN

In the experimental program, three different types of deck slab panels were designed and cast to carry out three types of experiments:

1) Study of crack pattern with regard to the amount of distribution steel under subcritical load (A1-series).

2) Study of punching capacity of slab weakened by critical orientation and nucleation of cracks (A2-series).

3) Static and limited fatigue tests in simulated girder-slab type deck panels (A3-series).

2.2 EXPERIMENTAL DETAILS

2.2.1 Test Specimens

2.2.1.1 A1-Series Panels

This series of panels were used to examine the effect of the distribution steel on the crack pattern. A total of nine panels were cast in two batches. A

typical panel consisted of a slab 1800 x 1200 mm and 80 mm thick, supported on two steel I-beams (W 8x15) providing a span of one metre. Studs of 12 mm diameter size at a spacing of 200 mm centre to centre were welded to the top flange of the I-beams to ensure composite action. Fig. 2.1 shows the details of a typical A1-series panel.

In all these panels, the amount of main transverse steel was kept unchanged and this consisted of 8 mm diameter steel rebars spaced at 100 mm centre to centre. The panels were labelled A1/ISO, A1/H, A1/M and A1/S, corresponding to four different amounts of distribution steel, namely isotropic reinforcement (ISO), high amount of reinforcement (H), medium amount of reinforcement (M) and small amount of reinforcement (S). Table 2.1 shows the details of reinforcement steel used in A1-series panels. Panel A1/H had distribution steel of 8 mm diameter spaced 150 mm centre to centre, which amounted to about 67% of the amount of main steel. This corresponds to the AASHTO specified maximum value for the distribution steel in deck slabs whose main steel is perpendicular to the direction of traffic. The distribution steel for panel A1/M consisted of 6 mm diameter bars spaced at 150 mm centre to centre (37% of main steel) and for panel A1/S, 6 mm diameter bars at 300 mm centre to centre (18% of main steel). The top steel consisted of isotropic reinforcement of 6 mm diameter bars spaced at 300 mm centre to centre for all the panels.

Electrical resistance strain gauges were fixed at the middle of three transverse steel bars and three longitudinal steel bars in four panels (one from

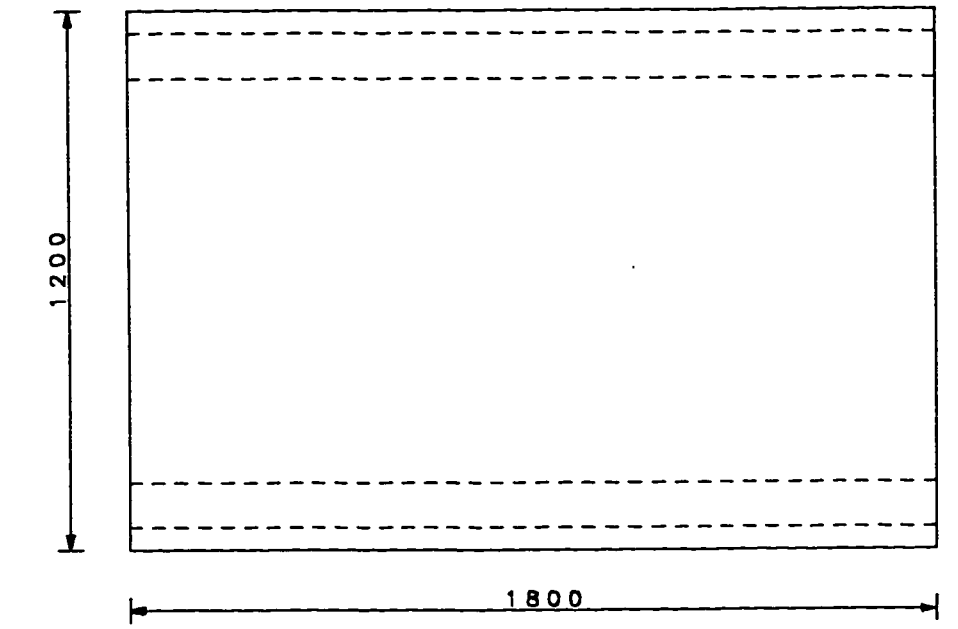

*All Dimensions in mm

Fig. 2.1: Typical A1-series Panel.

Table 2.1: Reinforcement Details of A1-Series Panels.

PANEL	MAIN STEEL		DISTRIBUTION STEEL		DISTRIBUTION STEEL AS PERCENTAGE OF MAIN STEEL
	diameter (mm)	spacing c/c (mm)	diameter (mm)	spacing c/c (mm)	
A1/ISO	8	100	8	100	100
A1/H	8	100	8	150	67
A1/M	8	100	6	150	37
A1/S	8	100	6	300	18

each type), to measure the steel strains at different load levels. Fig 2.2 shows the location of strain gauges in A1-series panels.

The crack pattern under sub-critical load level would be noted for these panels. The amount of main tension steel and other parameters (variables) were kept constant, while the amount of distribution steel was varied to study the effect of the distribution steel on the amount and pattern of stress (load) induced cracks at the bottom of the slab, and compare the crack formation and the punching load capacity. In this manner the amount of distribution steel that reduces or arrests the development of large size cracks by effectively distributing the load over a larger area would be determined.

2.2.1.2 A2-Series Panels

This series of panels were cast to examine the reduction in the punching capacity, if any, due to the cracking of panels. A total of twelve panels were cast in this series. A typical panel consisted of a slab of overall dimensions of 1850 x 1300 mm and 90 mm thick supported on two steel I-beams (W 8x15) providing a span of one metre. As in A1-series panels, 12 mm studs were welded at spacing of 200 mm centre to centre to ensure composite action. In some panels, a thin metallic insert in the form of a frustum of cone was embedded, which represented an initial crack geometry considered detrimental to the resistance offered by the panel against punching.

The slab thickness of 90 mm used in panels of this series was highest in the

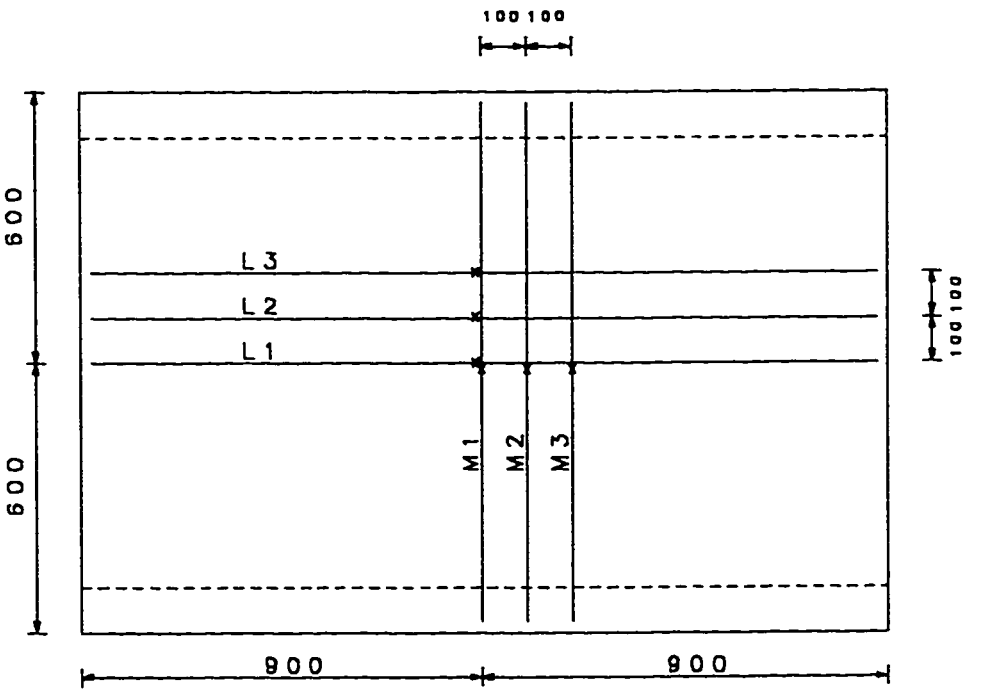

M-Transverse Steel Bars
L-Longitudinal Steel Bars
x-Location of Strain Gauge

*All Dimensions in mm

Fig. 2.2: Location of Steel Bars with Strain Gauges in A1-Series Panel.

panels of the three series. The thickness was increased to allow for the different heights of the inserts in order to determine the punching loads for the different crack geometry and depth. Fig. 2.3 shows the details of a typical A2-series panel.

The amount of both transverse and longitudinal steel was kept constant in all the panels, except for one panel, which was cast without any reinforcement. The transverse steel consisted of 10 mm diameter bars spaced 100 mm apart and the longitudinal steel consisted of 8 mm diameter bars at a spacing of 150 mm centre to centre. The top steel consisted of an isotropic reinforcement of 6 mm diameter bars at a spacing of 150 mm centre to centre.

The panels were divided into four groups. The first group consisted of two types of panels, A2C/P and A2C/S. Panel A2C/P was cast without conical insert and without any reinforcement. The second type A2C/S, consisted of two panels cast without conical inserts, to give the punching capacity of a perfect slab in the absence of a simulated flaw represented by the insert.

The second group consisting of five panels, were cast with a precast notch inserted in the form of a frustum of a cone (Plate 2.1). Fig. 2.4 shows the geometric details of the conical insert. Different angles of inclination of the conical inserts were used by varying the angle of inclination α from 20° to 90°. Panel A2/20, A2/30, A2/45, A2/60 and A2/90 had angles of inclinations of 20°, 30°, 45°, 60° and 90° respectively. These panels were cast with a crack depth projection of 44 mm, about half the slab depth. Table 2.2 give details of angles of inclination, base diameters and vertical projection of the cone which

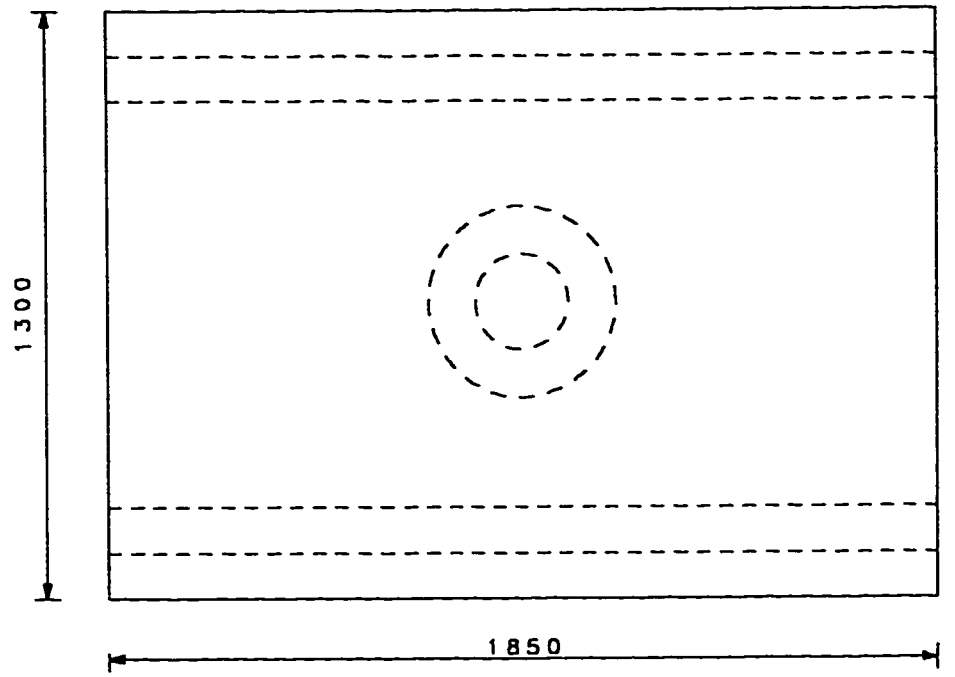

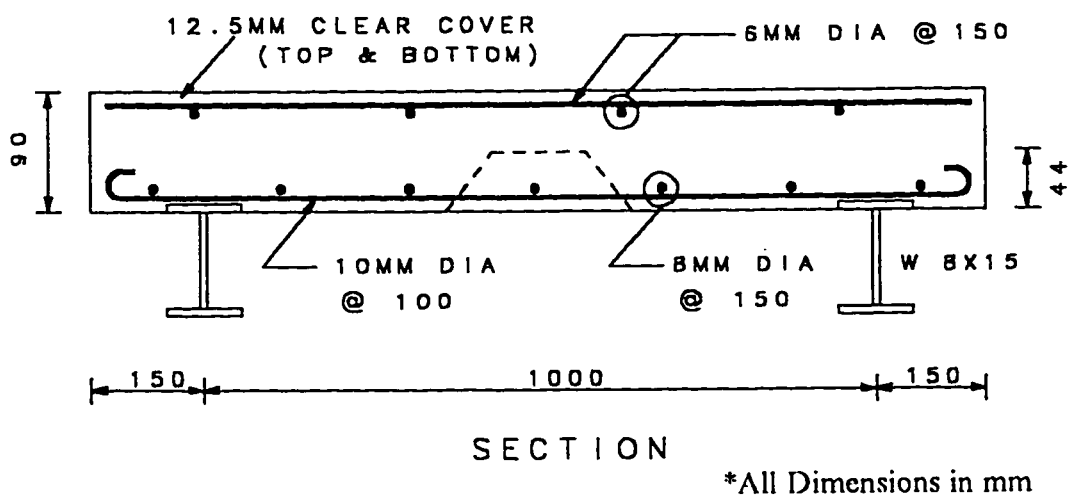

Fig. 2.3: Typical A2-Series Panel.

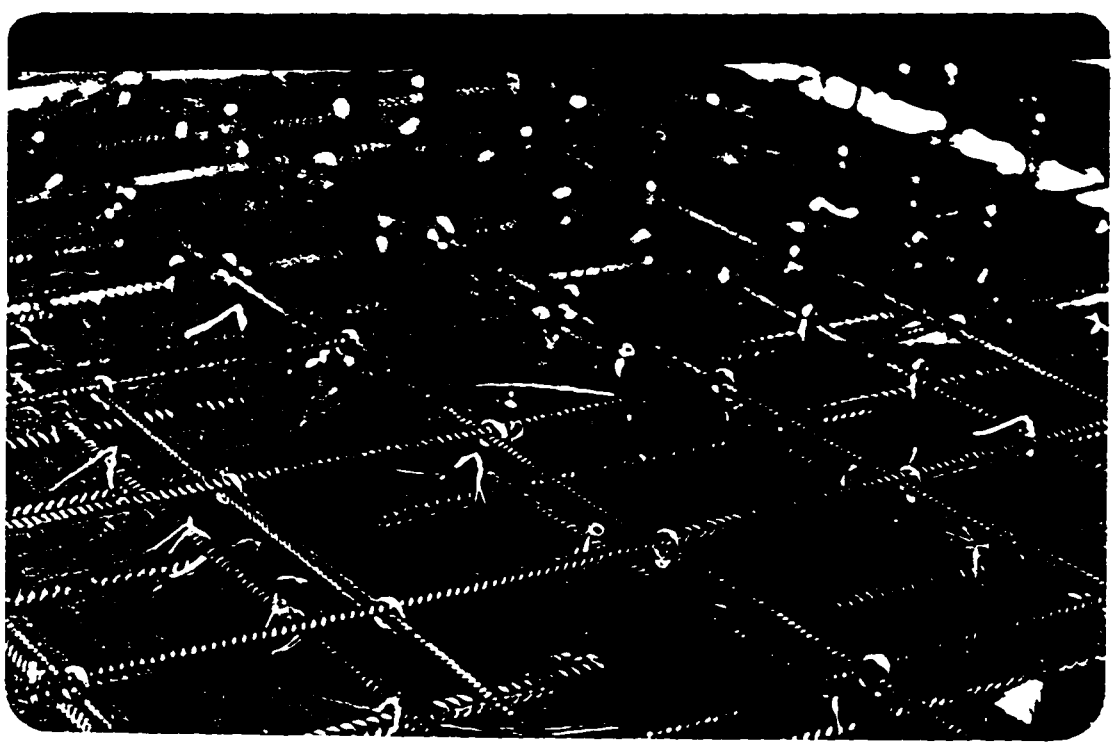

Plate 2.1: Typical A2-Series Panel with Conical Insert.

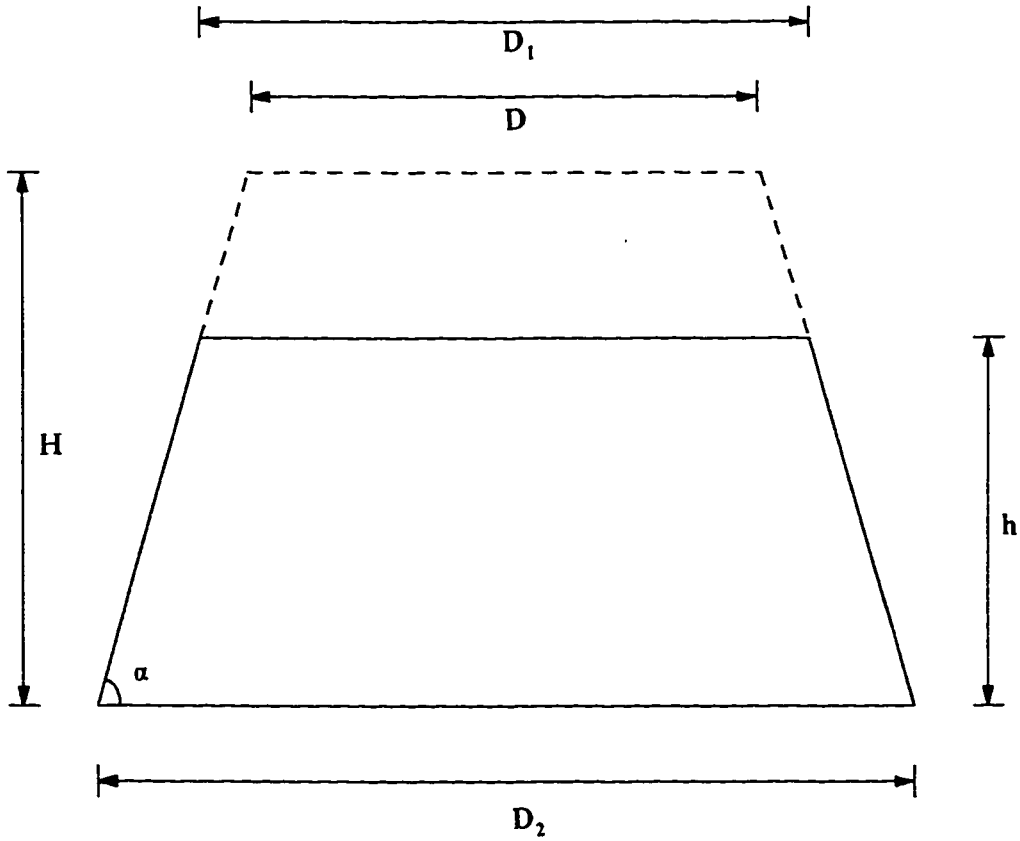

D -Diameter of Load Area
D_1-Diameter of Conical Insert at depth h
D_2-Diameter of Conical Insert at base
h -Depth of Conical Insert
H -Depth of the Slab

Fig. 2.4: Geometrical Details of Conical Insert used in in A2-Series Panels.

Table 2.2: Details of Conical Inserts of A2-Series Panels.

PANEL		ANGLE WITH PLANE OF SLAB (Degrees)	BASE DIAMETER OF CONICAL INSERT (mm)	HEIGHT OF INSERT (mm)
GROUP NO.	DESIGNATION			
1	A2C/P	-	-	-
	A2C/S	-	-	-
2	A2/20	20	580	44
	A2/30	30	400	44
	A2/45	45	265	44
	A2/60	60	190	44
	A2/90	90	88	44
3	A2/60/H	60	190	64
	A2/90/H	90	88	64
4	A2C/90/L	90	250	30
	A2C/90/H	90	250	64

represented the simulated crack. These panels were tested under a circular patch load to yield a relationship between the angle of notch insert α and the punching shear capacity of the panel. This relationship would yield a crack geometry which appears to be most critical from the point of punching failure i.e., which causes the greatest reduction in the punch capacity.

The third group consisting of two panels were cast with inserts of angle of inclination of 60° (A2/60/H) and 90° (A2/90/H). These panels were similar to the ones in the second group except that the depth of notch was 64 mm, extending almost upto the level of the top reinforcement. Test results on these panels would identify the contribution of the steel reinforcement to the punching shear capacity of the panels.

The fourth group consisted of two panels with angle of inclination of 90° only. Panel A2C/90/L was cast with a notch of depth 30 mm and other other panel A2C/90/H was cast with a notch of depth 64 mm. The notch depth of the latter panel (A2C/90/H) passed beyond the failure plane of angle α equal to 20° and the others well below the failure plane of α equal to 20°. The basic difference of these two panels from others is that they were cast with a wider insert base diameter of 250 mm. These would further help in indicating the influence of crack geometry on the punching shear reduction.

2.2.1.3 A3-Series Panels

A total of twelve panels consisting of three different sets of four panels

each were cast. A typical A3-series panel consisted of a continuous slab of dimensions of 1720 x 1500 mm and 68 mm thick, supported on three steel I-beams (W 8x15) spaced 710 mm apart. Fig. 2.5 shows the details of a typical A3-series panel. Studs of 12 mm diameter at a spacing of 200 mm were welded to the top flange of the I-beams to ensure composite action.

The amount of both transverse and longitudinal steel was varied in each of the three sets of A3-series panels. Table 2.3 shows the details of three types of reinforcements used in the panels. The first set (A3-1) had the highest amount of steel, with the main transverse steel consisting of 8 mm diameter bars at a spacing of 100 mm centre to centre and the longitudinal steel of 6 mm diameter bars at 100 mm centre to centre. In the panels of second set (A3-2) the main steel consisted of 6 mm diameter bars at 100 mm centre to centre and longitudinal steel consisted of 4 mm diameter bars at 100 mm centre to centre. The third set (A3-3) had isotropic reinforcement of 4 mm diameter bars at 100 mm centre to centre. The amount of top steel was the same as the bottom reinforcement in the panels of each set. The reinforcement ratio (steel area to effective concrete area) expressed as a percentage is also shown in Table 2.3.

Electrical strain gauges were fixed on the central three bars of main transverse steel in some panels. The strain gauge location corresponds to the midspan of one of the two spans of the panels (Fig. 2.6). The span which had the steel strain gauges was labelled span A and the other as span B.

These panels which were subjected to static and fatigue loads would highlight the failure mode of the bridge deck slab. The panels were cast with

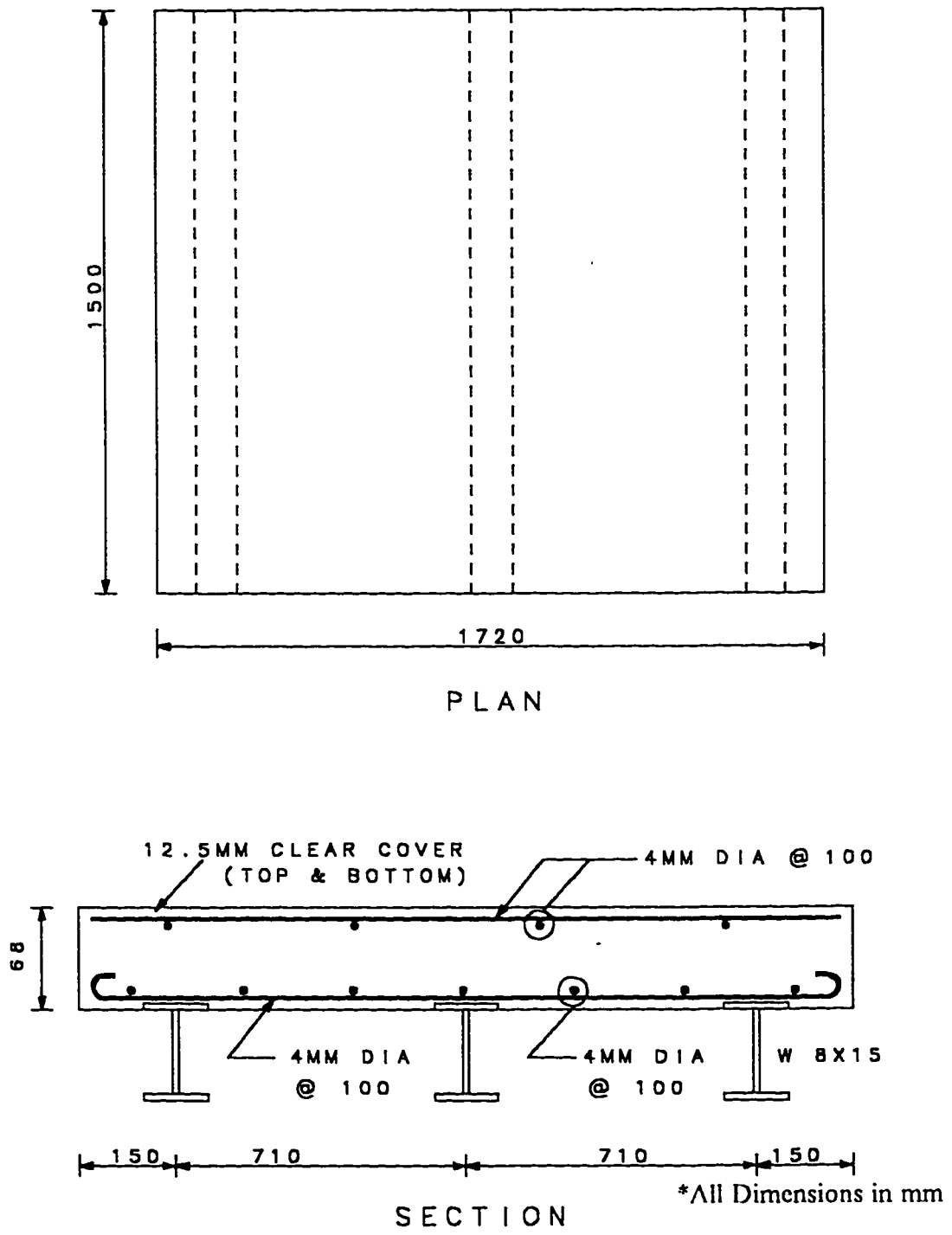

Fig. 2.5: Typical A3-Series Panel.

Table 2.3: Reinforcement Details of A3-Series Panels.

PANEL SET	MAIN STEEL			DISTRIBUTION STEEL	
	diameter (mm)	spacing c/c (mm)	steel ratio (%)	diameter (mm)	spacing c/c (mm)
A3-1	8	100	0.98	6	100
A3-2	6	100	0.54	4	100
A3-3	4	100	0.24	4	100

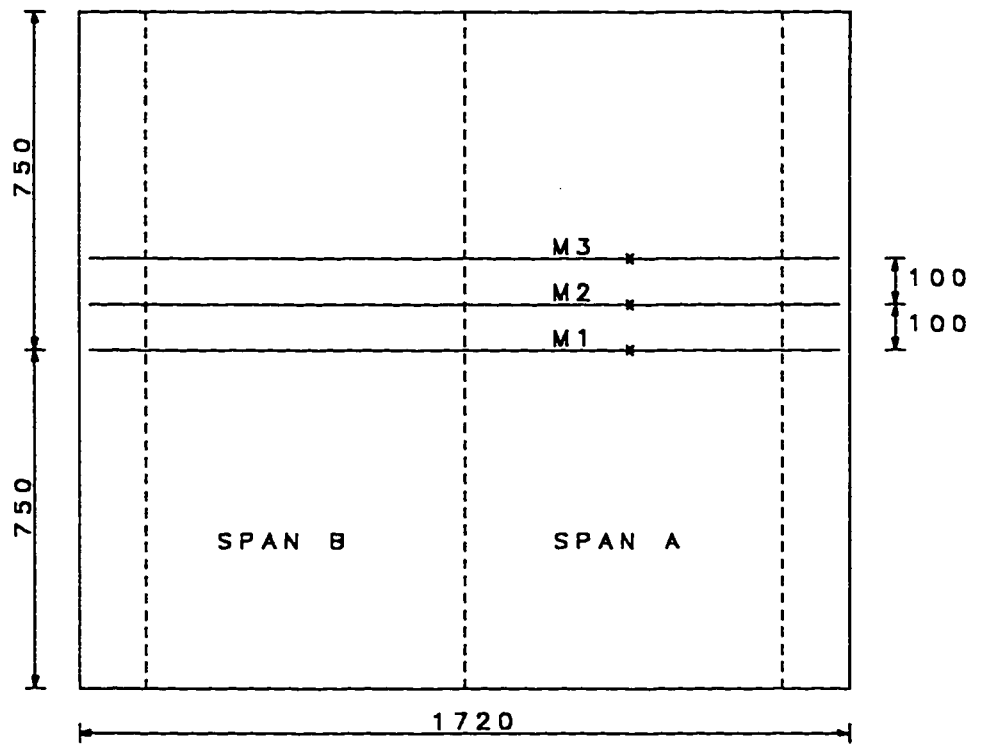

M-Transverse Steel Bars
x -Location of Strain Gauge

*All Dimensions in mm

Fig. 2.6: Location of Steel Bars with Strain Gauges in A3-Series Panels.

three I-beams to provide the lateral support restraint for the study of the favourable influence of the lateral support restraint on enhancement of the flexural capacity of the deck slab. By increasing the load areas, the increase in failure load would be noted and the transition of the mode of failure, if any, would be noted. To observe the threshold value of failure load under repetitive loading, limited fatigue tests were conducted on the span B of the panels for which span A was used in static tests with smaller load areas. The use of this span was possible as the failure was essentially a localized punching failure with hardly any damage to the edge of span or the other span.

2.3 MIX DESIGN AND CASTING

The same concrete mix design was used for all test panels. Since the casting involved large quantities of concrete, larger than the amount which can be handled in the laboratory, a local ready-mix concrete supplier was contracted for the supply of concrete. Table 2.4 shows the details of the concrete mix design. A mixture of washed aggregate of 20 mm size and 10 mm size in a ratio of 1:2 was specified. The coarse aggregate was crushed limestone obtained from Dhahran area and was a typical representative of aggregate used commonly in the Eastern province of Saudi Arabia. The slump of concrete varied between 19 to 23 mm for different batches.

Timber formwork was used for casting. The two layers of reinforcement assembled following the rebar arrangement for a particular panel were placed in the formwork with the required amount of top and bottom cover. Plate 2.2

Table 2.4: Concrete Mix Design.

CONSTITUENT	WEIGHT (kg/ m^3)
Cement	380
Aggregate 20 mm	430
Aggregate 10 mm	880
Sand	730
Water	200
Water/Cement	0.53
CA/FA	1.79

CA : Coarse Aggregate
FA : Fine Aggregate

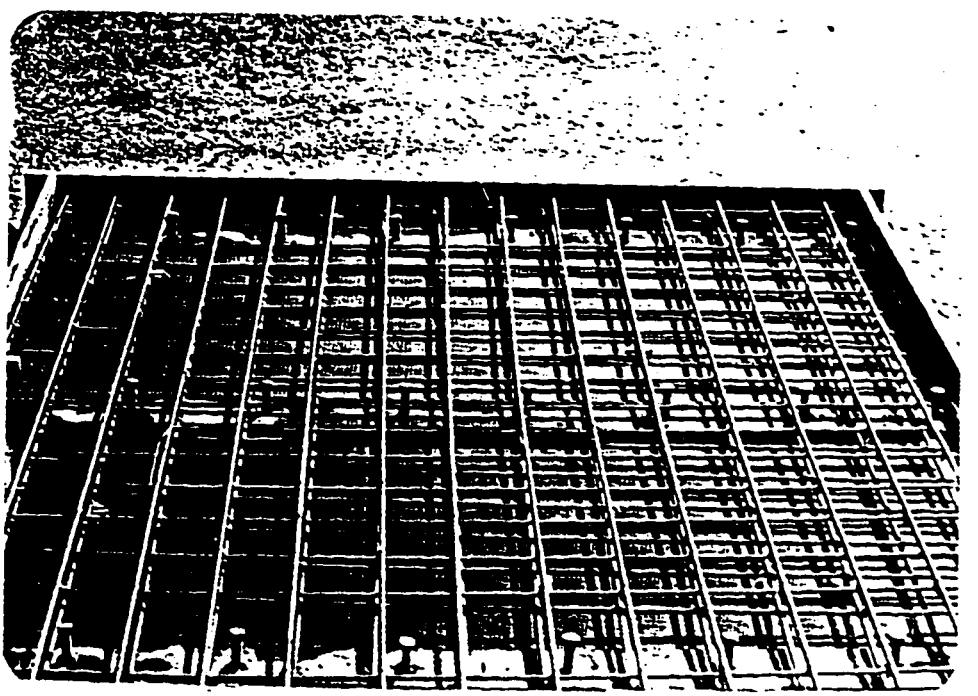

Plate 2.2: View of Reinforcement Layout in Typical A3-Series Panel.

shows a typical A3-series panel prior to casting. After casting, compacting and finishing, the panels were covered immediately with polyethylene sheets, to avoid development of any non-structural cracks. Plate 2.3 shows the panels covered with polyethylene sheets immediately after casting. The test panels were cured for one week with water sprayed twice a day.

For determining the compressive strength, cylinders of 75 x 150 mm and also 100 x 200 mm were obtained. The cylinders were also cured along with the panels. Three tension test samples were taken from each diameter reinforcement steel bar for determining the yield stress and the ultimate tensile strength.

2.4 TEST SET-UP AND TEST PROCEDURE

All panels were tested using a test frame fitted with MTS 500 kN capacity hydraulic actuator. A single load was applied by the actuator through a rubber padded steel plate to distribute the load on a small area, simulating the action of a wheel load. The panels in A1-series were tested under a load area of 75 x 150 mm. A2-series panels were tested under a circular patch load of 88 mm diameter. A3-series panels were tested with four different load areas of 75 x 150 mm, 100 x 200 mm, 200 x 400 mm and 200 x 500 mm. For fatigue tests, the load area was confined to 75 x 150 mm. A frequency of 2 to 2.5 Hz was used for fatigue tests. Plate 2.4 shows the view of typical test set-up for the panels.

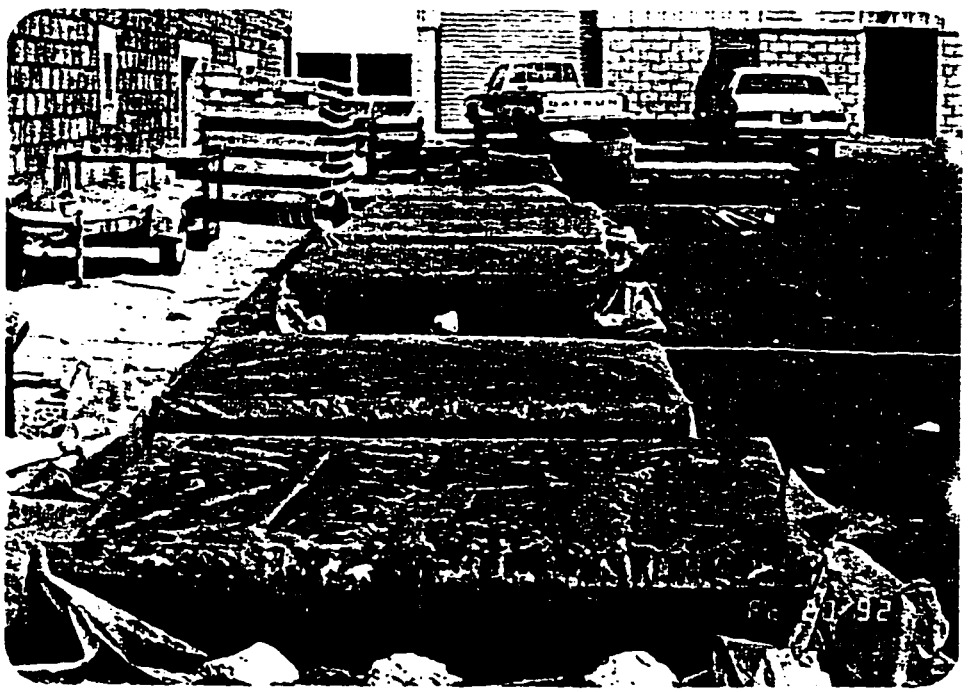

Plate 2.3: View of Panels Covered with Polyethylene Sheets after Casting.

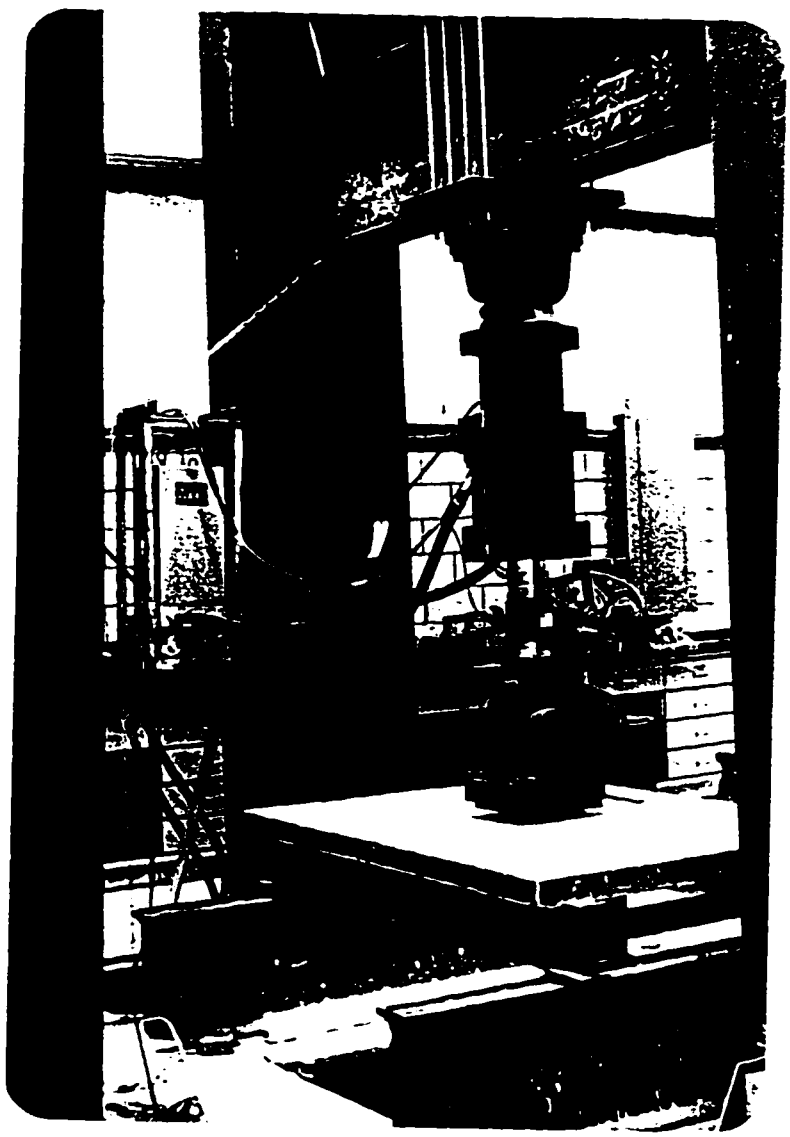

Plate 2.4: Test Set-Up for Panels.

2.4.1 Test Procedure for A1-Series Panels

The panels were supported by two large steel I-beams providing a span of 1750 mm. The panels were tested under a patch load which was moved to three different locations along the span to simulate the effect of a moving wheel load. A load P on an area of 75 x 150 mm was applied at three different locations on the slab, in succession, first at the centre, then at 450 mm from the centre on one side and finally at the third location, 350 mm from the centre on the other side, moving the load from one end to the other end of the panel. Fig. 2.7 shows the three load locations. The distances of the load positions on either side of the panel centre could not be kept the same due to difficulties encountered in the movement of the panel.

A certain amount of load P was applied at one location and the cracks developed at the bottom of the slab were marked with a color marker. The load was retained till all the cracks were marked. Then the load was shifted to the second location and the cracks developed were marked and similarly at the third location same procedure was followed. When one cycle of moving the load to three locations from one end to the other end was complete for the load P and cracks marked, a photograph of the slab was taken to record the crack pattern. Since there was not enough room below the panel to go under and take photograph, a mirror was placed below the panel on the ground and a photograph of the reflection of the cracks was taken. The load was then increased and same procedure was followed again. When the load was at the centre position strains were measured in steel for the panels with strain gauges,

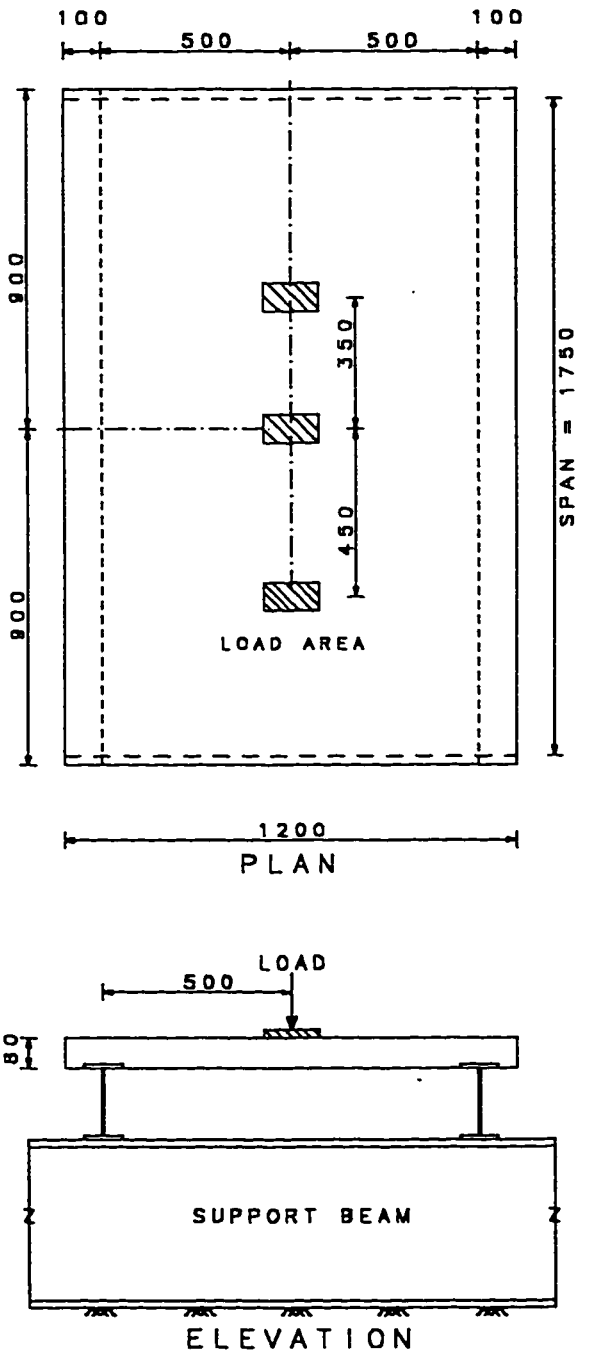

*All Dimensions in mm

Fig. 2.7: Location of load positions for A1-series Panel.

in each cycle of moving the load. After reaching a load of 70% to 80% of the ultimate load, the panel was tested to failure by applying the load at the central position. The failure load was recorded and the failure pattern and failure mode was observed for each panel. A final photograph of the failed panel was taken. The dimensions of failure surface at top and bottom of the slab were measured.

2.4.2 Test Procedure for A2-Series Panels

These panels were also supported by the two large I-beams, providing a span of 1800 mm. The panels were tested under a single concentrated load spread over a circular patch of diameter 88 mm placed at the centre of the panel. Fig. 2.8 shows the location of load for these panels. Loading was applied monotonically at a slow rate till failure. In each test, the failure load and the mode of failure was recorded.

Since the conical inserts were of different inclinations and base diameters, close observation was made to see the development of cracks both at the bottom and at the top, and the cracking of the concrete within the conical insert and outside the conical insert.

2.4.3 Test Procedure for A3-Series Panels

These panels were used in static tests and in a limited number of fatigue tests using a pulsating load. Each panel was supported by two large steel I-beams to provide a span of 1450 mm. All static tests were conducted under a

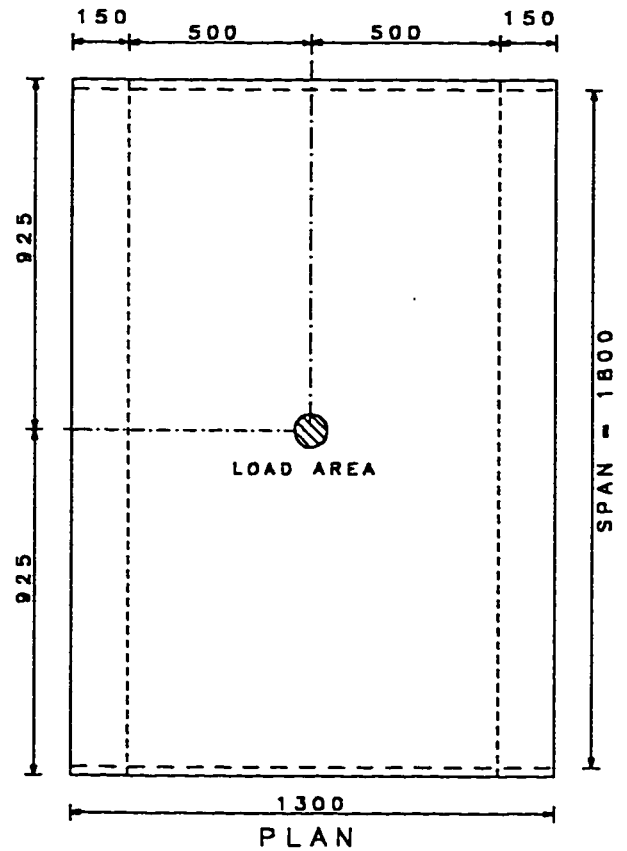

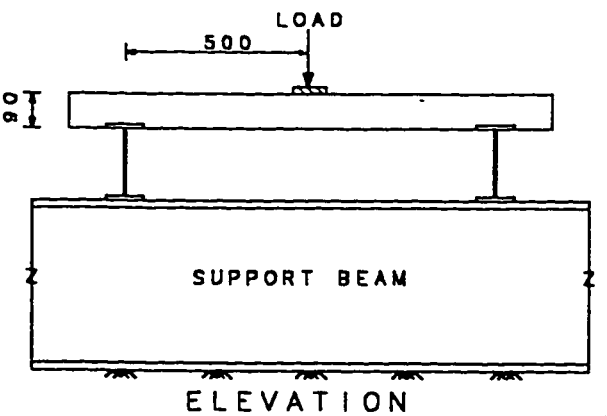

*All Dimensions in mm

Fig. 2.8: Location of Load Position for A2-Series Panel.

single patch load applied at the centre of one span of the slab. Fig 2.9 shows the load position and the support system of the panel. To avoid possible uplifting of the unloaded span of the slab, the three I-beams supporting the slab were clamped down to the large I-beams by C-clamps.

Four different load areas were used in static tests: 75 x 150 mm, 100 x 200 mm, 200 x 400 mm and 200 x 500 mm. In each static test, the load applied by the actuator on the padded steel plate was increased monotonically at a slow rate till failure, pausing briefly at different load levels for measurements of deflection and rebar strains and for the observation of the crack pattern. Deflections of the slab under the load point and at the midspans of the two slabs supporting I-beams were recorded with displacement transducers (LVDTs). The strain in the rebars fitted with strain gauges were recorded automatically on a strain recorder.

Prior to the application of the load, the readings of the LVDTs and the strain gauges were initialized close to zero. In each test, the first level of the load at which the slab cracked first was also recorded as the first cracking load. In the slowly increased load steps, test measurements included the record of deflection and rebar strains and also the observation of the emerging crack pattern and crack growth. At failure, the failure load and the mode of failure was recorded. The punched zone at the bottom of the deck was measured approximately to quantify the area of damage.

As the damage due to punching was essentially localized, especially for the case of smaller load areas, it was possible to test both spans of the slab between

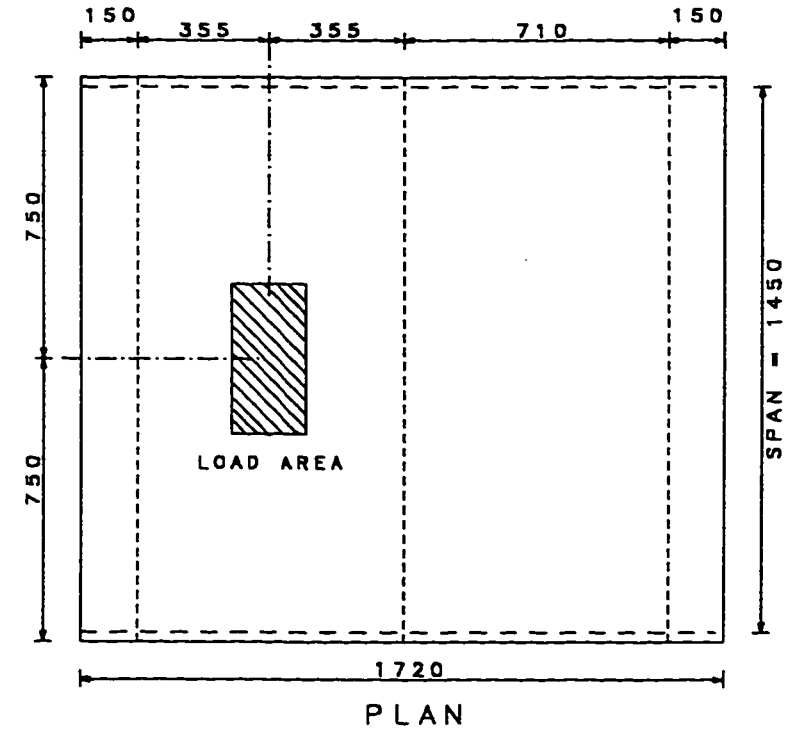

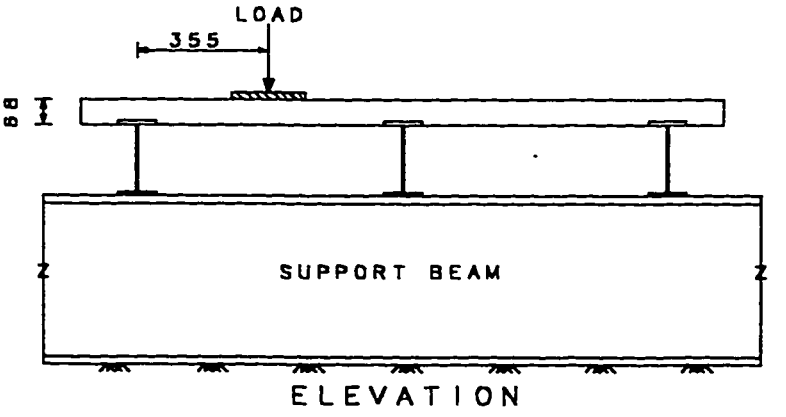

*All Dimensions in mm

Fig. 2.9: Location of load position for A3-series Panel.

the three supporting beams(Fig. 2.9) to generate two sets of test data. For the case when two static tests were conducted on the same panel, first the testing was done with smaller load areas(75 x 150 mm or 100 x 200 mm) in one span followed by the test on the other side to minimize the possible minor damages, if any. A total of sixteen static load tests were conducted on A3-series panels.

Three fatigue tests were conducted on these panels by utilizing the span of slabs which was not used in static tests. All fatigue tests were conducted with a pulsating load on an area of 75 x 150 mm. The untested span of panels used in static tests with 75 x 150 mm load area was utilized in fatigue tests. The magnitude of the maximum load level was restricted to about 60% of the value of the ultimate static load capacity P_u obtained with 75 x 150 mm load area. The ratio R of the minimum to the maximum load was kept close to 0.1 to avoid any possible uplifting of the panel under the cyclic loading. The frequency of the pulsating load was about 2.0 to 2.5 Hz. The number of load cycles were recorded automatically by a monitor hooked to the actuator.

Chapter 3

TEST RESULTS

3.1 CONCRETE AND STEEL STRENGTH

The casting of the panels in this test program was on a large scale. Concrete was used in different batches using the same mix design given in Table 2.4. The tests on cylinders taken from various batches at the time of cast, showed that the concrete strength varied significantly for different batches. This could be attributed to negligence on the part of ready mix contractor in strictly adhering to the mix design, the time lag in the casting of the panels which caused variation in the absorption of water by the aggregate and the loss of moisture due to evaporation in the hot outside environment. In view of this possibility that the concrete strength may vary due to variation in placement time and finishing, concrete cores of 50 mm diameter were extracted from each panel to obtain a better estimate of the actual concrete strength. The strength obtained were corrected for the height to depth ratio in accordance with ASTM specifications [35]. For comparison purposes, the concrete strength obtained from these cores were used for the assessment of test data.

Tables 3.1 to 3.3 show the core strength obtained for panels of A1, A2, and A3-series respectively. Due to variation of core strengths, an average of all core strengths obtained for different panels of a particular series was taken as the

Table 3.1: Compressive Strength of Core Samples Taken from A1-Series Panels.

PANEL	AVERAGE CORE STRENGTH OF PANEL (MPa)	AVERAGE CORE STRENGTH FOR A1-SERIES (MPa)
A1/ISO	27.9	27.1
A1/H	27.8	
A1/M	26.5	
A1/S	26.2	

Table 3.2: Compressive Strength of Core Samples Taken from A2-Series Panels.

PANEL		AVERAGE CORE STRENGTH OF PANEL (MPa)	AVERAGE CORE STRENGTH FOR A2-SERIES (MPa)
GROUP NO.	DESIGNATION		
1	A2C/P	25.2	
	A2C/S	25.5	
2	A2/20	27.4	
	A2/30	30.6	
	A2/45	32.8	28.2
	A2/60	30.6	(Excluding
	A2/90	27.9	A2C/P)
3	A2/60/H	29.2	
	A2/90/H	28.8	
4	A2C/90/L	25.0	
	A2C/90/H	24.4	

Table 3.3: Compressive Strength of Core Samples Taken from A3-Series Panels.

PANEL SET	AVERAGE CORE STRENGTH OF PANEL SET (MPa)	AVERAGE CORE STRENGTH FOR A3-SERIES (MPa)
A3-1	25.2	
A3-2	24.1	26.6
A3-3	30.6	

reference core strength for that particular series. This average core strength for the series are also shown in the tables. The failure load values could be adjusted for the variation in concrete core strength from that of the average core strength for that series to facilitate comparison based on an identical values of core strengths.

The ratio of the average core strength to that of the cylinders strength approximately varied from 0.88 to 0.92 with an average of 0.9. This compares favorably also with the result of past study [36] on the relationship between the core strength and cylinder strength of concrete.

The steel used was a high strength steel rebars, manufactured locally, in the Eastern Province of Saudi Arabia. The steel yield stress of 6 mm, 8 mm and 10 mm diameter bars was around 550 MPa (80 ksi) and a ultimate strength of 775 MPa (112 ksi). The yield strength of 4 mm bars was a little higher than the other bars, with a value of 590 MPa (85 ksi) and an ultimate strength of 633 MPa (92 ksi).

3.2 A1-SERIES TEST RESULTS

The various test data gathered from the tests on the A1-series panels include the crack mapping and its documentation at selected steps of increased loading, to record the strains in some of the main transverse steel rebars and in some of the longitudinal steel rebars which were fitted with strain gauges.

3.2.1 Cracking

In order to show the progressive crack growth under a moving wheel load from one end to the other end of the slab, crudely simulated by applying load at three locations in successive steps, photographs were taken at different load levels after each cycle of moving the load from one end to the other end of the panel. The photographs were taken for each panel type namely A1/ISO, A1/H, A1/M and A1/S for the load levels of 40 kN, 60 kN, 70 kN and 80 kN. Plates 3.1 to 3.4 show the cracking pattern of the four panels at these load levels. These photographs would serve to indicate the density of cracks for panels with different amounts of distribution steel at identical load levels and identical load passages.

3.2.2 Strains

In order to record the level of stress under different load level, strains were measured from a selected number of main steel rebars fitted with strain gauges. The location of these bars are shown in Fig. 2.2. In some of the panels, the strain gauges malfunctioned due to possible damage of the strain gauges because of cracking and possible abrasion resulting from any bond slip. These values were rejected and are not shown. Figs. 3.1 to 3.12 show the strains in the transverse steel rebars plotted against load for the panels A1/S, A1/H and A1/ISO at different load levels.

Also the strains in some of the rebars of longitudinal steel were measured

A1/S

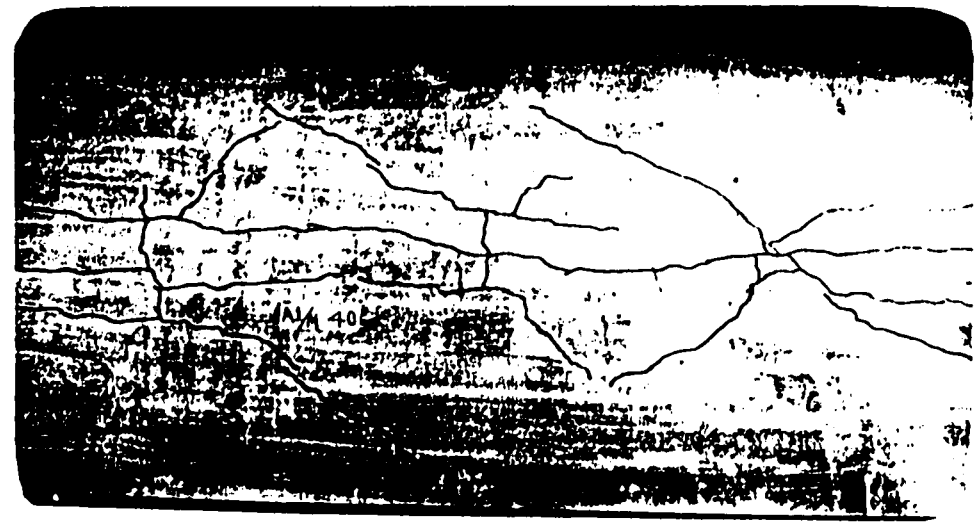

A1/M

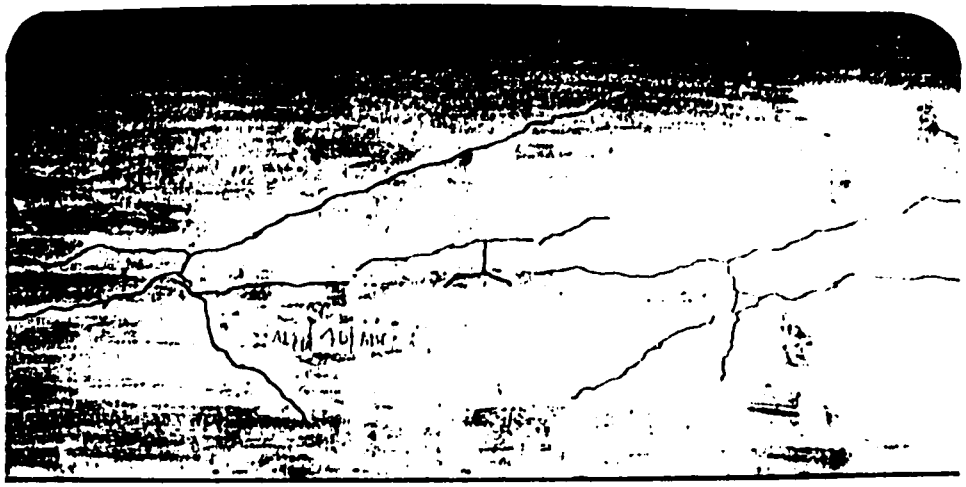

A1/H

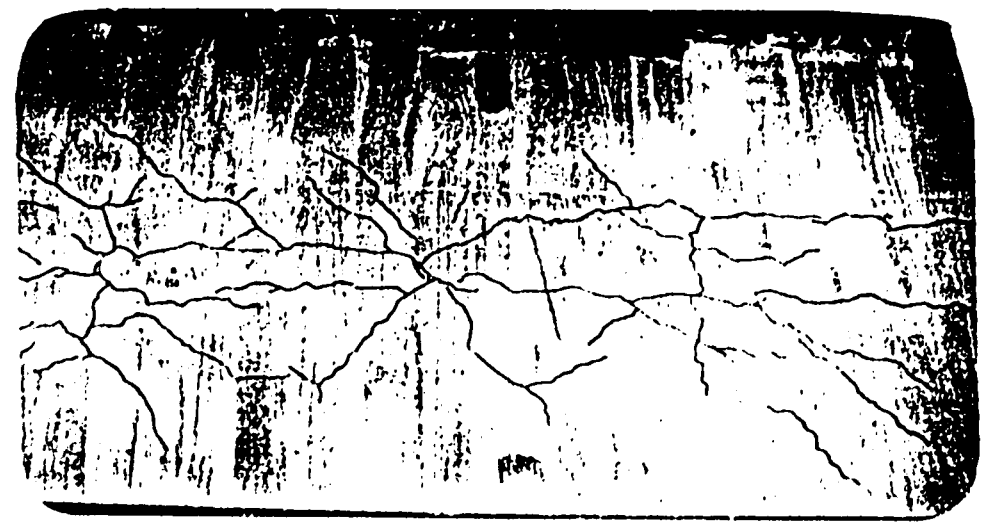

A1/ISO

Plate 3.1: Cracks Developed in Different A1-Series Panels at 40 kN Load.

A1/S

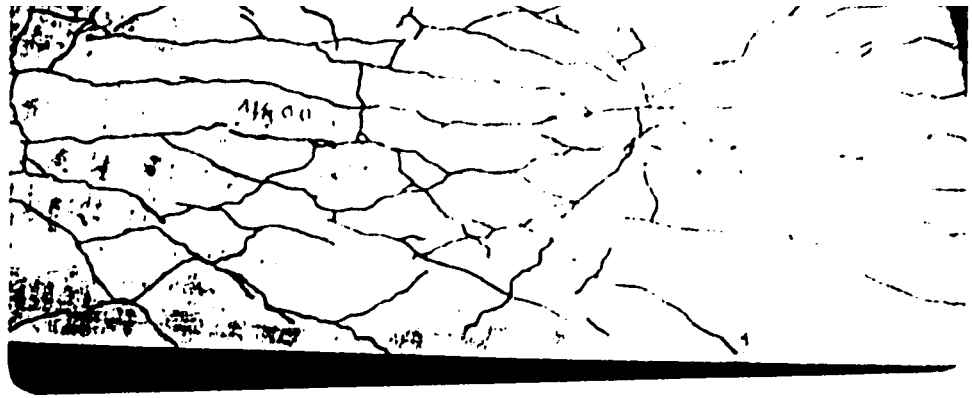

A1/M

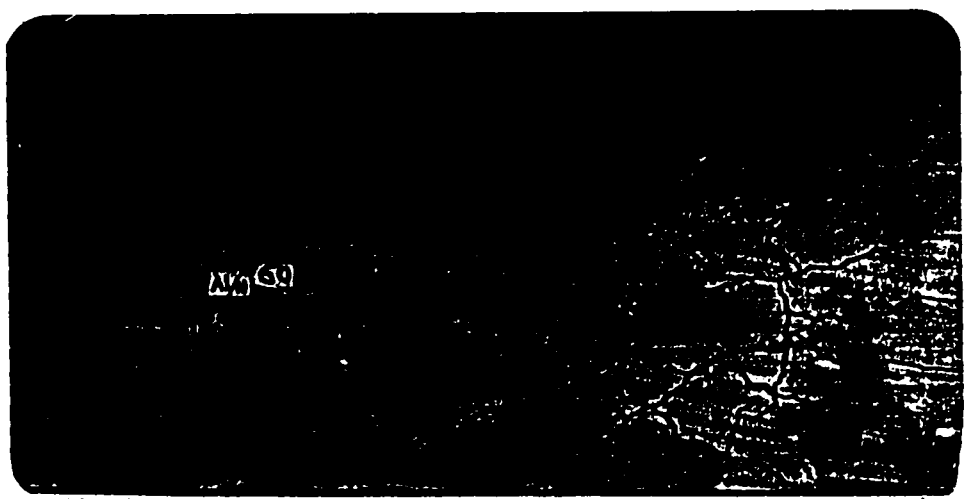

A1/H

A1/ISO

Plate 3.2: Cracks Developed in Different A1-Series Panels at 60 kN Load.

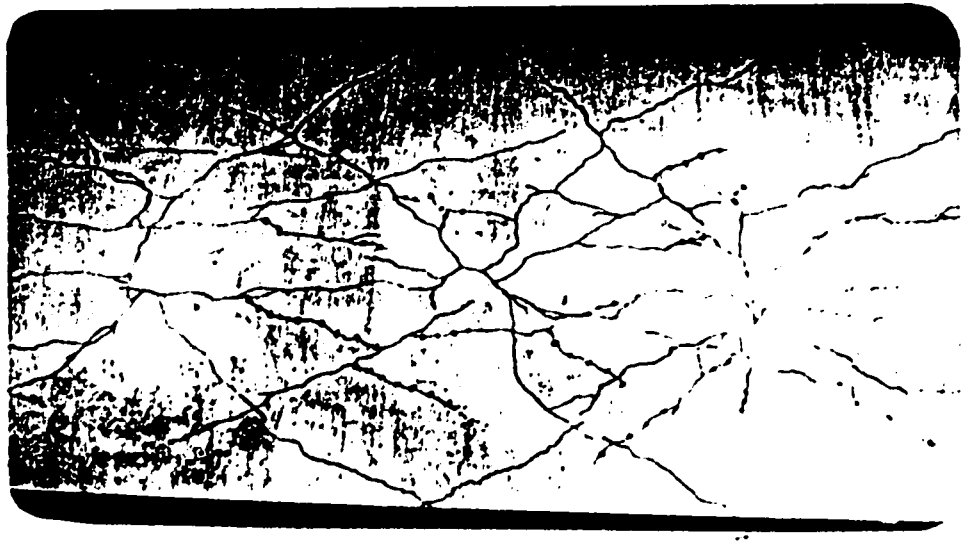

A1/S

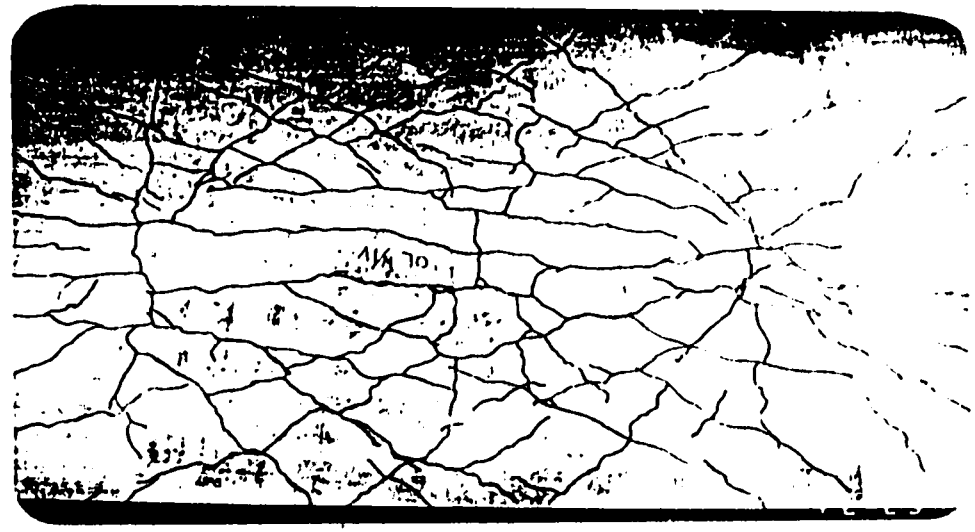

A1/M

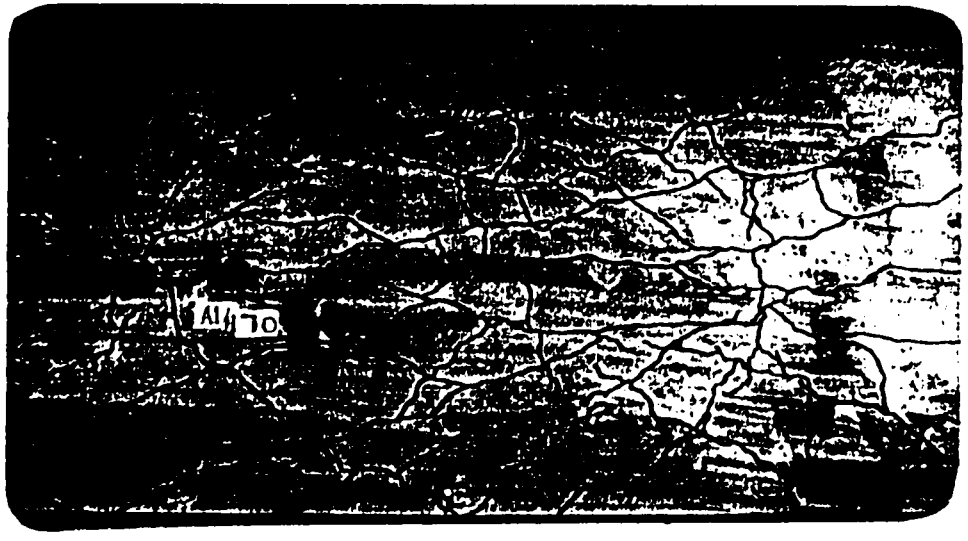

A1/H

A1/ISO

Plate 3.3: Cracks Developed in Different A1-Series Panels at 70 kN Load.

A1/S

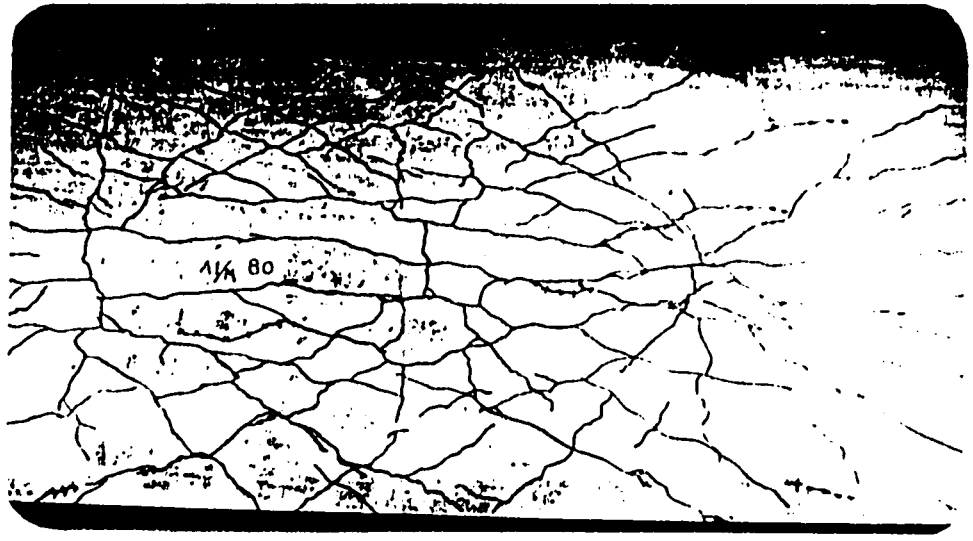

A1/M

A1/H

Plate 3.4: Cracks Developed in Different A1-Series Panels at 80 kN Load.

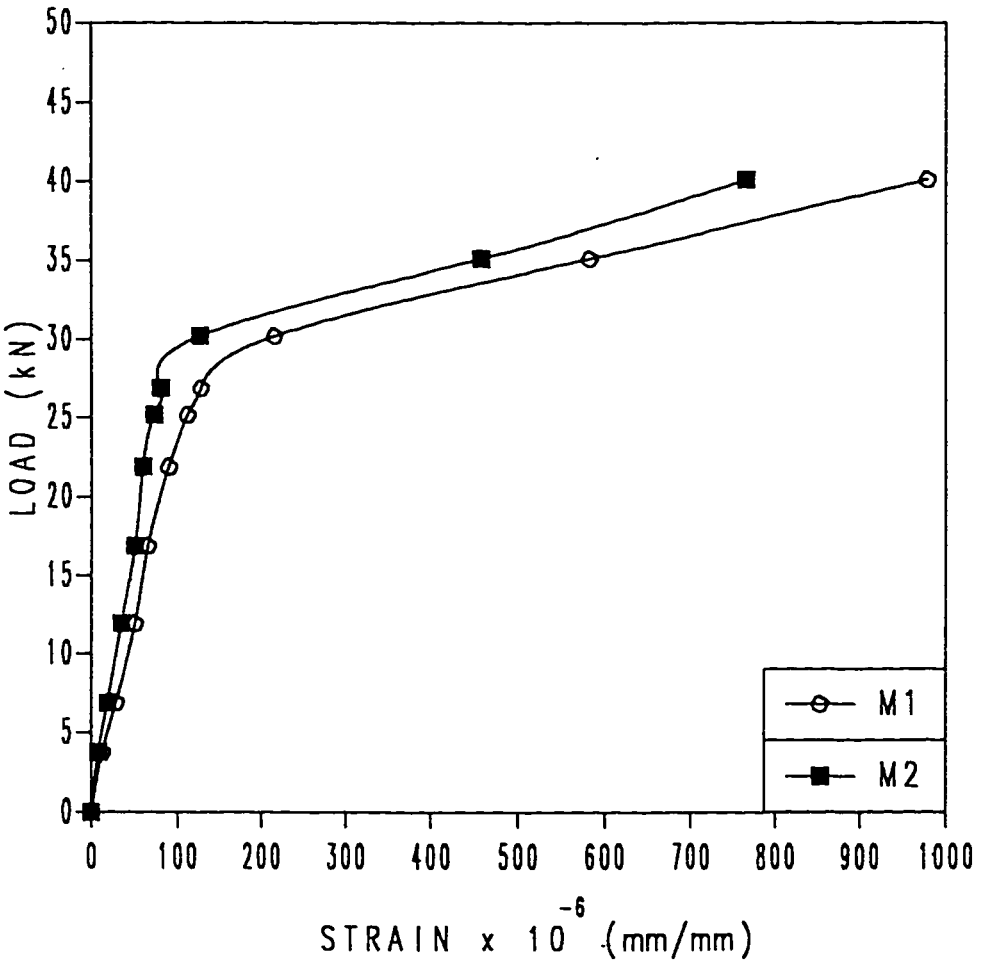

Fig. 3.1: Load-Strain Relationship in Transverse Steel Bars of Panel A1/S Loaded upto 40 kN.

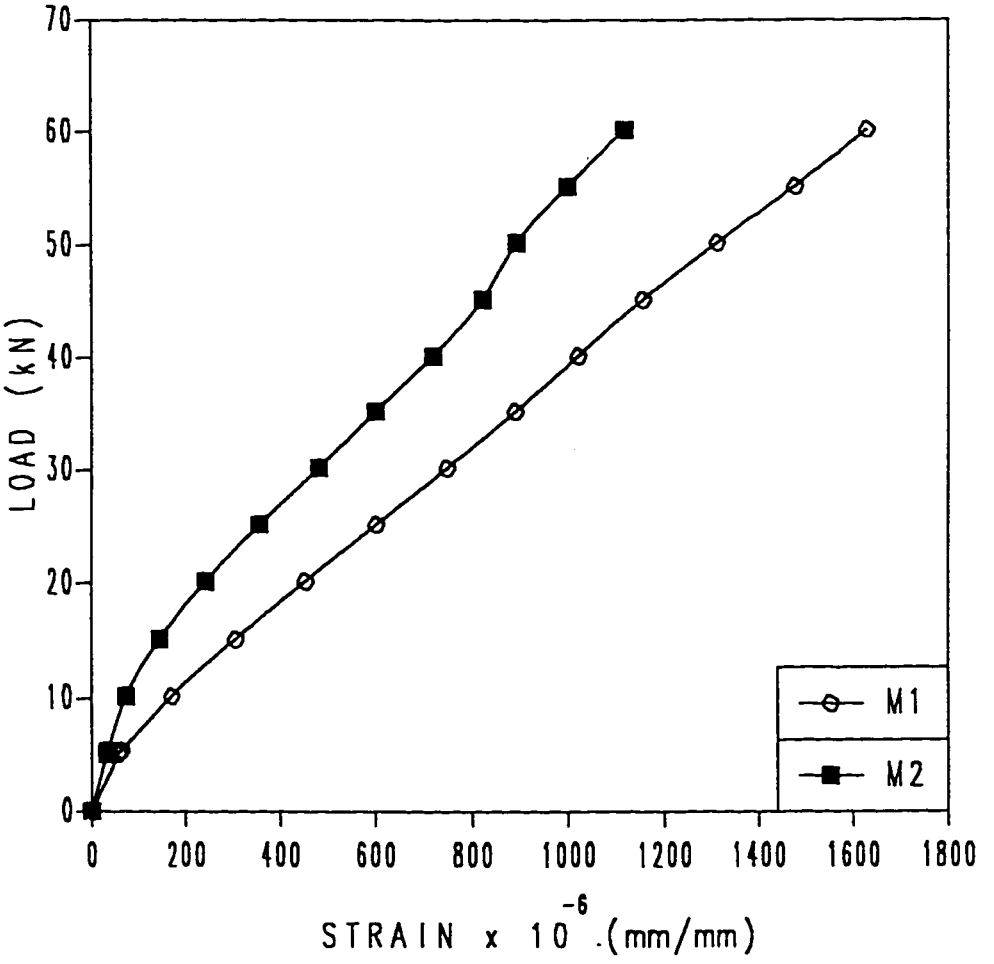

Fig. 3.2: Load-Strain Relationship in Transverse Steel Bars of Panel A1/S Loaded upto 60 kN.

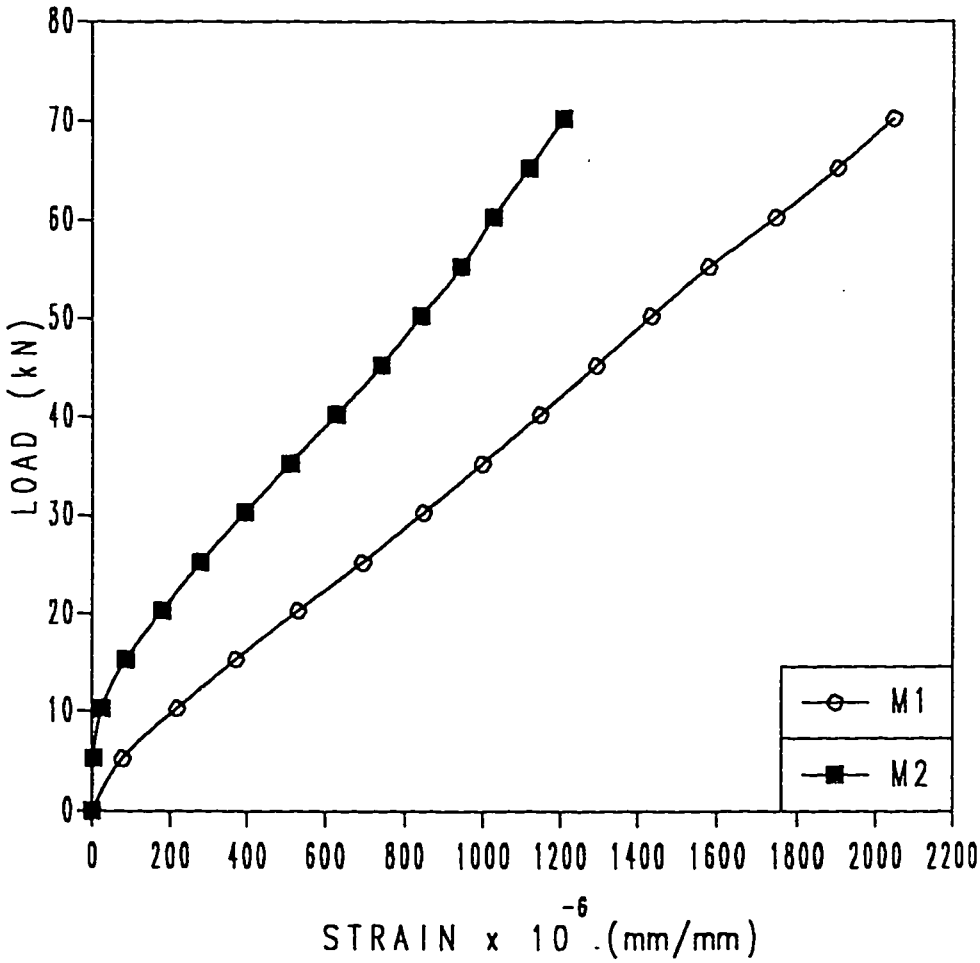

Fig. 3.3: Load-Strain Relationship in Transverse Steel Bars of Panel A1/S Loaded upto 70 kN.

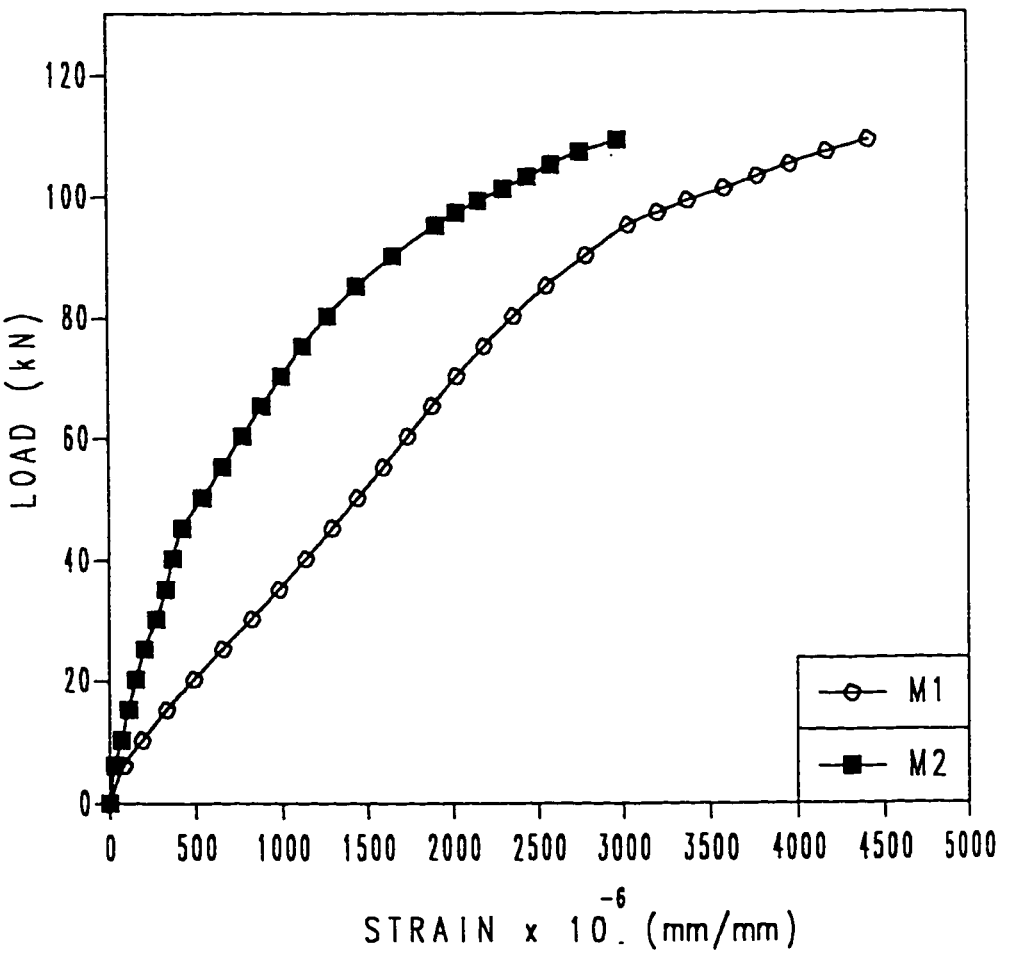

Fig. 3.4: Load-Strain Relationship in Transverse Steel Bars of Panel A1/S Loaded to Failure.

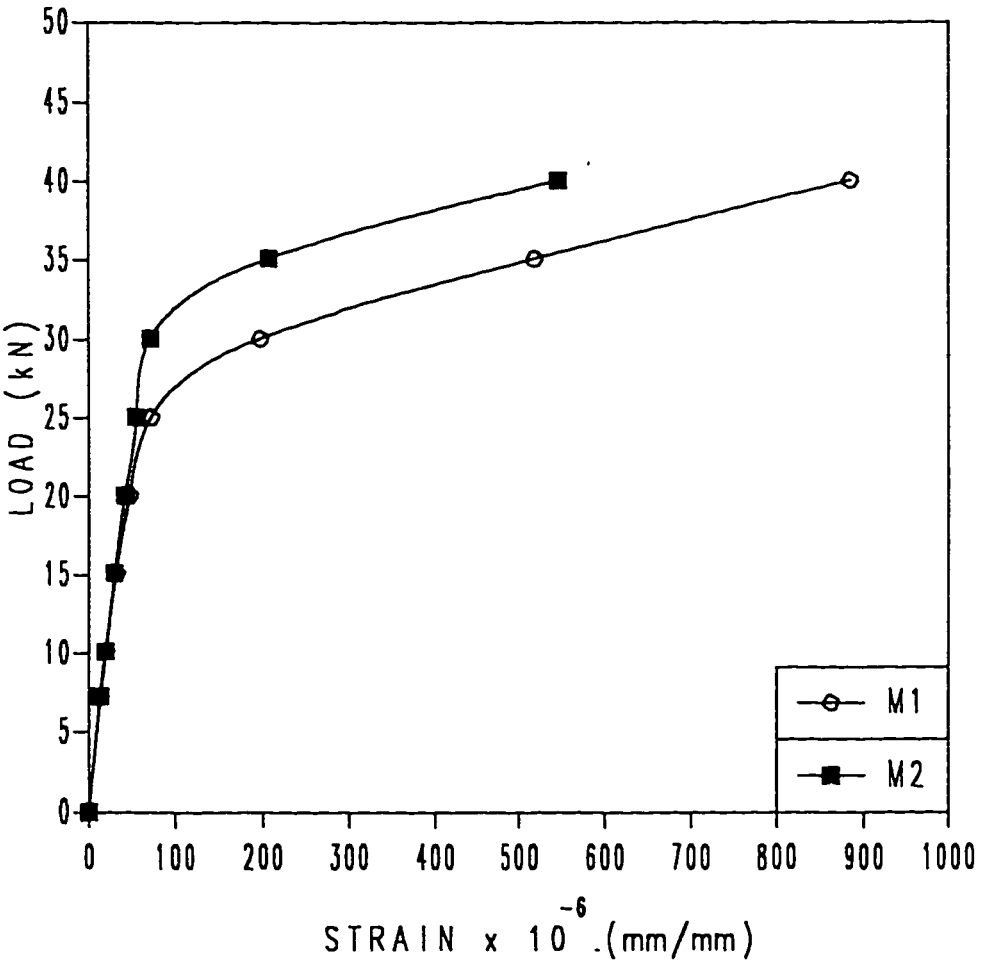

Fig. 3.5: Load-Strain Relationship in Transverse Steel Bars of Panel A1/H Loaded upto 40 kN.

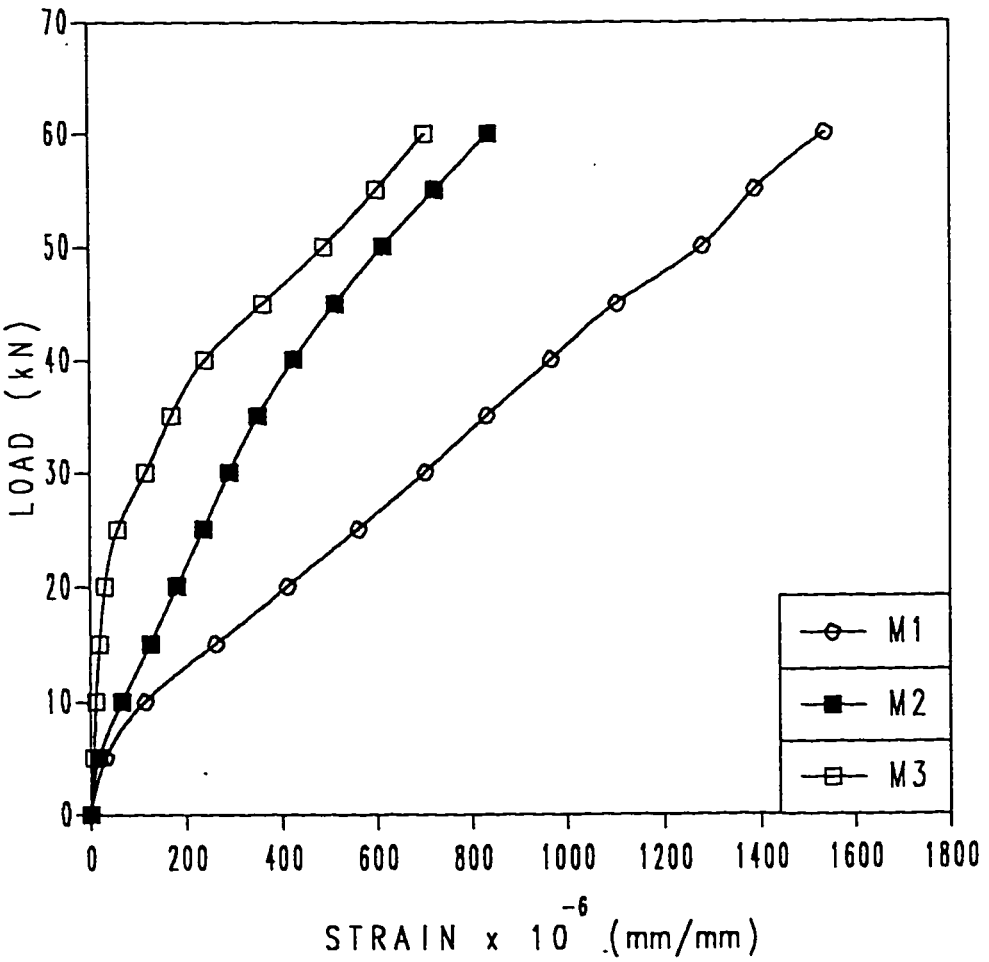

Fig. 3.6: Load-Strain Relationship in Transverse Steel Bars of Panel A1/H Loaded upto 60 kN.

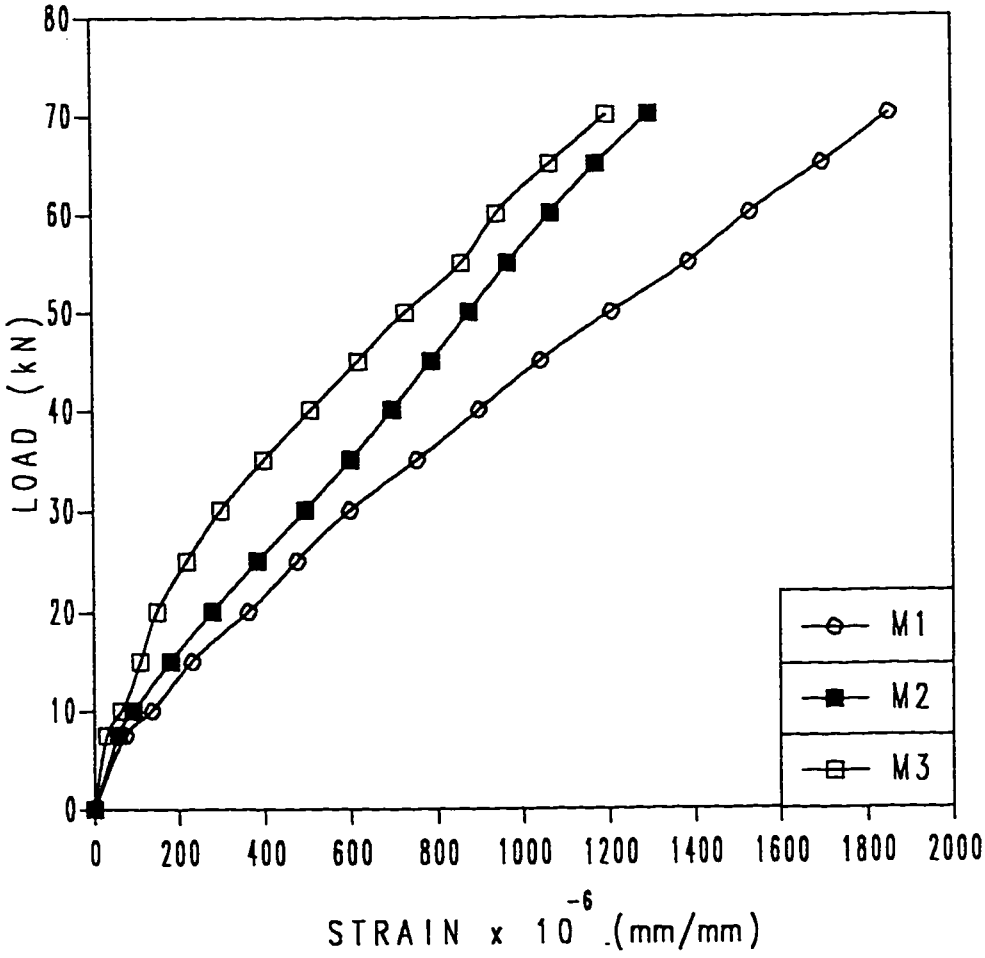

Fig. 3.7: Load-Strain Relationship in Transverse Steel Bars of Panel A1/H Loaded upto 70 kN.

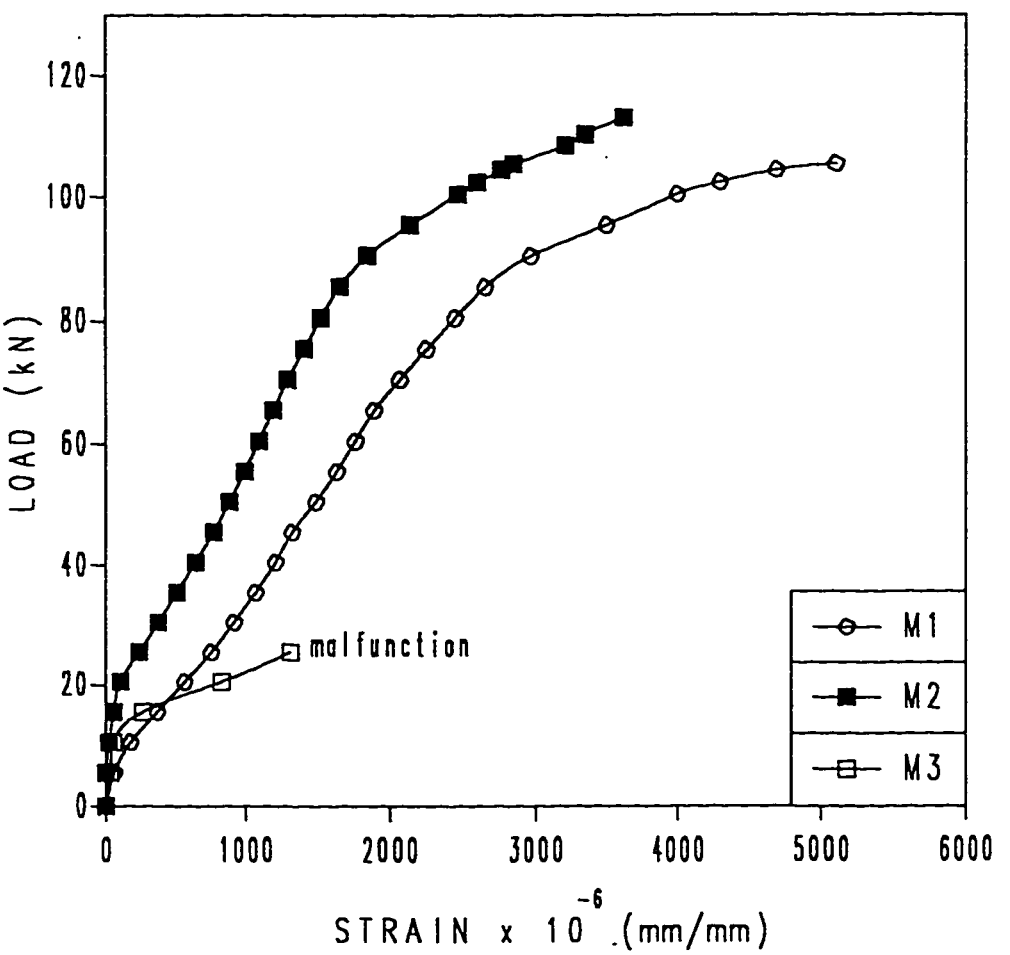

Fig. 3.8: Load-Strain Relationship in Transverse Steel Bars of Panel A1/H Loaded to Failure.

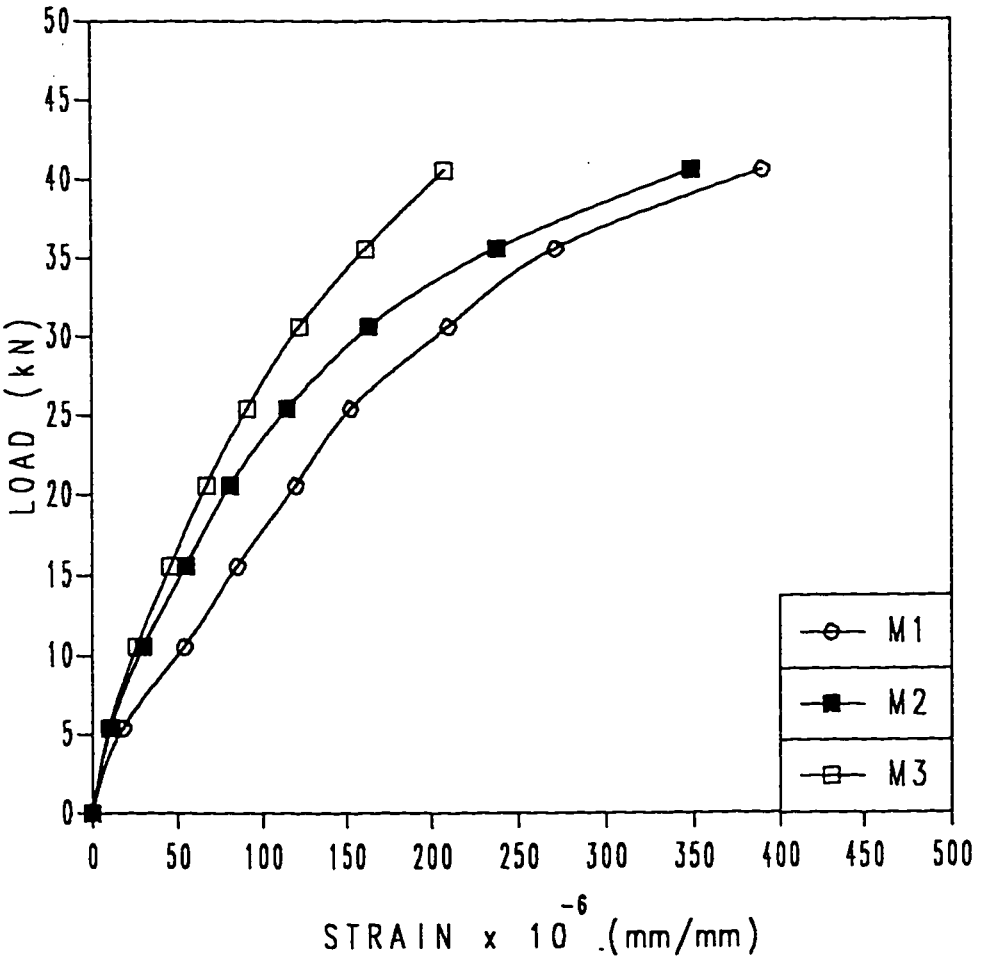

Fig. 3.9: Load-Strain Relationship in Transverse Steel Bars of Panel A1/ISO Loaded upto 40 kN.

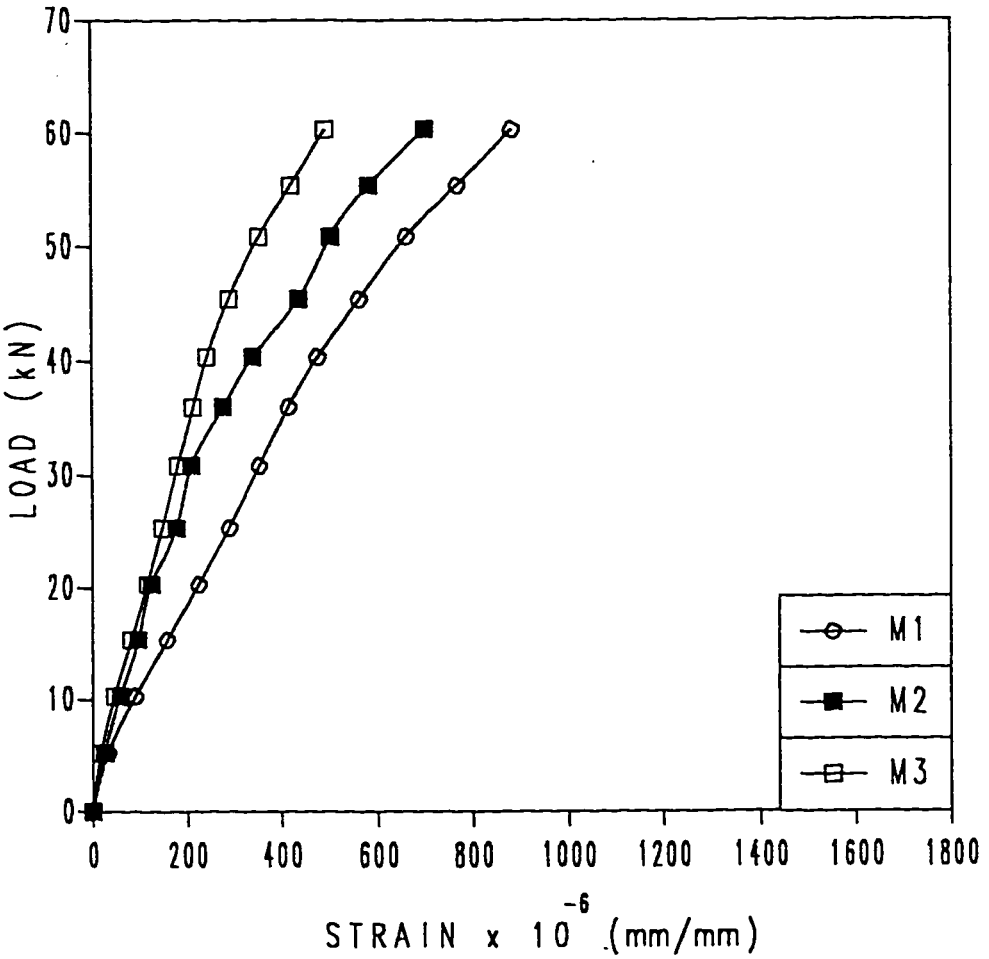

Fig. 3.10: Load-Strain Relationship in Transverse Steel Bars of Panel A1/ISO Loaded upto 60 kN.

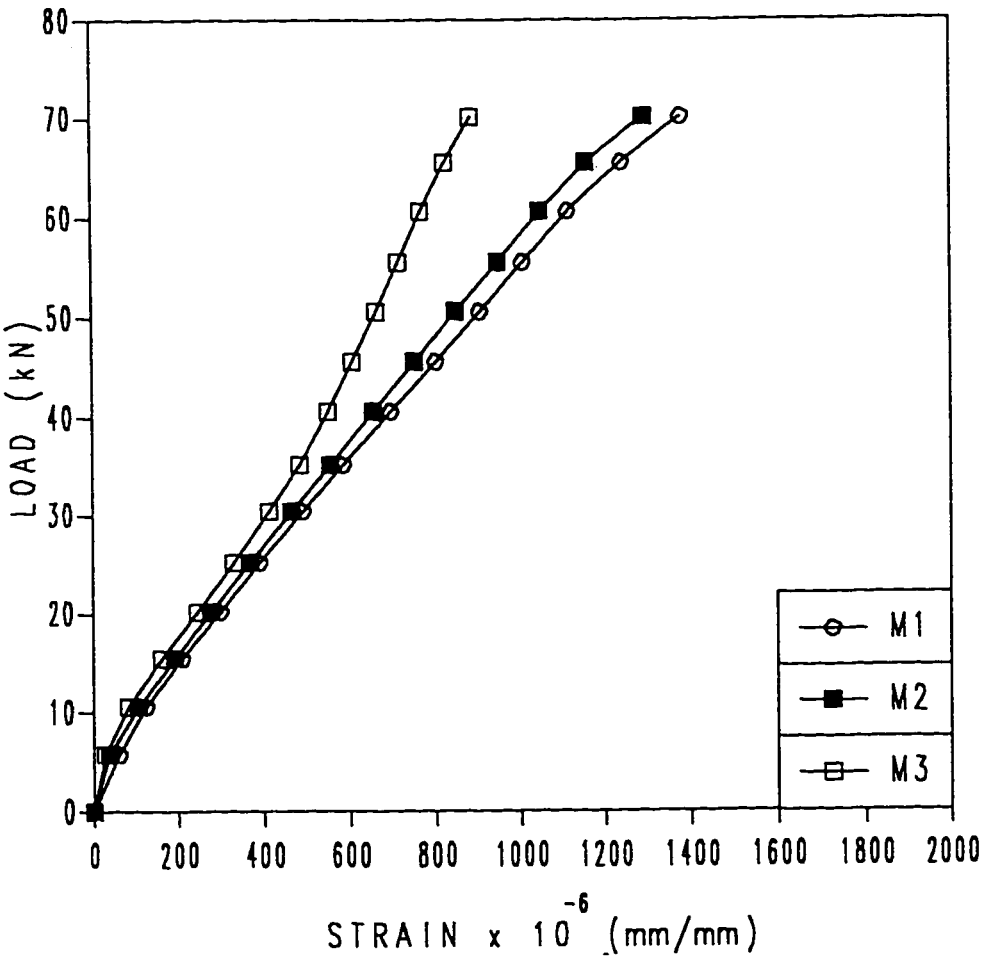

Fig. 3.11: Load-Strain Relationship in Transverse Steel Bars of Panel A1/ISO Loaded upto 70 kN.

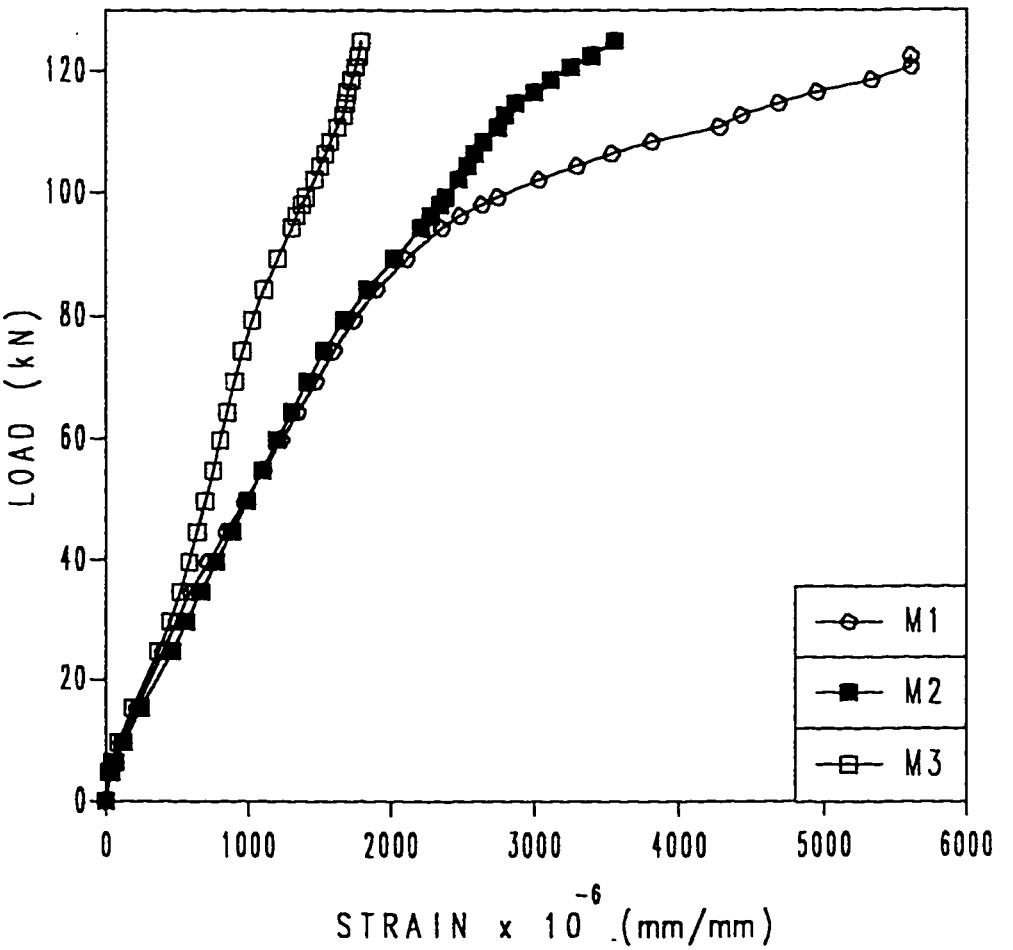

Fig. 3.12: Load-Strain Relationship in Transverse Steel Bars of Panel A1/ISO Loaded to Failure.

to see the level of stress which may give an indication of the amount of load or moment in the longitudinal direction. Figs. 3.13 to 3.23 show the strain in longitudinal steel bars plotted against load for different panels at different load levels.

Comparison of the strains for identically placed bars at the same load level would indicate the amount of stress in the rebars in different panels. This would also indicate the effective role played by the longitudinal steel in distributing the load over larger area or to bring in a wider width of slab to resist the load.

3.2.3 Failure Loads

After the travel of load P equal to 80 kN, the panel was loaded to failure by positioning the load at the centre location of the panel. The failure loads were recorded for each panel. Table 3.4 shows the failure load for different panels of A1-series. Also shown are the values of concrete compressive strength for cores taken from the panels. Failure was essentially in punching for all panels, with a top failure surface equal to load area and a large dislocated area at the bottom. Plate 3.5 shows a top failure surface, which is typical of failure in all the panels. Plate 3.6 shows the bottom failure surfaces for all the panels. No crack was visibly observed at the top surface of the slab.

The length and breadth of the failure zone at bottom were measured to record the approximate size of pot hole. In all cases the top failure surface was equal to the load area but the bottom failure surfaces varied. Table 3.4 also

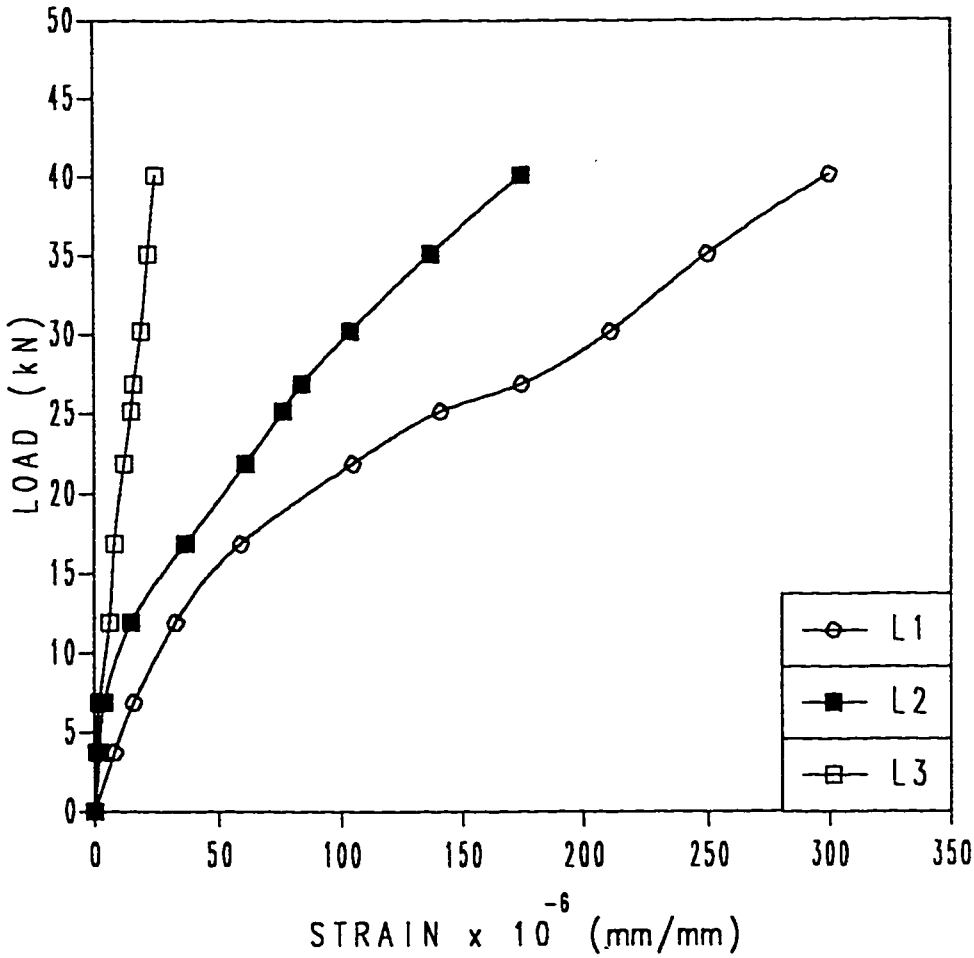

Fig. 3.13: Load-Strain Relationship in Longitudinal Steel Bars of Panel A1/S Loaded upto 40 kN.

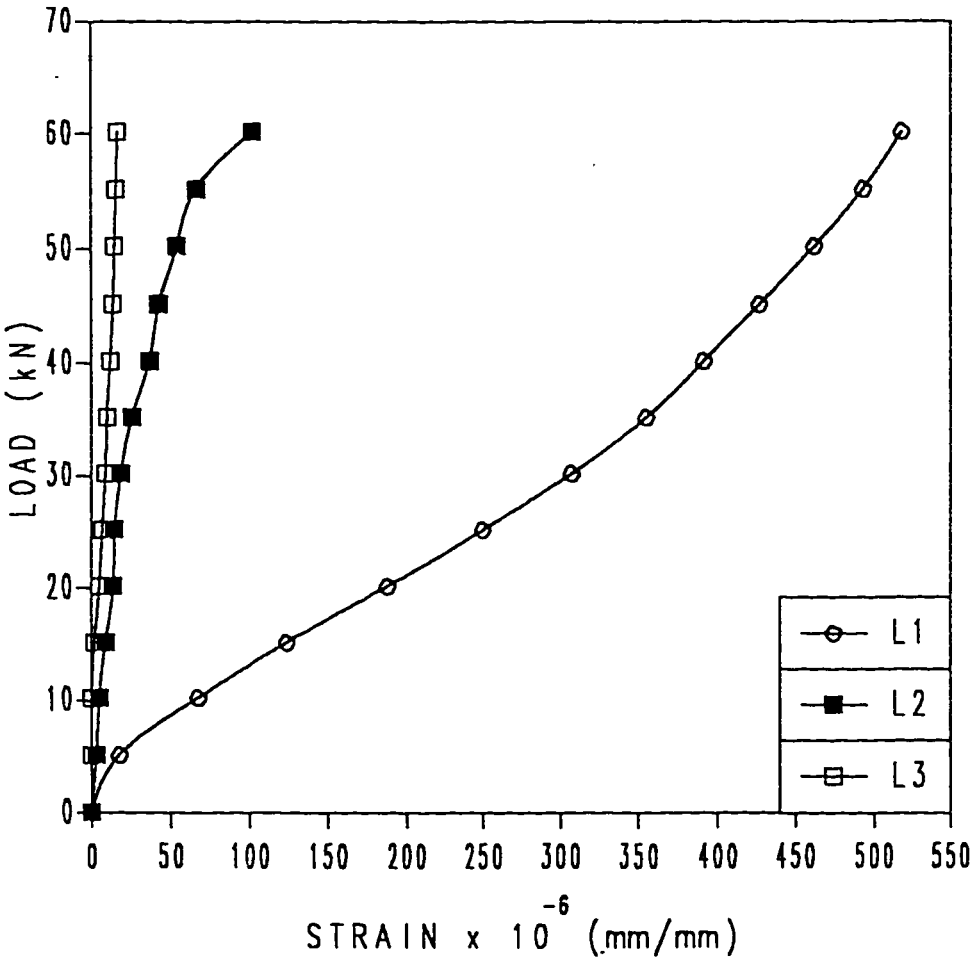

Fig. 3.14: Load-Strain Relationship in Longitudinal Steel Bars of Panel A1/S Loaded upto 60 kN.

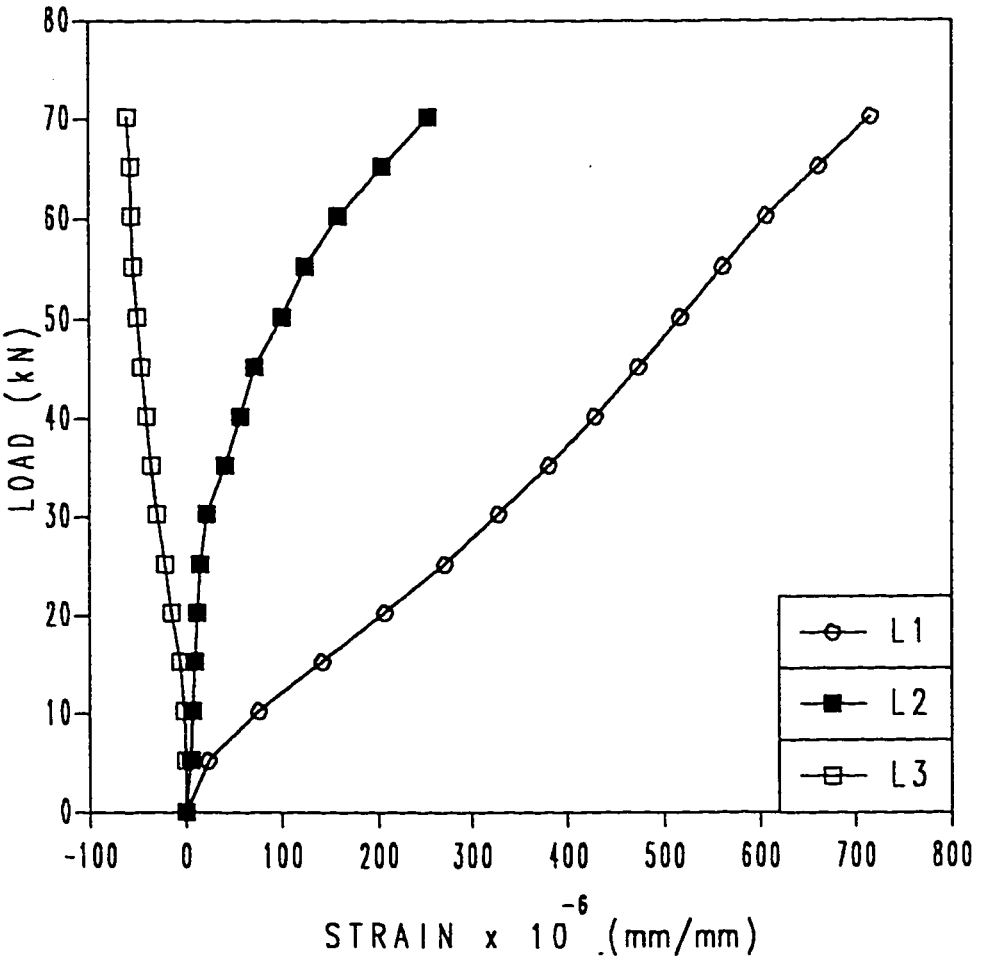

Fig. 3.15: Load-Strain Relationship in Longitudinal Steel Bars of Panel A1/S Loaded upto 70 kN.

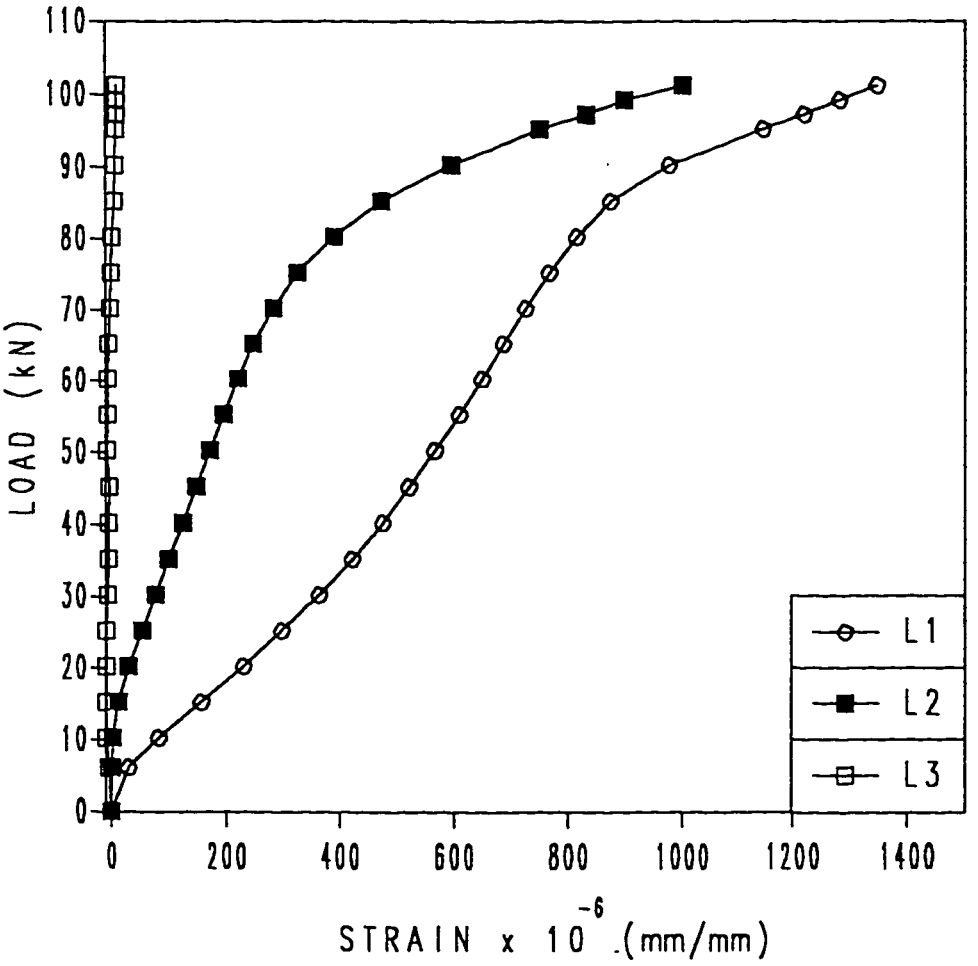

Fig. 3.16: Load-Strain Relationship in Longitudinal Steel Bars of Panel A1/S Loaded to Failure.

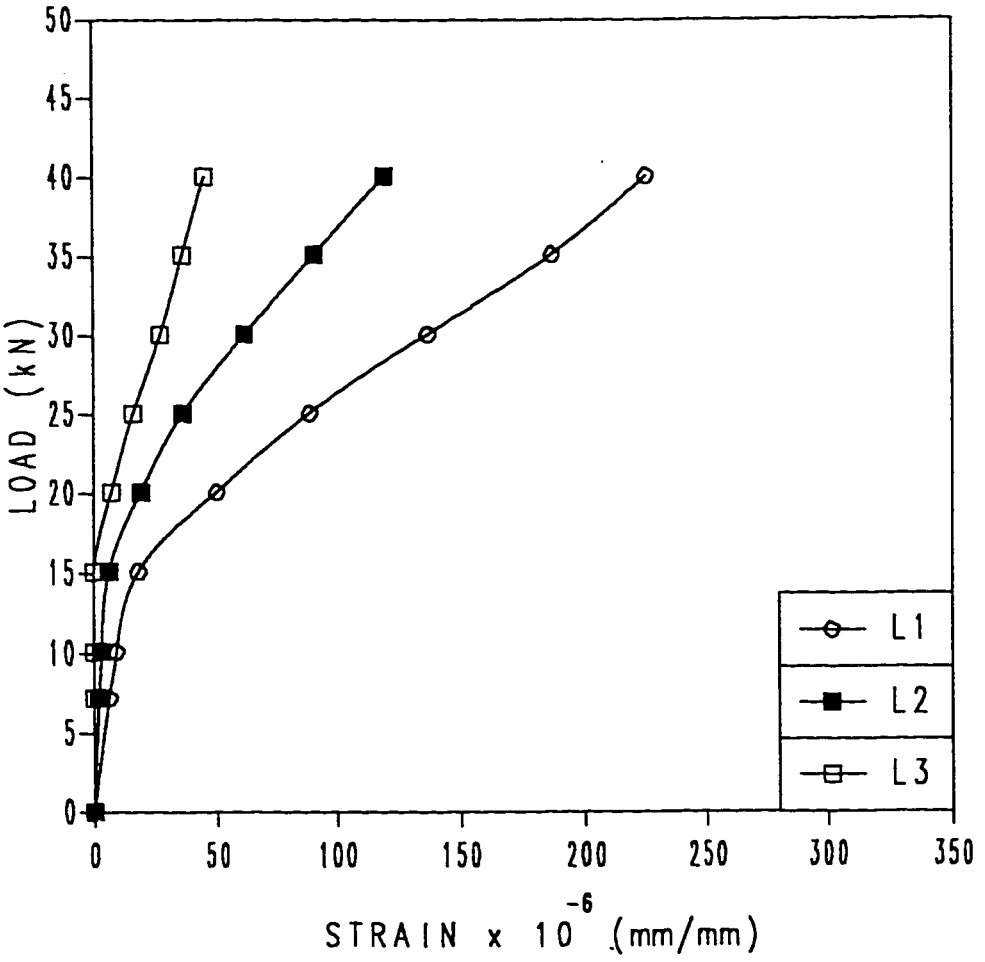

Fig. 3.17: Load-Strain Relationship in Longitudinal Steel Bars of Panel A1/H Loaded upto 40 kN.

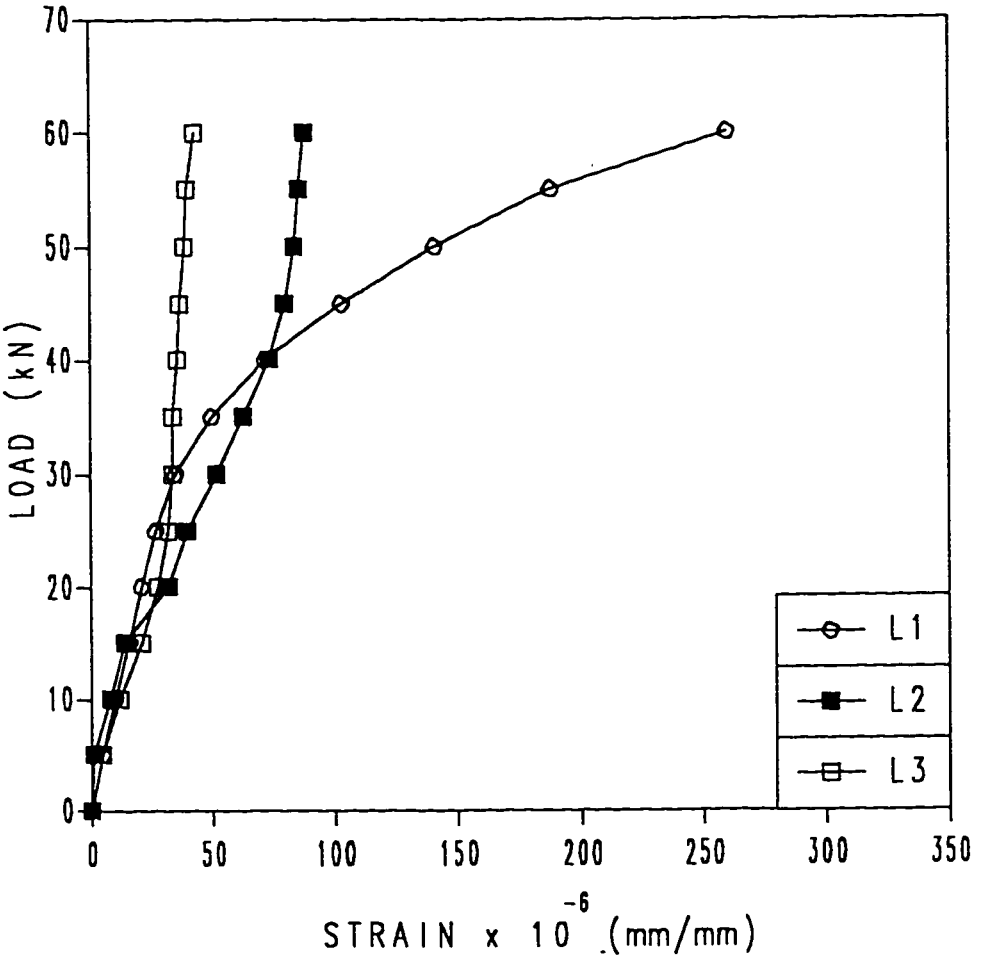

Fig. 3.18: Load-Strain Relationship in Longitudinal Steel Bars of Panel A1/H Loaded upto 60 kN.

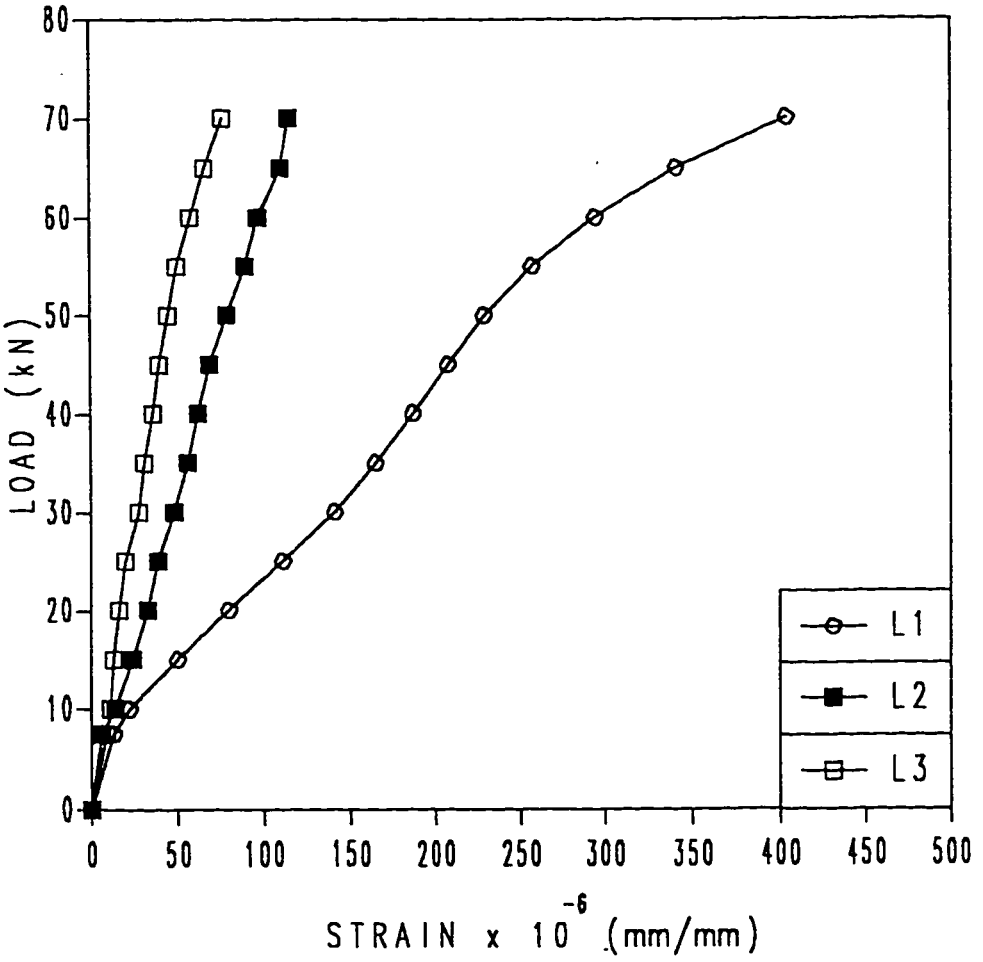

Fig. 3.19: Load-Strain Relationship in Longitudinal Steel Bars of Panel A1/H Loaded upto 70 kN.

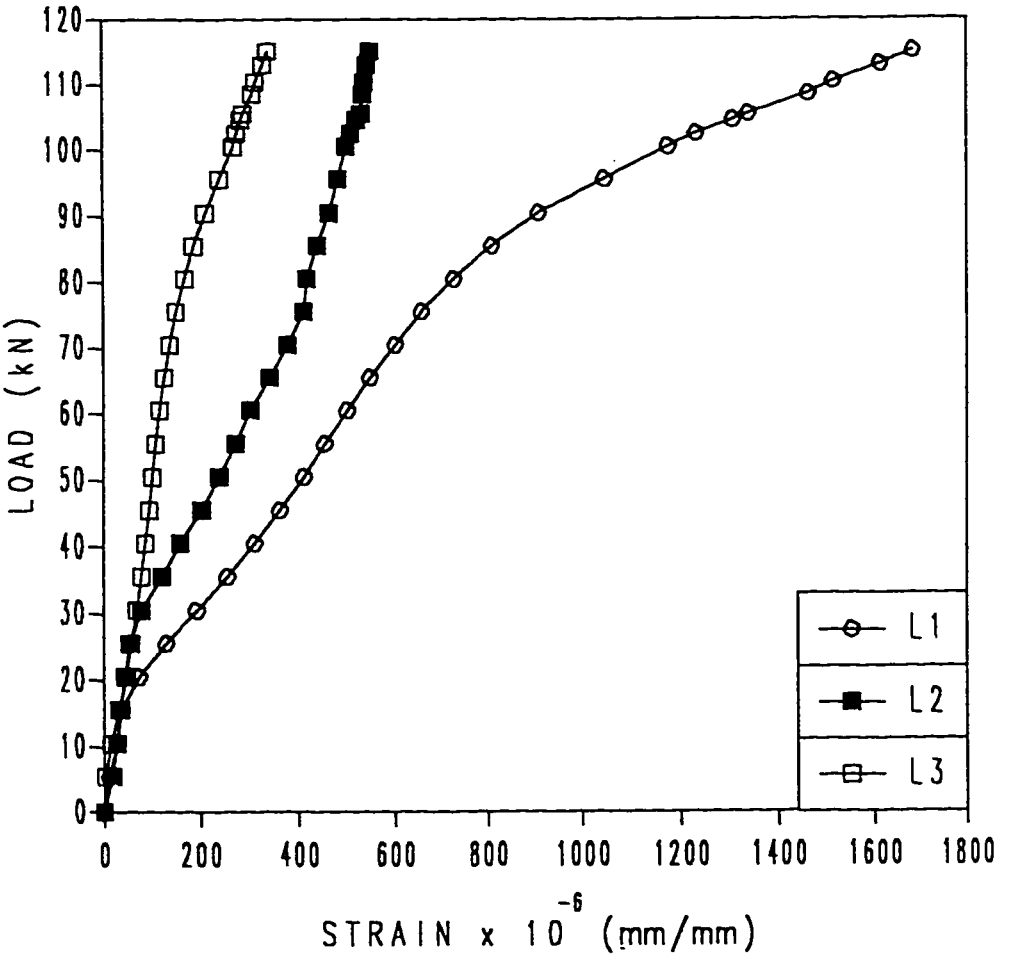

Fig. 3.20: Load-Strain Relationship in Longitudinal Steel Bars of Panel A1/H Loaded to Failure.

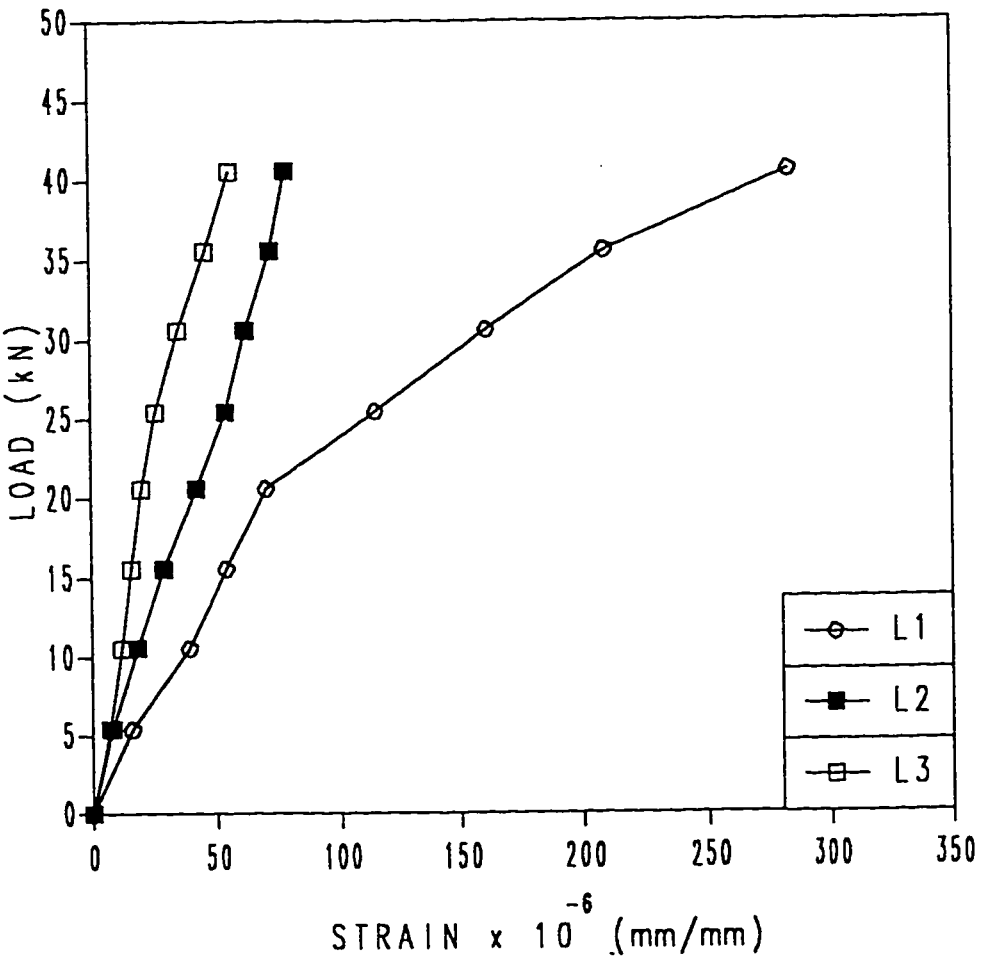

Fig. 3.21: Load-Strain Relationship in Longitudinal Steel Bars of Panel A1/ISO Loaded upto 40 kN.

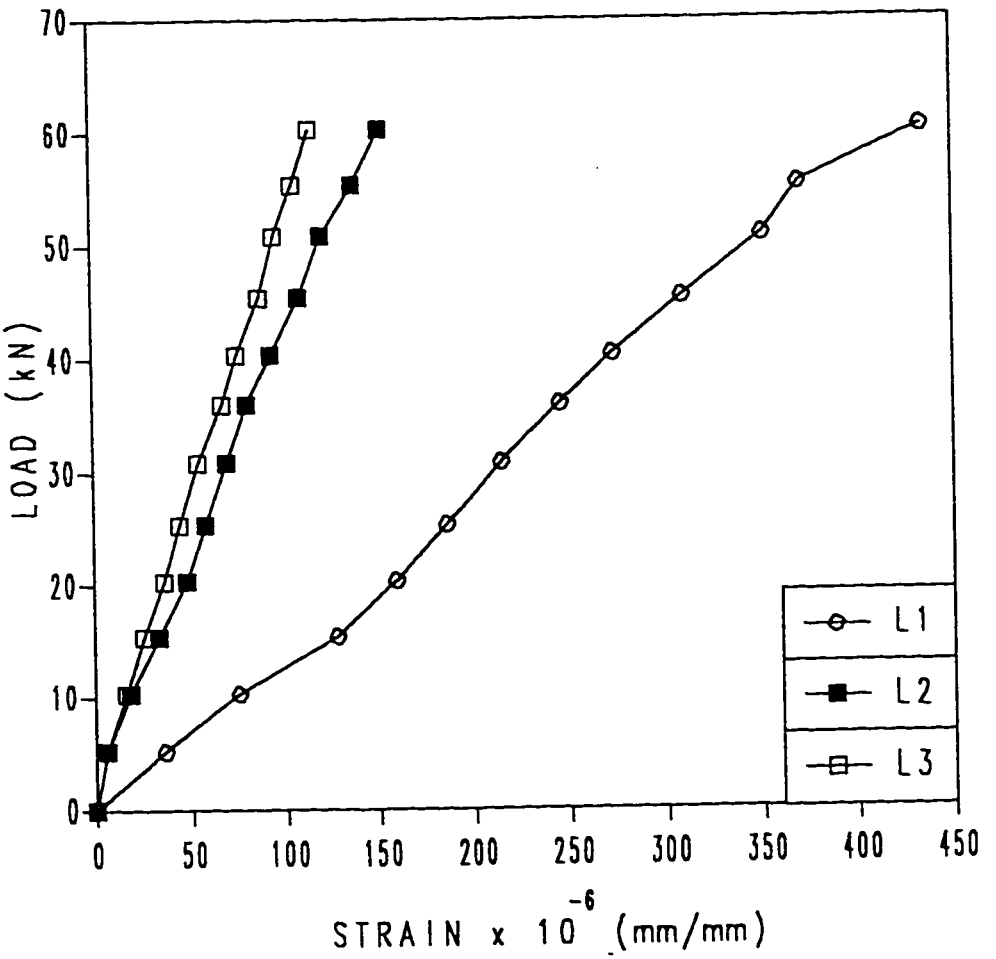

Fig. 3.22: Load-Strain Relationship in Longitudinal Steel Bars of Panel A1/ISO Loaded upto 60 kN.

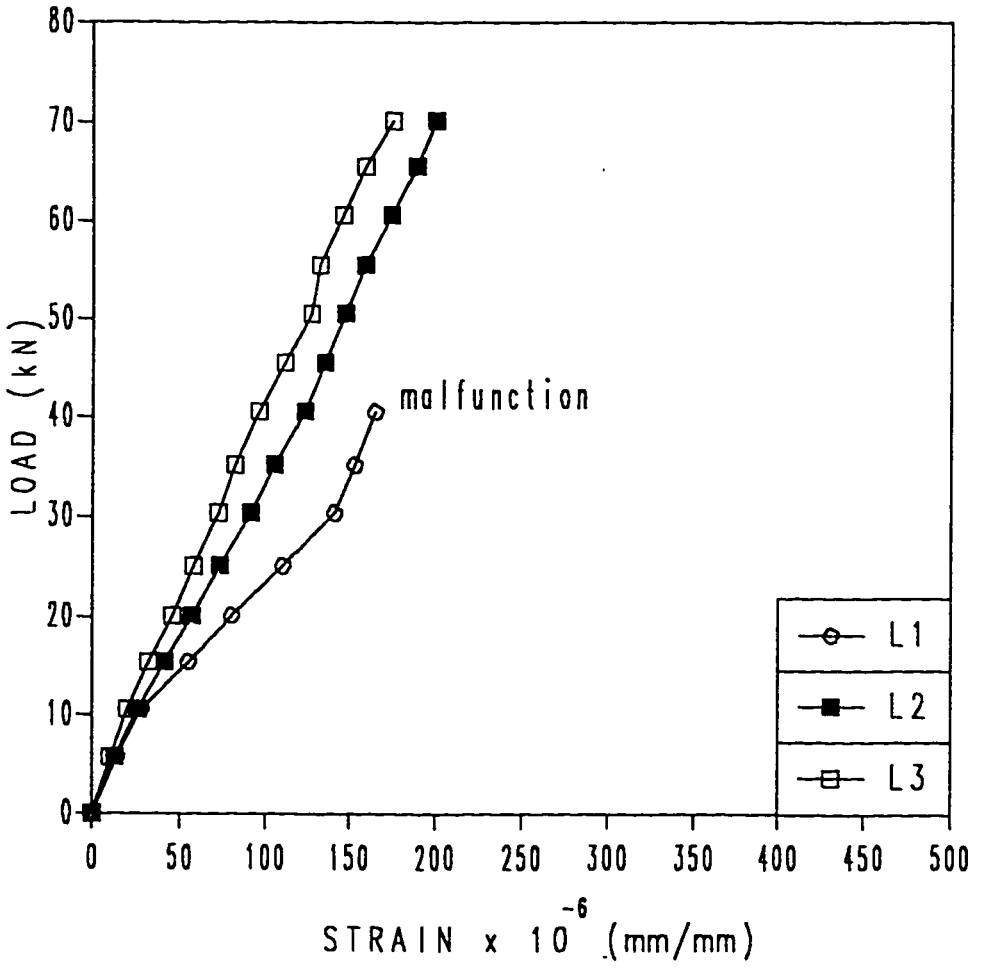

Fig. 3.23: Load-Strain Relationship in Longitudinal Steel Bars of Panel A1/ISO Loaded upto 70 kN.

Table 3.4: Test Results of A1-Series Panels.

PANEL	AVERAGE CORE STRENGTH (MPa)	FAILURE LOAD (kN)	DIMENSIONS OF BOTTOM FAILURE SURFACE (mm)	
			WIDTH	LENGTH
A1/ISO	27.9	127.0	600	800
A1/H	27.8	117.0	600	700
A1/M	26.5	105.0	560	600
A1/S	26.2	101.0	500	550

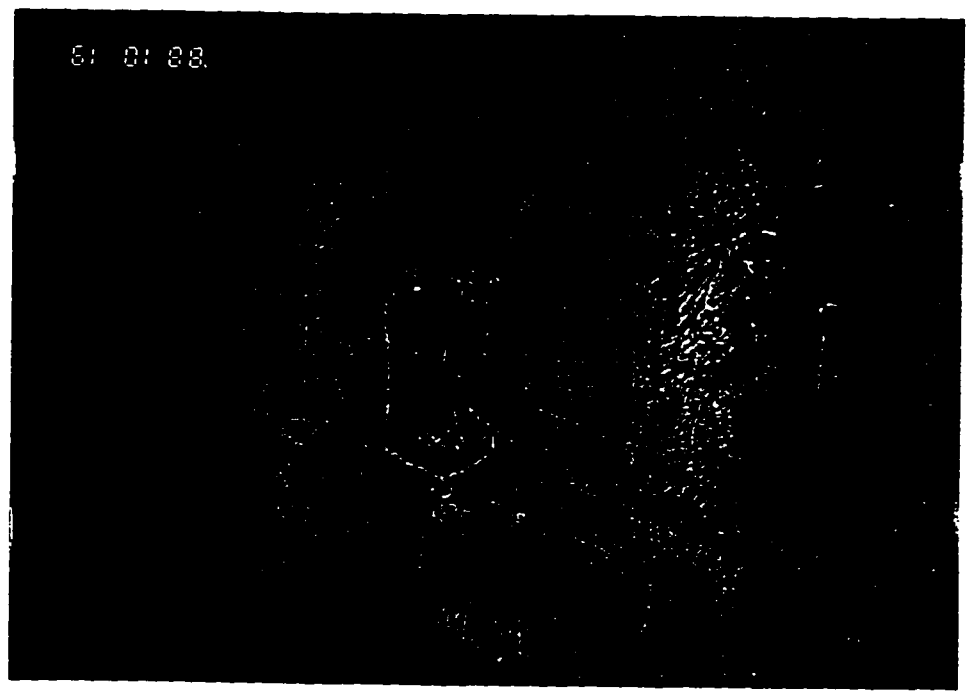

Plate 3.5: View of Typical Top Failure Surface of A1-Series Panels.

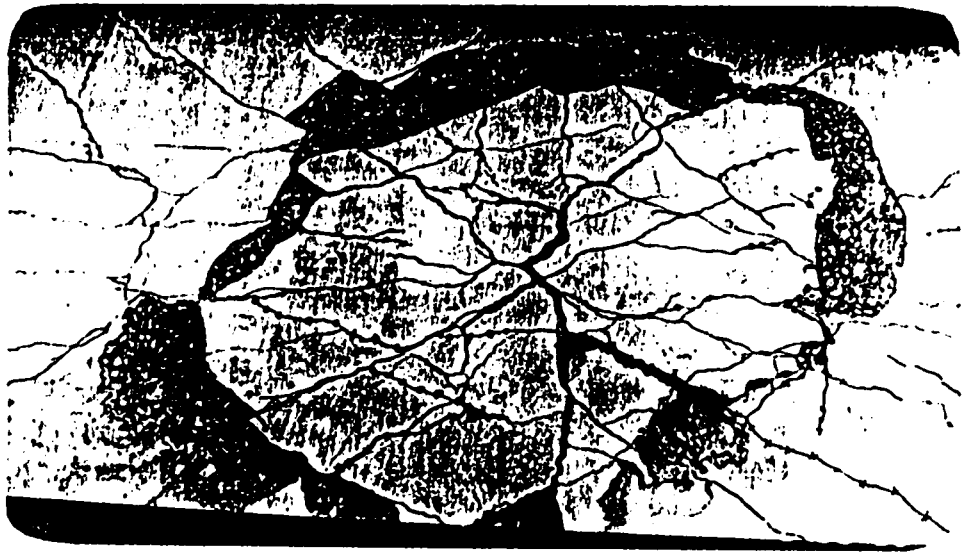

A1/S

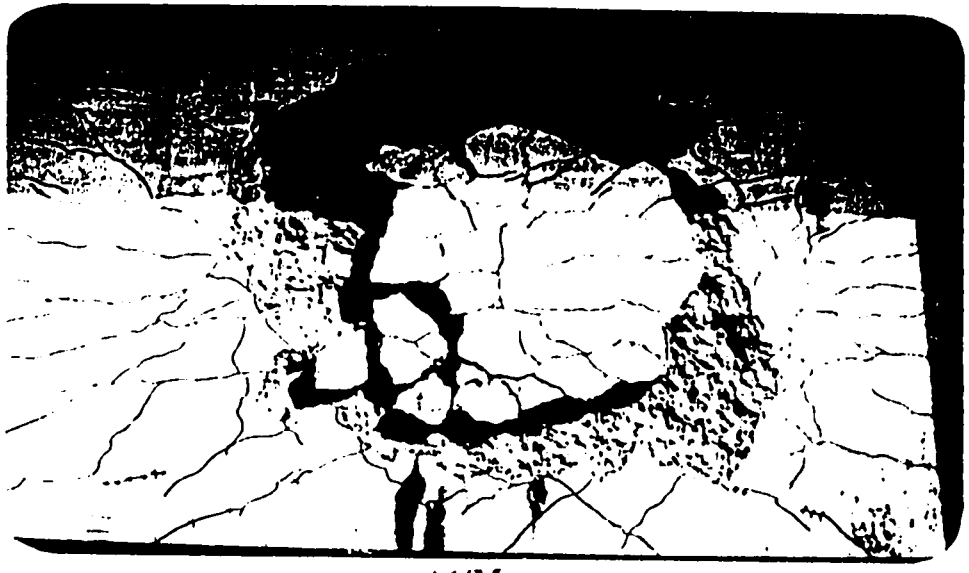

A1/M

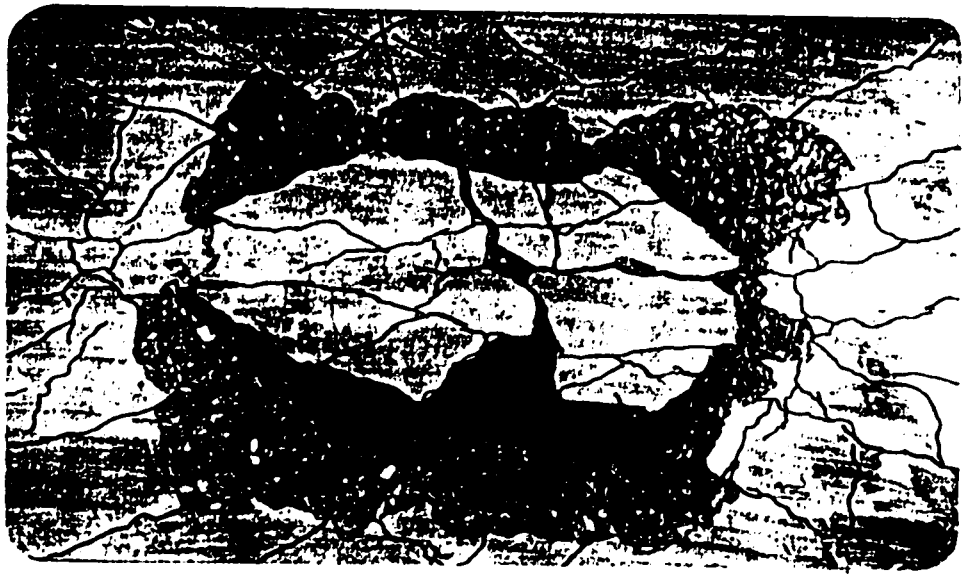

A1/H

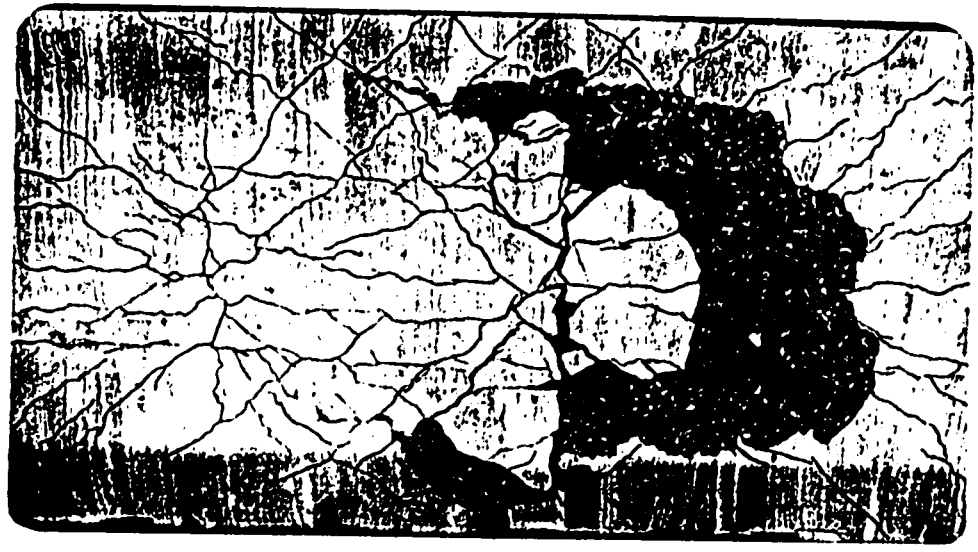

A1/ISO

Plate 3.6: View of Bottom Failure Surfaces of Different A1-Series Panels.

shows the dimensions of failure zone, across the length and width.

3.3 A2-SERIES TEST RESULTS

These panels were tested to examine the reduction in punching capacity of the panels in the presence of a flaw. The test data for this series essentially consisted of recording the failure load and observe closely the mode of failure for each panel. Table 3.5 shows the values of failure loads for all A2-series panels. The core compressive strength of cores taken from the panels are also shown in Table 3.5.

All panels failed in punching except for panel A2C/P of Group 1. This panel was of plain concrete i.e., no reinforcement was used. Plate 3.7 shows the flexure mode failure of A2C/P panel. The punching capacity of panel A2C/S, cast without any conical insert would give the base value for the possible reduction in the punching capacity, if any, of the panels with different conical inserts.

The panels of Group 2 to 4 had different type of conical inserts whose details are given in Table 2.2. The comparison of failure loads of Group 2 panels cast with same insert depth but with different inclinations of inserts would indicate the critical crack geometry for the punching capacity of the panel. The comparison of the failure loads of Group 2 and Group 3 panels will indicate the influence of initial crack depth on punching capacity and further comparison with Group 4 panels will indicate the influence of the perimeter of

Table 3.5: Test Results of A2-Series Panels.

PANEL		AVERAGE CORE STRENGTH OF PANEL (MPa)	EXPERIMENTAL FAILURE LOAD (kN)
GROUP NO.	DESIGNATION		
1	A2C/P	25.2	30.0
	A2C/S	25.5	123.0
2	A2/20	27.4	71.0
	A2/30	30.6	74.0
	A2/45	32.8	106.0
	A2/60	30.6	128.0
	A2/90	27.9	124.0
3	A2/60/H	29.2	65.0
	A2/90/H	28.8	132.0
4	A2C/90/L	25.0	120.0
	A2C/90/H	24.4	50.0

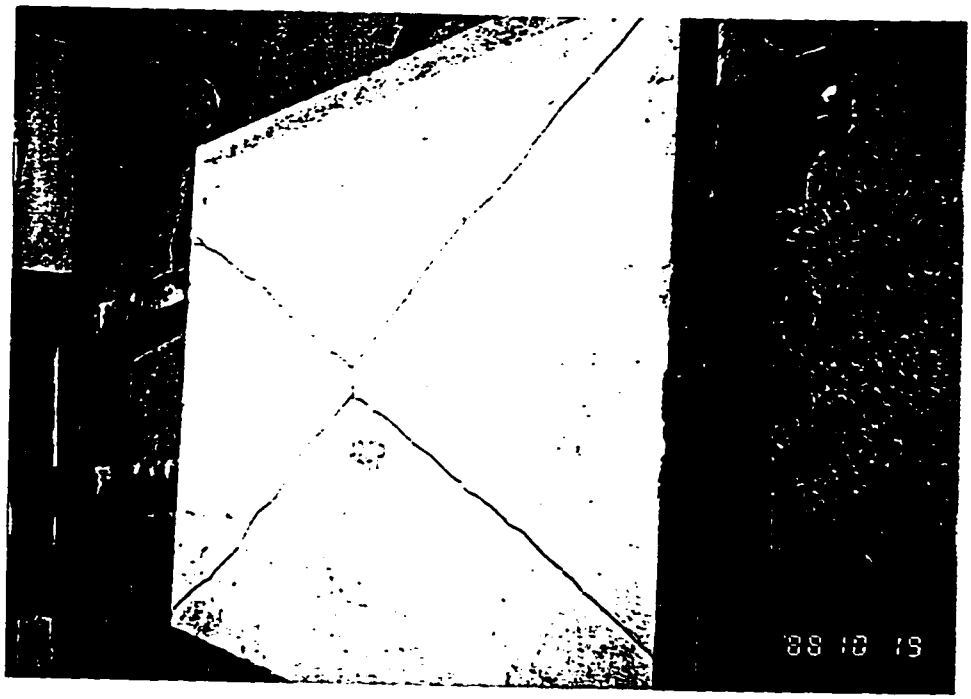

(a) Top Surface

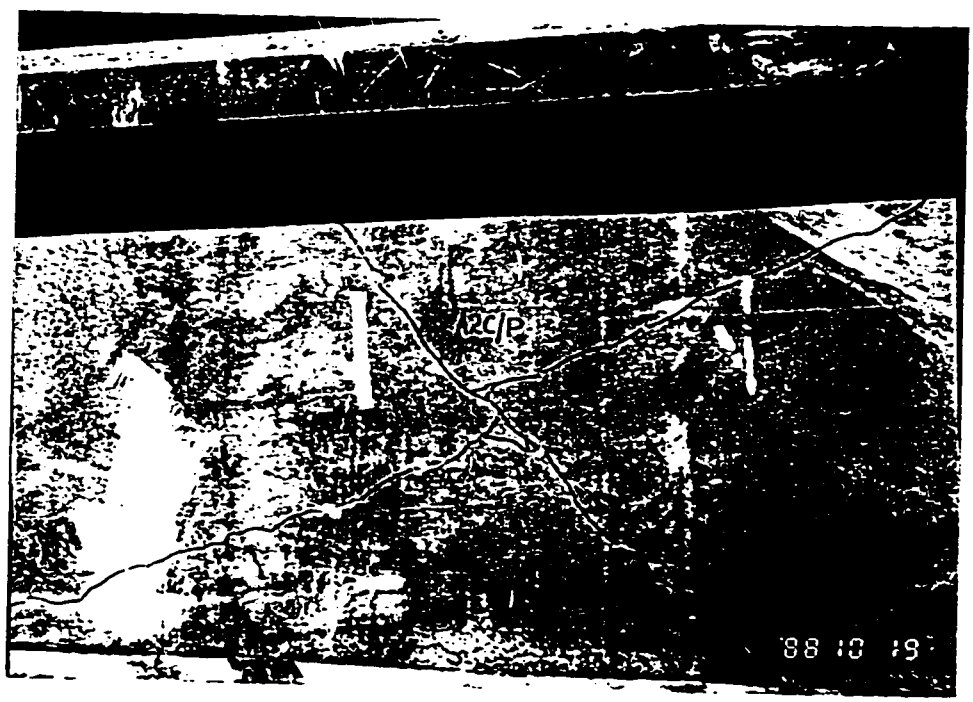

(b) Bottom Surface

Plate 3.7: View of Top and Bottom Failure Surfaces of Panel A2C/P.

the cracked zone on the punching capacity. Plate 3.8 shows a typical top and bottom failure surfaces with the path of failure zone lying within the conical inserts. Plate 3.9 shows the top and bottom failure surfaces, with the path of the failure zone lying well outside the conical insert.

3.4 A3-SERIES TEST RESULTS

In this series there were three different sets of panels with different amounts of main transverse steel and longitudinal steel. The set A3-1 had the highest amount of steel and set A3-3 had the lowest amount of steel. Details of these panels are given in Table 2.3.

Two types of test conducted on these panels are: (i) Static load tests and (ii) Fatigue load tests.

3.4.1 Static Load Tests

3.4.1.1 Deflections

The net slab deflections under the load point were obtained by subtracting the average of the deflection readings at the centre of the two supporting edge beams and the deflection readings of the slab below the load point. The deflections were measured by LVDT and data recorded automatically.

The net slab deflections are plotted against the applied load for panels of different set for same load areas and are shown in Figs. 3.24 to 3.27. This would

(a) Top Surface

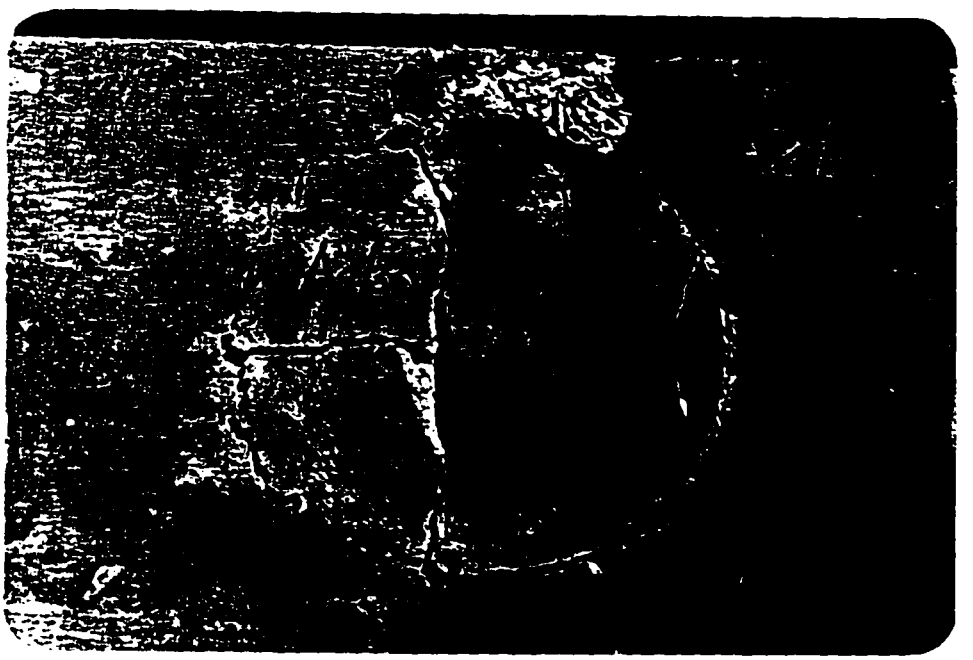

(b) Bottom Surface

Plate 3.8: View of Top and Bottom Failure Surfaces of Panel A2/30.

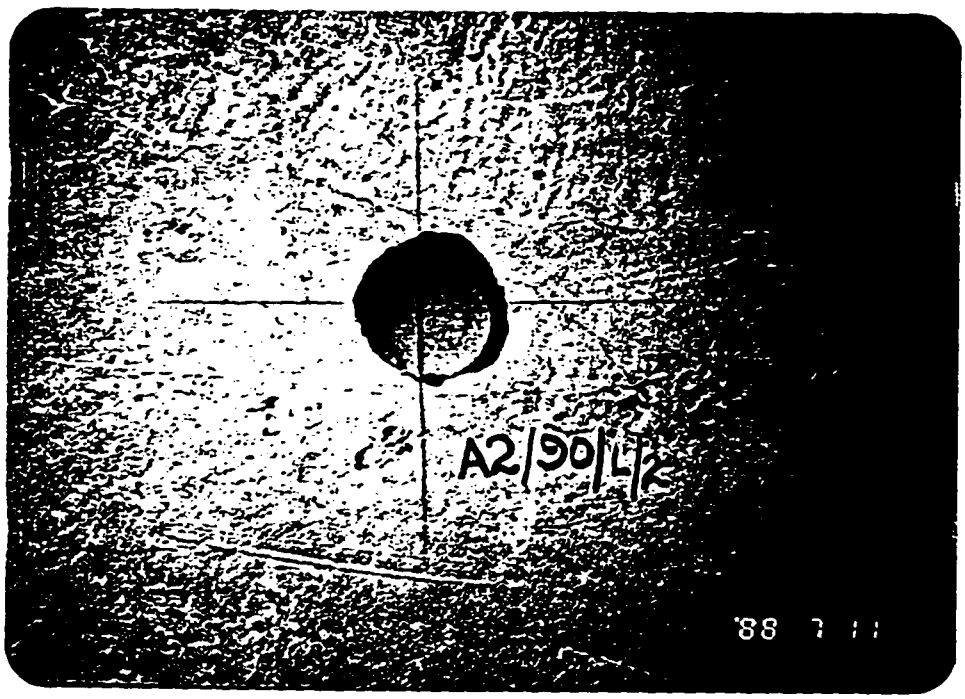

(a) Top Surface

(b) Bottom Surface

Plate 3.9: View of Top and Bottom Failure Surfaces of Panel A2/90.

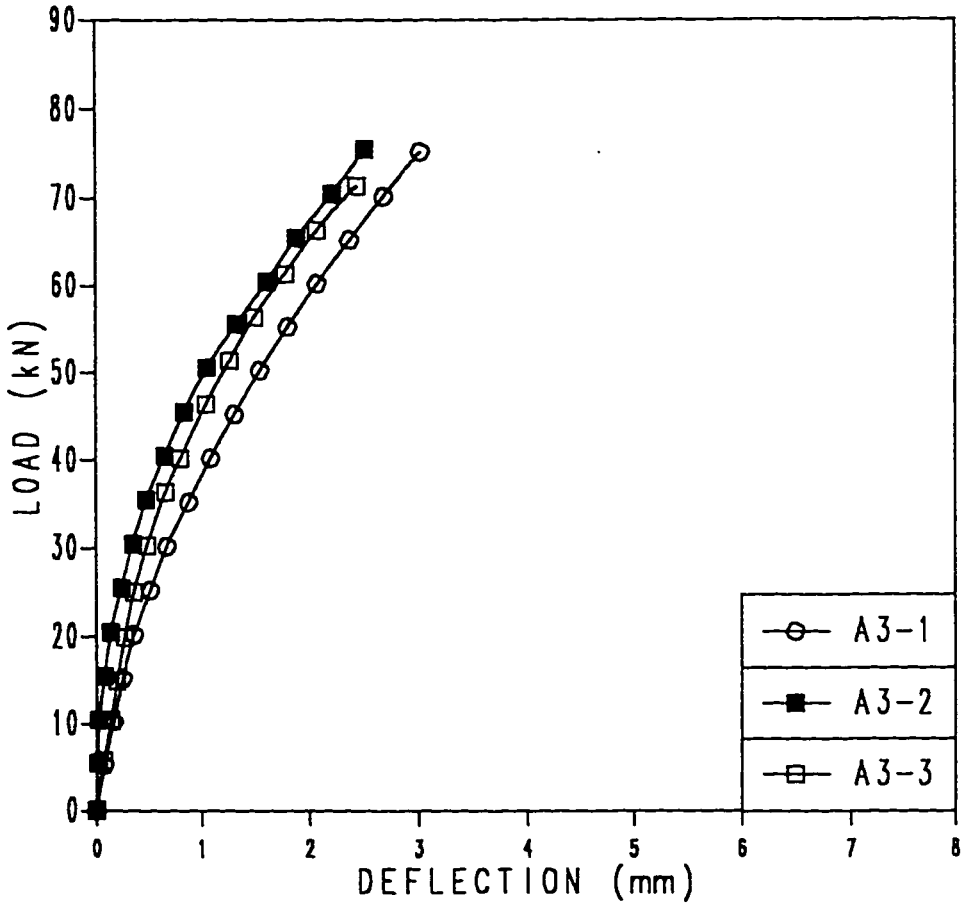

Fig. 3.24: Load-Deflection Response of A3-Series Panels for Load Area of 75 x 150 mm.

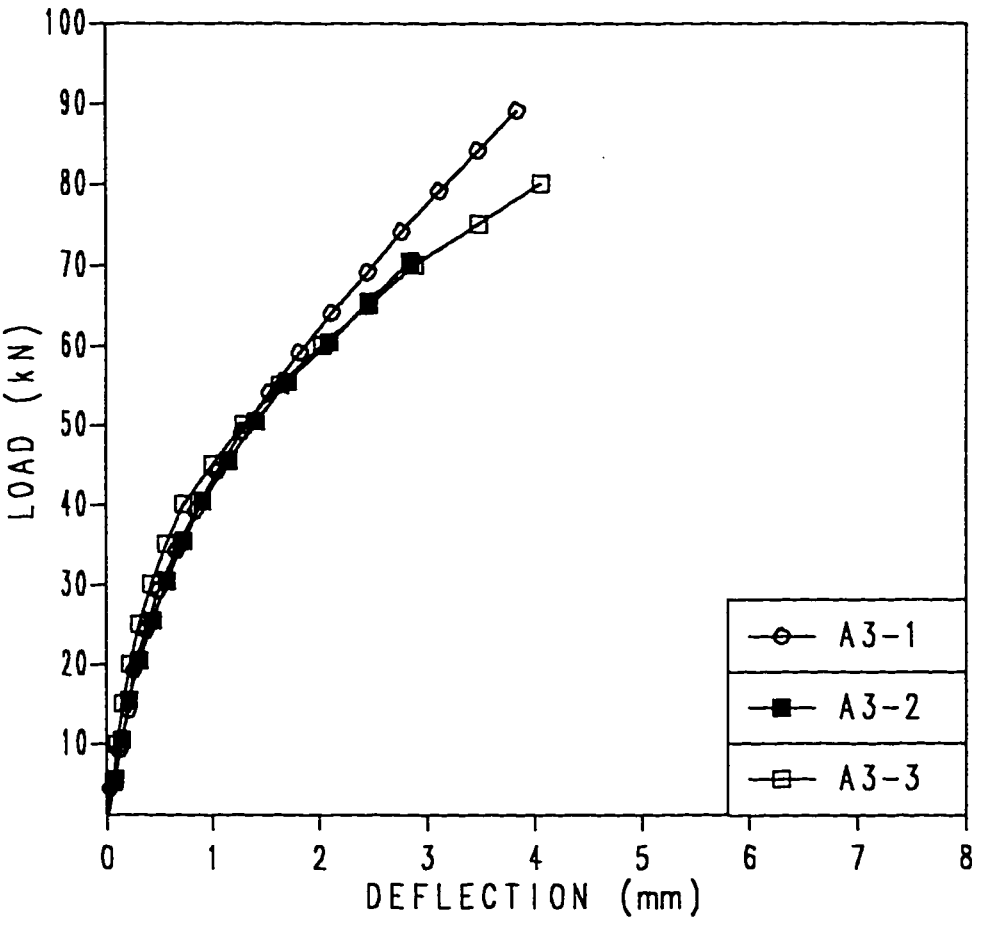

Fig. 3.25: Load-Deflection Response of A3-Series Panels for Load Area of 100 x 200 mm.

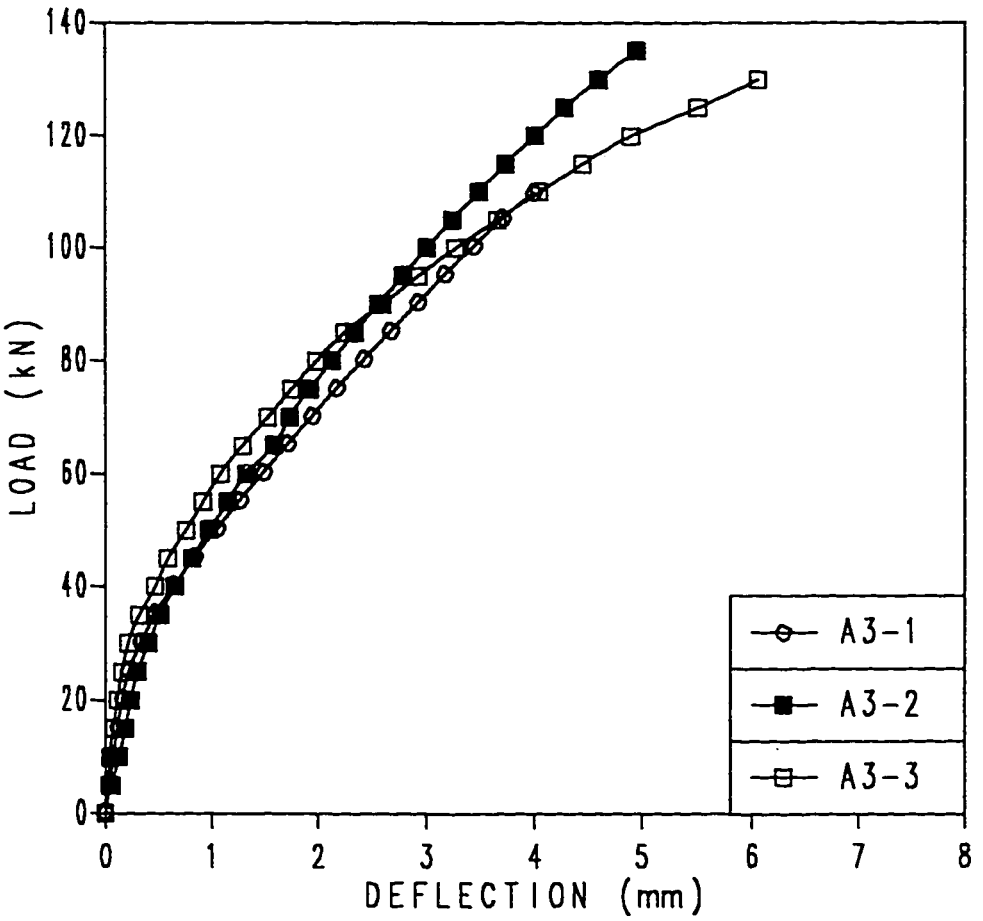

Fig. 3.26: Load-Deflection Response of A3-Series Panels for Load Area of 200 x 400 mm.

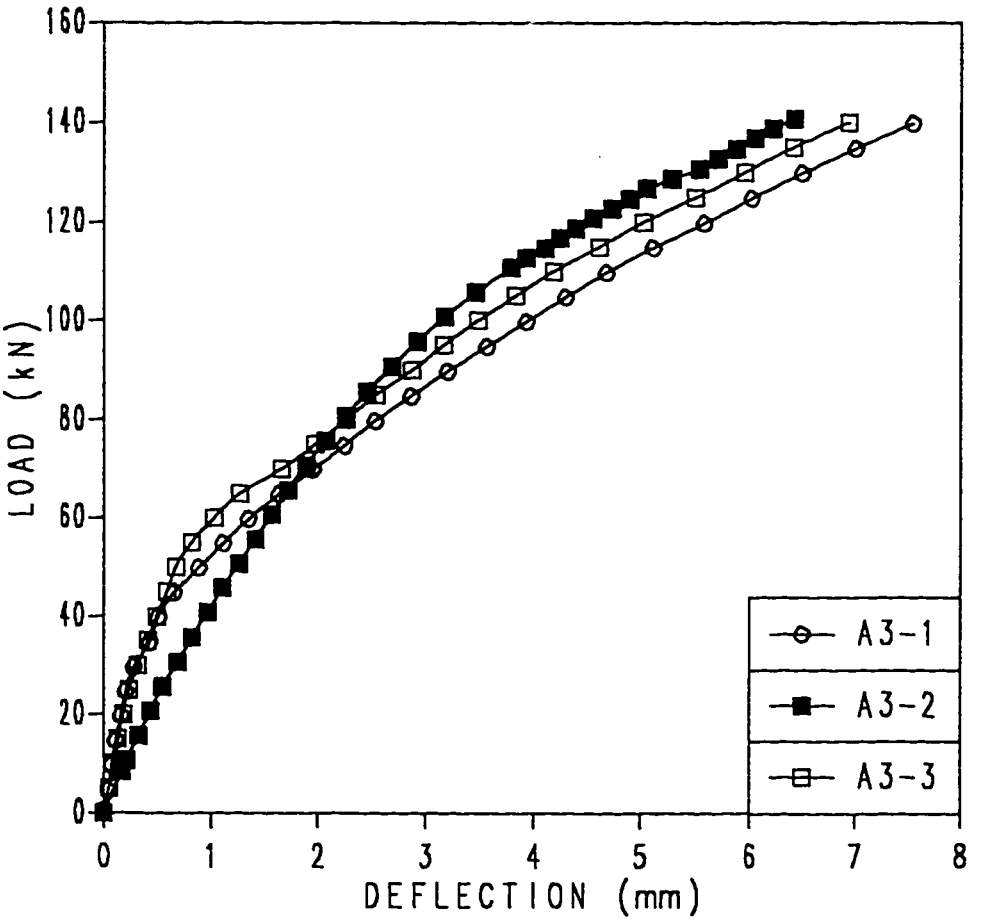

Fig. 3.27: Load-Deflection Response of A3-Series Panels for Load Area of 200 x 500 mm.

indicate the load deflection response for different panel sets and the behavior of the slab for different amounts of steel from ductility point of view. Figs. 3.28 to 3.30 show the load vs deflection plots for different load areas of same panel set. The deflections were not recorded at higher load level because of the risk of damaging the measuring the equipments.

3.4.1.2 Strains

In order to record the level of stress under different load levels, strains were measured from some of the main steel rebars fitted with strain gauges. The location of these steel bars are shown in Fig. 2.6. Figs. 3.31 to 3.35 show the plots of the load vs strain in transverse steel bars of different panels for different load areas. These plots would indicate the cracking load level, the load at which the steel starts yielding for different panels under different load areas. The strains in different bars would indicate the width of slab resisting the load. As mentioned for A1-series panels some of the strain gauges malfunctioned for this series and the values are not shown.

One panel was tested to study the effect of loading on the unloaded span of the panel by testing the span B first, with smaller load area of 75 x 150 mm and strains read from the strain gauges in the span A showed a maximum reading of -115×10^{-6} mm/mm . This would indicate the level of stress on the unloaded span due to the load on the other span of a panel.

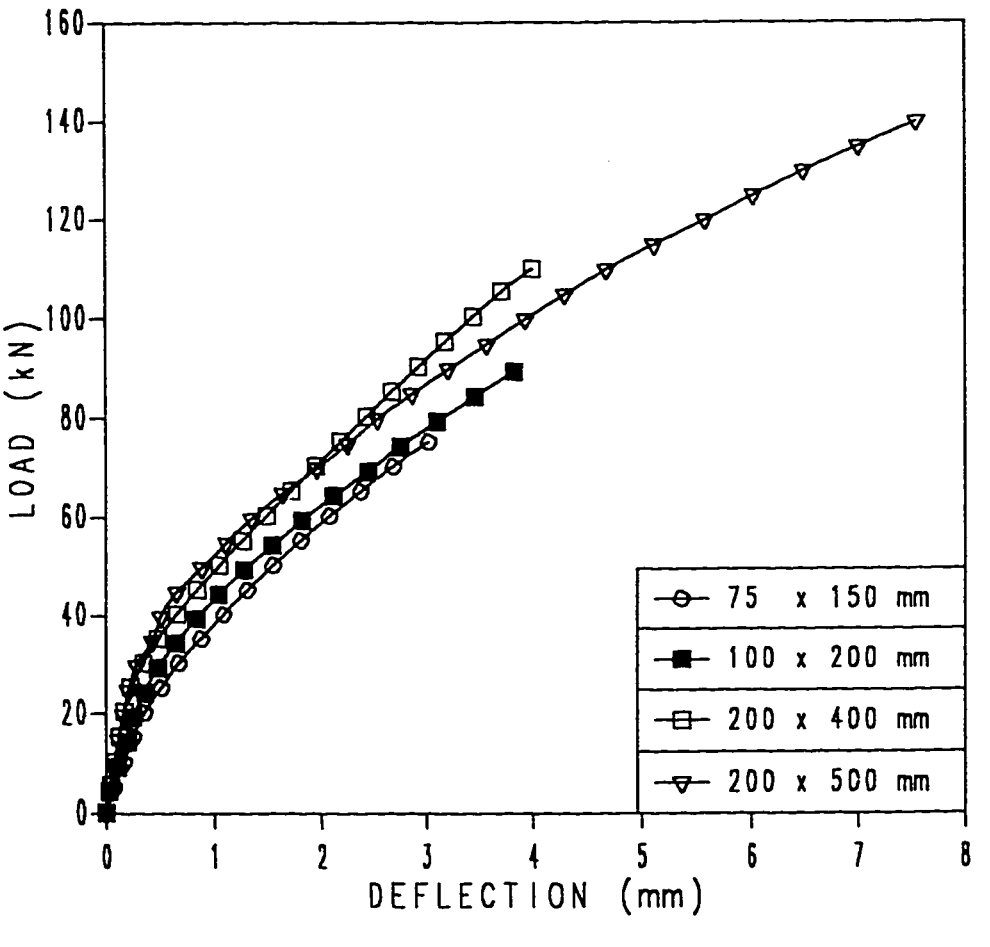

Fig. 3.28: Load-Deflection Response of A3-1 Panels for Different Load Areas.

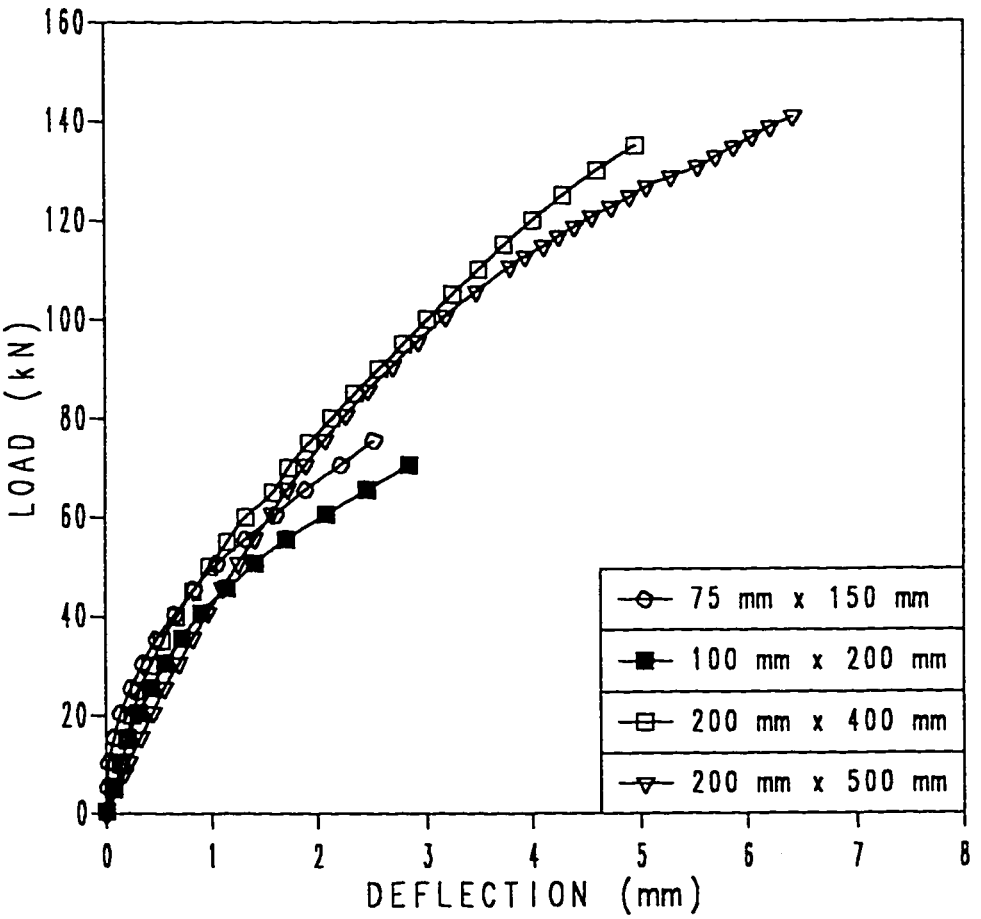

Fig. 3.29: Load-Deflection Response of A3-2 Panels for Different Load Areas.

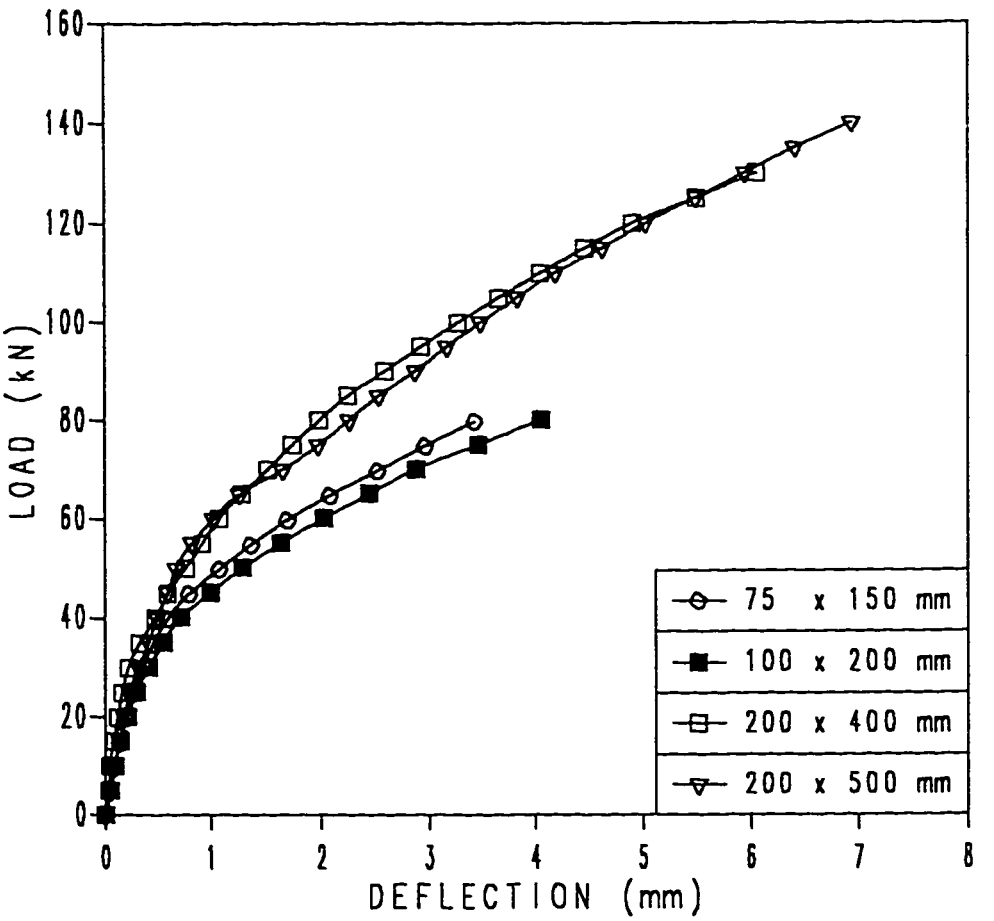

Fig. 3.30: Load-Deflection Response of A3-3 Panels for Different Load Areas.

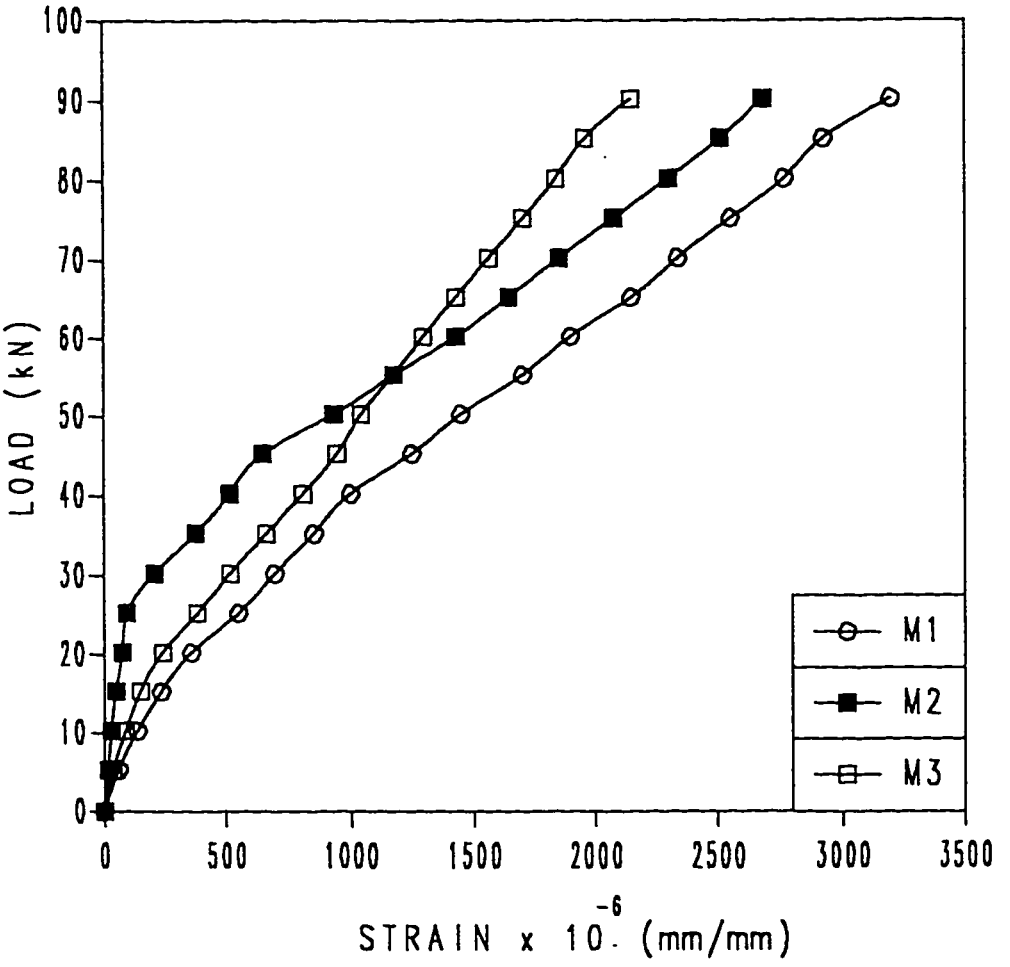

Fig. 3.31: Load-Strain Relationship in Transverse Steel Bars of Panel A3-1 for Load Area of 75 x 150 mm.

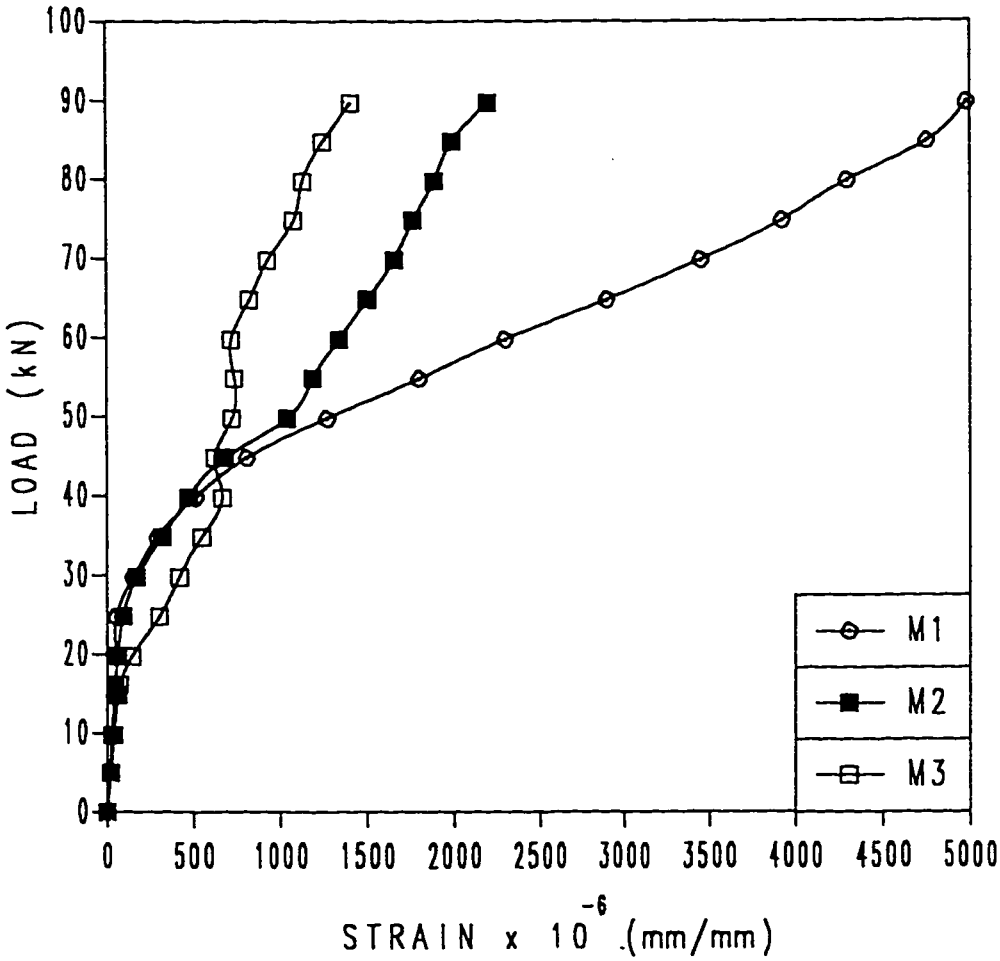

Fig. 3.32: Load-Strain Relationship in Transverse Steel Bars of Panel A3-3 for Load Area of 75 x 150 mm.

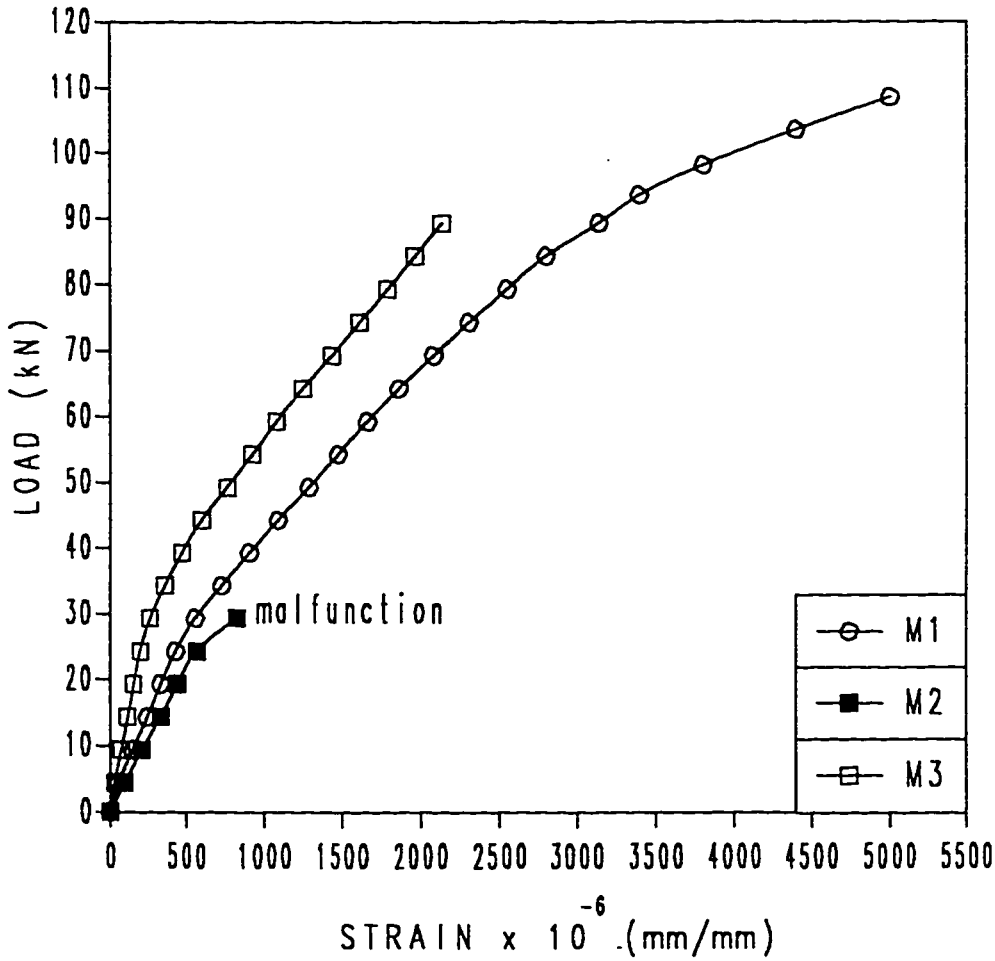

Fig. 3.33: Load-Strain Relationship in Transverse Steel Bars of Panel A3-1 for Load Area of 100 x 200 mm.

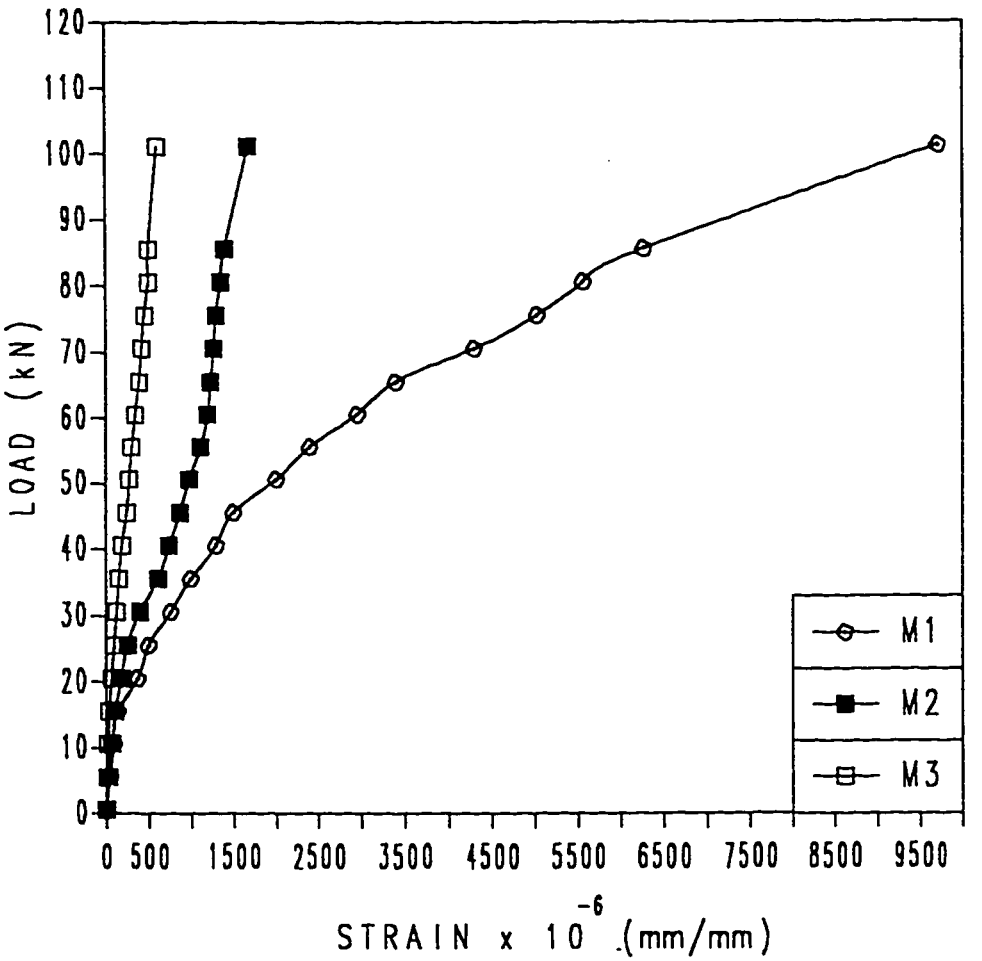

Fig. 3.34: Load-Strain Relationship in Transverse Steel Bars of Panel A3-2 for Load Area of 100 x 200 mm.

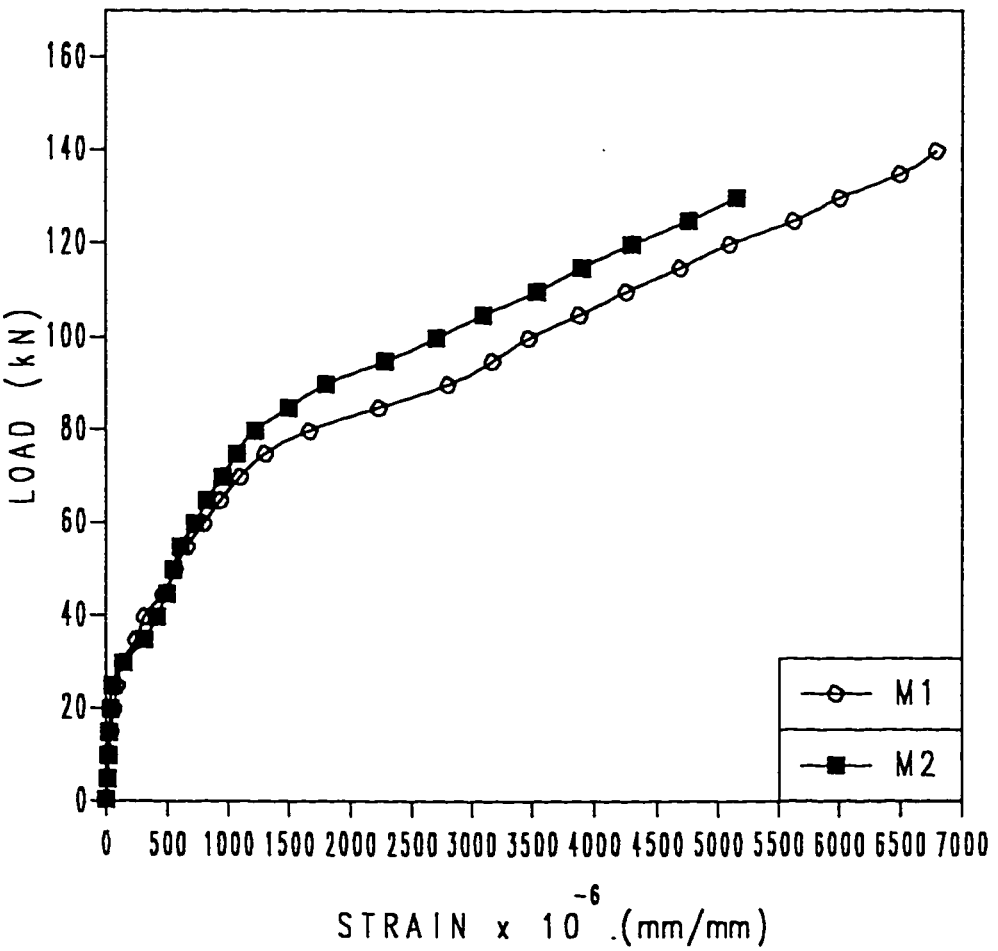

Fig. 3.35: Load-Strain Relationship in Transverse Steel Bars of Panel A3-3 for Load Area of 200 x 500 mm.

3.4.1.3 Failure Loads

In the static tests, the failure loads were recorded and the mode of failure was observed for different load areas. Table 3.6 shows the static test results of each set of panels for different load areas. These values of failure loads shown are average values for each set of panels. Also shown are the values of the concrete core strengths of each set. The comparison of this data would show the influence of different loading areas on the punching capacity for the panels. Table 3.7 shows the failure loads of panels of different sets for each load area. The comparison of the failure loads for panels of different sets (having different amounts of steel) for a particular load area would help in finding the influence of the main transverse steel on the punching capacity of the panels.

Punching shear type failure was noted in all the panels tested under static loading. The top failure surfaces were equal to the load area and a large dislocated area at the bottom. Plates 3.10 and 3.11 show the views of the typical top and bottom failure surfaces, for different load areas.

The approximate size of the bottom area of the fractured concrete was measured and from this the angle of inclination of failed concrete area was found. It varied between 20° to 30°. This value of angle would also help in proposing the critical shear plane path in the test results obtained from A2-series.

Table 3.6: Test Results of A3-Series Panels.

PANEL SET	LOAD AREA (mm x mm)	AVERAGE CORE STRENGTH OF PANEL SET (MPa)	EXPERIMENTAL FAILURE LOAD (kN)
A3-1	75 x 150	25.2	97.0
	100 x 200		113.0
	200 x 400		169.0
	200 x 500		189.0
A3-2	75 x 150	24.1	92.0
	100 x 200		102.0
	200 x 400		163.0
	200 x 500		179.0
A3-3	75 x 150	30.6	98.0
	100 x 200		113.0
	200 x 400		161.0
	200 x 500		168.0

Table 3.7: Test Results of Different A3-Series Panels for Same Load Area.

LOAD AREA (mm x mm)	PANEL SET	EXPERIMENTAL FAILURE LOAD (kN)
75	A3-1	97.0
x	A3-2	92.0
150	A3-3	98.0
100	A3-1	113.0
x	A3-2	102.0
200	A3-3	113.0
200	A3-1	169.0
x	A3-2	163.0
400	A3-3	161.0
200	A3-1	189.0
x	A3-2	179.0
500	A3-3	168.0

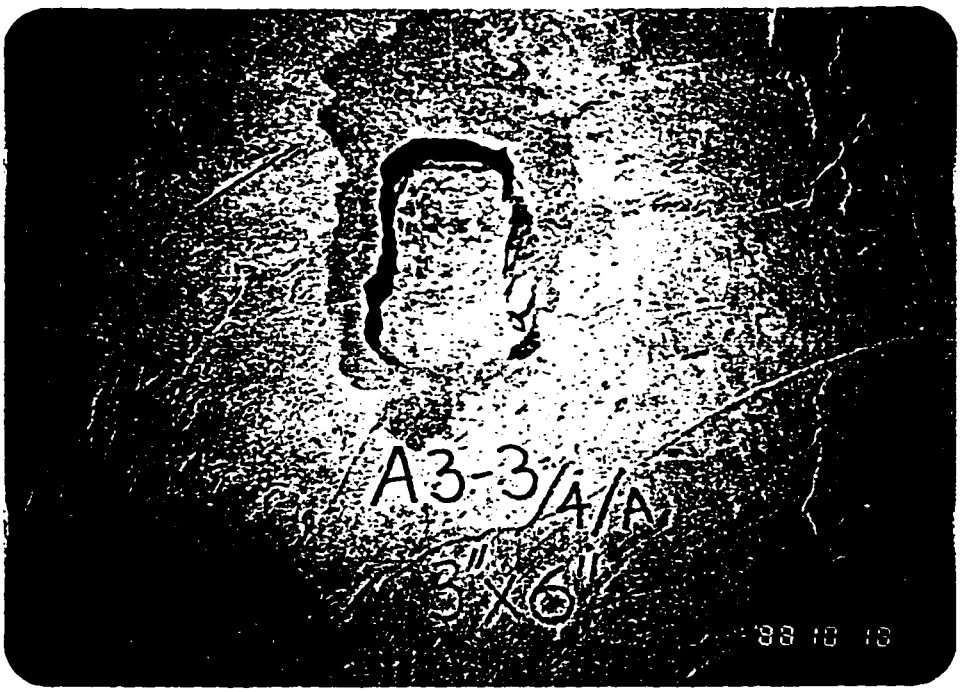

(a) Top Surface

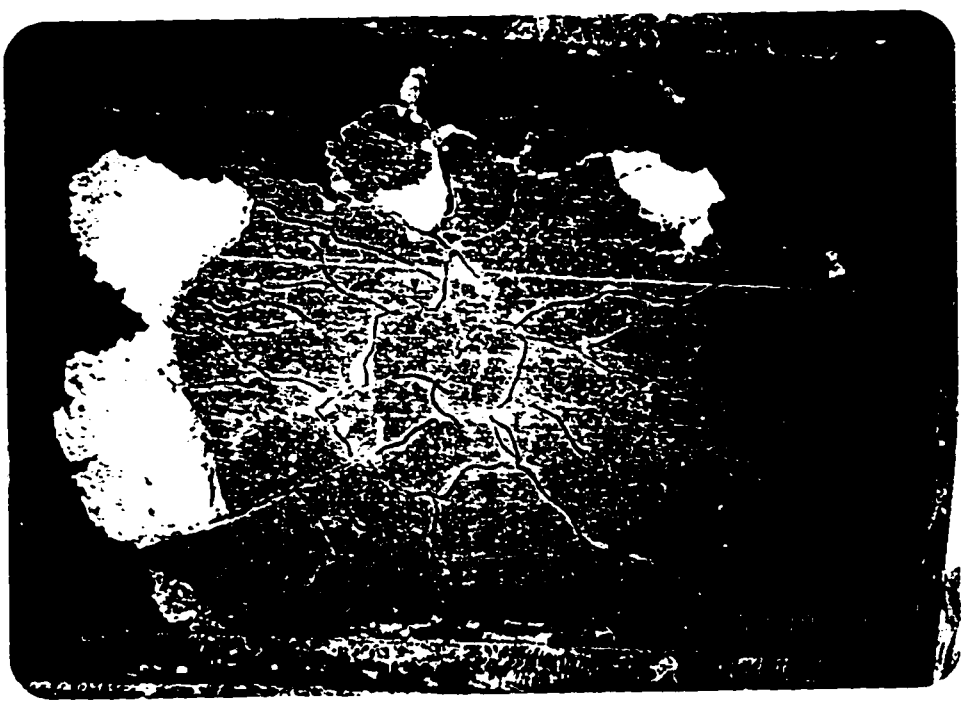

(b) Bottom Surface

Plate 3.10: View of Top and Bottom Failure Surfaces of Typical A3-Series Panel for Load Area of 75 x 150 mm.

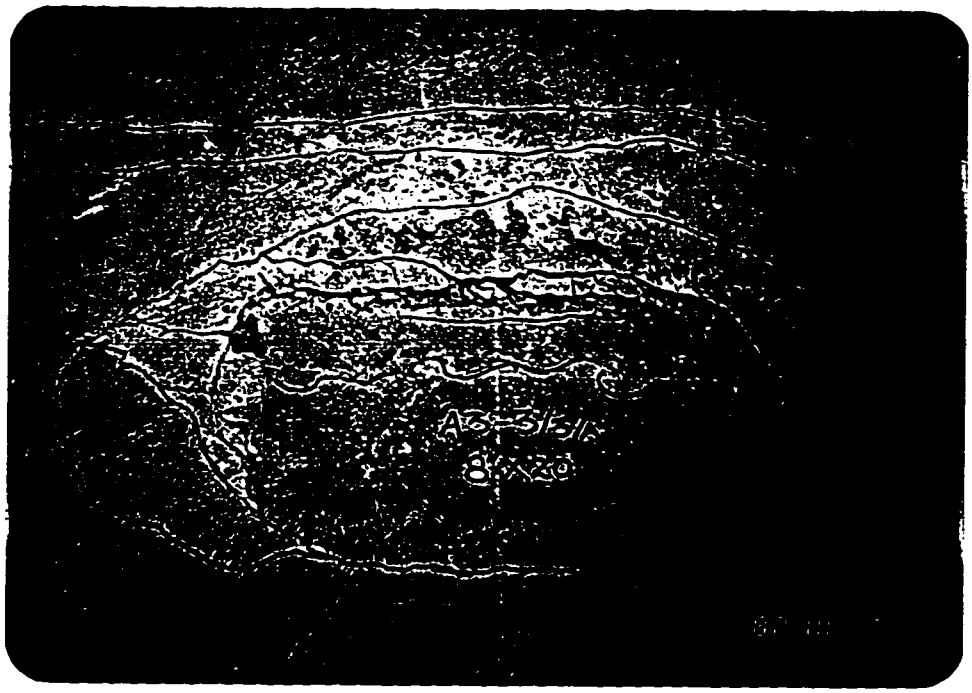

(a) Top Surface

(b) Bottom Surface

Plate 3.11: View of Top and Bottom Failure Surfaces of Typical A3-Series Panel for Load Area of 200 x 500 mm.

3.4.2 FATIGUE TESTS

Only three panels have been tested in fatigue. The panels were tested with a load area of 75 x 150 mm under a maximum load of 60% of the ultimate load capacity of the panel obtained from the static test of the other span of the panel for that area. The ratio R of the minimum stress to the maximum stress was kept equal to 0.1. The number of cycles exceeded one million cycles in these panels and test was aborted. For panel A3-2, the test was extended to more than two million cycles and still the panel did not fail. The results from these test would indicate the maximum load level below which the fatigue failure would be inhibited, under a pulsating load.

Chapter 4

THEORETICAL COMPUTATION OF FAILURE LOADS

In this chapter, an attempt has been made to compute theoretical values of failure loads of A3-series panels, under a single patch load considering both the flexural and the punching type failures. Yield line method was considered to be more appropriate for calculating the flexural capacity of slabs and for the calculation of punching capacity, several methods have been used.

4.1 FLEXURAL CAPACITY

4.1.1 Yield Line Theory

The method for the limit analysis of reinforced concrete slabs known as yield line theory was initiated by Ingerslev [20], expanded and advanced by K. W. Johansen [1]. This is an upper bound approach, in which the strength of slab is assumed to be governed by flexure alone. The ultimate load of a slab is estimated by postulating a collapse mechanism compatible with the boundary conditions. Complete failure theoretically cannot occur until yielding has been occured at several locations so that a condition of unstable equilibrium is formed. The moment at the plastic hinge lines are the ultimate moments of

resistance of the sections and the ultimate load is determined using the principle of virtual work or the equation of equilibrium. This approach gives ultimate load which is correct only when the assumed collapse mechanism corresponds to the correct one, else an overestimated ultimate load would be given.

The fundamental assumptions in the yield line theory are:

1) The collapse mode is a flexural one.

2) The steel has fully yielded along the yield lines at failure.

3) The slab deforms plastically at failure and is separated into segments by the yield lines.

4) The bending and twisting moments are uniformly distributed along the yield line and they are the maximum values provided by the moment strengths in two orthogonal directions.

5) The elastic deformations are negligible compared with the plastic deformations, thus the slab parts rotate as plane segments in the collapse condition.

The collapse mechanism in nearly all common cases are well known and therefore one is not often faced with the uncertainty of whether alternatives exist.

4.1.1.1 Analysis of A3-Series Panels

Virtual work method of yield line theory could be employed to determine the collapse load of A3-series panels by considering them as continuous two way slabs.

A yield line pattern producing a collapse mechanism is assumed. Since the moments and loads are in equilibrium, when the yield line pattern has formed, an infinitesimal increase in load will cause the structure to deflect further. The external work done by the loads to cause a small arbitrary virtual deflection must equal to accommodate this deflection. The slab is therefore given a virtual displacement, and the corresponding rotations at the various yield line can be calculated. By equating internal work and external work, the relation between the ultimate loading in terms of slab dimensions and ultimate resisting moments of slab per unit length is obtained.

The assumed failure mechanism for a typical A3-series panel is shown in Fig. 4.1. This pattern which is considered to be the most appropriate depends on three variables a, b, and c. The lengths of the yield lines a, b, and c must be determined to produce minimum value of ultimate load. The yield line analysis gives the ultimate flexure capacity P_{FLEX} of the slab as given in Equation 3.1 of Ref. 25 which is reproduced below:

$$P_{FLEX} = 2\frac{M_u}{L}\left\{2a + b + \frac{(b-a)(2b-c-a)}{(a-2c+b)}\right\} + \frac{16\,M_t\,L}{(a-2c+b)} \quad \ldots (4.1)$$

in which M_u is the moment capacity per unit length in the direction of u and

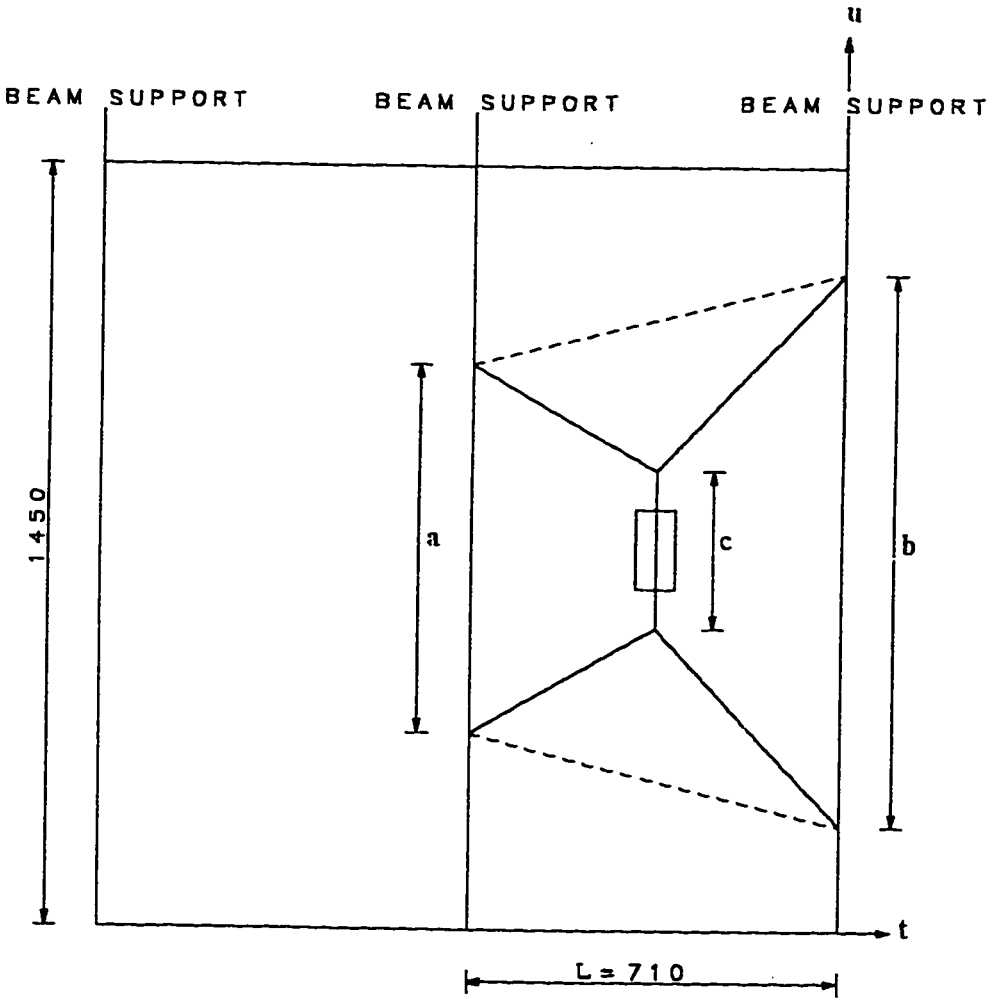

Fig. 4.1: Yield Line Pattern for A3-Series Panels.

M_t is the moment capacity per unit length in the direction of t (Fig. 4.1) and L is equal to 710 mm.

Using a computer program, minimum value of P_{FLEX} was determined by a search procedure in which the three variables a, b, and c were progressively varied, one at a time. It was found that the ultimate capacity of the panels is a linear function of the dimension c, i.e., the smallest capacity corresponds to the minimum value of c. The minimum feasible value that c can take must be the width of the loading plate. Also the minimum value was obtained when a and b were equal.

The values of P_{FLEX} computed are shown in Table 4.1, along with the yield line dimension for various load plates. The values of M_u and M_t are also shown in Table 4.1, which were calculated using the yield stress of steel bars as given in Section 3.1.

4.2 PUNCHING CAPACITY

The following approaches were used to evaluate the punching capacity of A3-series panels:

(1) The Kinnunen and Nylander model

(2) The Plasticity Approach

(3) The Yield Line Analysis of Punching

Table 4.1: Ultimate Flexural Capacity of A3-Series Panels by Yield Line Analysis [1].

PANEL SET	M_u (kN-mm/mm)	M_t (kN-mm/mm)	LOAD AREA (mm x mm)	a,b (mm)	c (mm)	P_{FLEX} (kN)
A3-1	12.8	6.5	75 x 150	737	150	143
			100 x 200	787	200	148
			200 x 400	991	400	168
			200 x 500	1092	500	179
A3-2	7.7	3.3	75 x 150	689	150	76
			100 x 200	737	200	79
			200 x 400	940	400	92
			200 x 500	1041	500	98
A3-3	3.8	3.5	75 x 150	914	150	52
			100 x 200	991	200	53
			200 x 400	1194	400	59
			200 x 500	1295	500	62

(4) The ACI Code Formula

4.2.1 Kinnunen and Nylander Model

This model developed by Kinnunen and Nylander [8] was based on a number of tests on circular slabs with radial and circumferential reinforcement and circular load area. Fig. 4.2 shows the idealized model proposed by Kinnunen and Nylander. The outer portion of the slab which is bounded by the shear crack and radial cracks, is considered loaded through a compressed conical shell that develops from the loaded area to the end of the shear crack. The conical shell is assumed to have shape as shown in Fig. 4.2a and its thickness is assumed to vary in such a way that the compressive stresses at intersection with the loaded area and at the root of shear crack are approximately equal.

The element in Fig. 4.2b is acted upon by the forces: (1) The external load or reaction $P\beta/2\pi$, (2) The oblique compression force in the compressed conical shell $T\beta/2\pi$, (3) The resultant of the tangential forces in the reinforcement at right angles to the radial cracks R_1, (4) The resultant of the radial forces in the reinforcement cutting across the shear crack R_2, and (5) The resultant of the tangential compressive forces in the concrete R_3.

The failure is described as the failure of the conical shell in compression. This takes place when the tangential strain at the top surface slab, taken as a measure of supporting strength of the conical shell reaches the characteristic

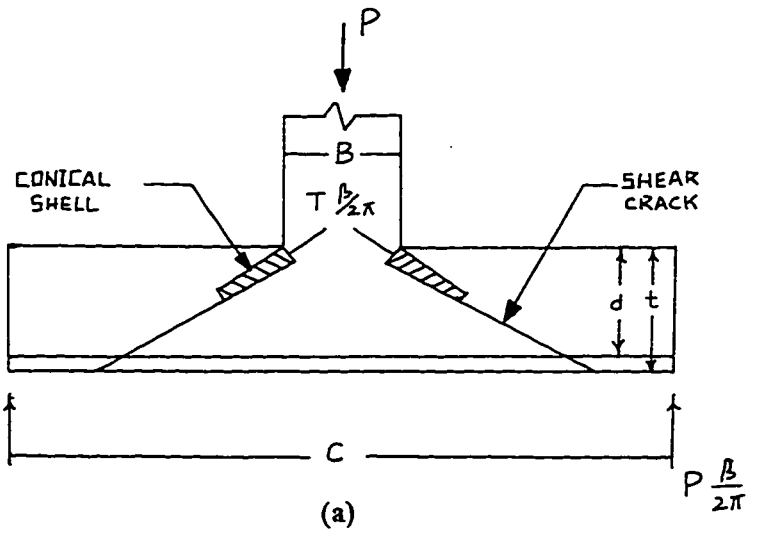

Fig. 4.2: Kinnunen and Nylander Model.

value. Kinnunen and Nylander established relationships between the characteristic tangential strain and load area dimension and between the tangential stress and the stress in the conical shell, which yielded agreement between test and theoretical results. An increase of 15% to 20% in the values given by this model, for the dowel action has been suggested.

The calculation of punching load involves iterative process. With the help of a small computer program, using the equations given in Ref. 8 the values of the punching capacity by this model ($P_{K\text{-}N}$) were calculated. The strength of concrete used was the average core strength for the A3-series (Table 3.3) increased by 10% to represent the actual concrete strengths f'_c which is about 29.3 MPa and the strength of steel as given in Section 3.1. The equivalent diameter of the noncircular slab of A3-series panels was taken as the diameter of the largest circle that could be inscribed within the area of slab (dia. = 710 mm). The values of $P_{K\text{-}N}$ calculated for A3-series panels are shown in Table 4.2.

4.2.2 Plasticity Approach

To evaluate the punching capacity of A3-series panels by plasticity approach, the theoretical solution proposed by Da-Hua Jiang and Jing-Hua Shen [27] was used. This is a modified solution similar to Braestrap-Nielson solution [26], to solve the punching shear strength of plain concrete slab using plasticity approach. A parabolic Coulomb-Mohr intrinsic equation was chosen for the failure criterion of concrete in this approach.

Table 4.2: Punching Capacity of A3-Series Panels by Kinnunen and Nylander Model [8].

PANEL SET	LOAD AREA (mm x mm)	EQUIVALENT CIRC. DIA. OF LOAD (mm)	$P_{K\text{-}N}$ (kN)
A3-1	75 x 150	122	55
	100 x 200	162	71
	200 x 400	324	144
	200 x 500	363	163
A3-2	75 x 150	122	44
	100 x 200	162	57
	200 x 400	324	87
	200 x 500	363	95
A3-3	75 x 150	122	27
	100 x 200	162	31
	200 x 400	324	42
	200 x 500	363	46

The collapse mechanism assumed is shown in Fig. 4.3a, in which, a solid of revolution I is punched out of the remaining part II of the slab. The upper bound ultimate punching load is found by equating the work done by the external load to the internal energy dissipated in the failure surface III. The lowest upper bound is determined by calculus of variation. The main weakness of this model lies in the fact that its application is confined to the axisymmetric case and that it does not take into account the effect of steel reinforcement.

The punching load by this approach (P_{PLAS}) was calculated using the equations given in Ref. 27 which are reproduced below

$$P_{PLAS} = \pi f_t \left(\frac{d_1^2}{4} - \frac{d^2}{4} + \frac{2Kh^2}{\ln d_1 - \ln d}\right) \quad . \ . \ . \quad (4.2)$$

The value of P_{PLAS} depends among others on the value of K given by

$$K = \frac{1}{4}\{m + 2(1 - \sqrt{m+1})\} \quad . \ . \ . \quad (4.2a)$$

where

$$m = \frac{f_c}{f_t} = \frac{\nu_c f_c}{\nu_t f_t} \quad . \ . \ . \quad (4.2b)$$

ν_c, ν_t are effectiveness factors which must be determined from the tests or must be known to apply this method. A value of m = 11 was assumed for this concrete which gave K = 1.52, f_c is compressive strength of concrete which was taken same as used for the Kinnunen and Nylander model equal to 29.3 MPa.

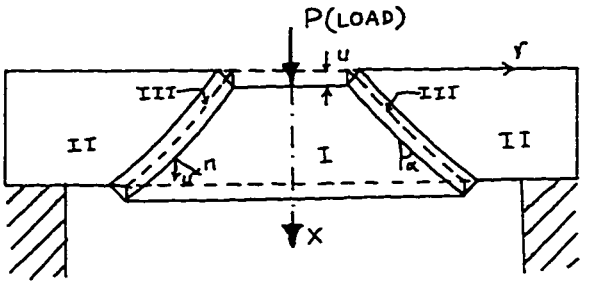

(a) Collapse Mechanism

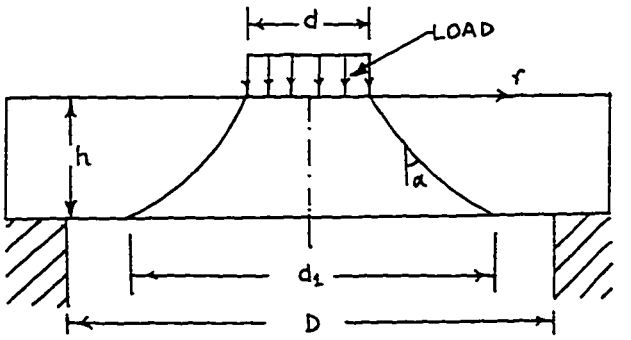

(b)

Fig. 4.3: Failure Mode in Plasticity Approach.

f_t is the tensile strength of concrete taken as 7 $\sqrt{f'_c}$ equal to 3.1 MPa.

Table 4.3 shows the values of P_{PLAS} in terms of v_t. In Ref. 27, authors suggested a value of v_c = 0.35. Based on this and m = 11, the value of v_t=0.3 calculated from Eq. 4.2b was taken for the calculation of P_{PLAS} and are also shown in Table 4.3.

4.2.3 Yield Line Analysis of Punching

By the analysis of the experimental data available in the literature, Gesund and Dikshit [32] showed that in many cases, the bending rather than shear strength of the slab governs its punching capacity. A semi-empirical parameter Q was developed in Ref. 39 given as Eq. 1 in Ref. 32, to separate shear and bending failures.

$$Q = \frac{p^2 f_y d^2}{\sqrt{f'_c}\, b\, B} \qquad . \; . \; . \qquad (4.3)$$

where p is the reinforcement ratio for the negative moment reinforcement alone when the positive moment reinforcement extends into the column. Otherwise it is to be taken as the sum of the positive and the negative reinforcement ratios. B is the perimeter of the slab supported by the column (load area), b is the perimeter of the load and d is the effective depth of the slab. f_y is the steel yield stress and f'_c is the cylinder compression strength of concrete. When $Q < 2$ the failure is by bending-punching and when $Q > 4$ the

Table 4.3: Punching Capacity of A3-Series Panels by Jiang-Shen Plasticity Model [27].

PANEL SET	LOAD AREA (mm x mm)	$v_t P_{PLAS}$	P^*_{PLAS} (kN)
A3-1 & A3-2 & A3-3	75 x 150	309	93
	100 x 200	381	114
	200 x 400	658	197
	200 x 500	723	217

*v_t = 0.3 has been assumed

shear failure is predominant. Generally for all practical reinforced concrete slab design, Q will be less than 2 and hence a real possibility of bending punching failures at most slab-column intersections. In view of the foregoing, expressions were derived in Ref. 32 for the bending-punching strength of uniformly loaded flat slabs supported on column using yield line theory.

The negative slab reinforcement was assumed to provide a yield moment m per unit length of slab in two mutually perpendicular directions, while the positive slab reinforcement was assumed to provide a yield moment ($m \times k_m$) in all directions for simplicity. k_m is the ratio of the top and bottom reinforcements. They assumed that shear stresses do not affect the yield line theory solutions, and that the punching failure of slabs at the loaded area will be the first failure to occur in the structure.

The appropriate failure mechanism is as shown in Fig. 4.4a. Assuming the average shear per unit length on the perimeter of the yield fan be q, writing virtual work equations and summing up the virtual energy inputs and outputs of the individual segments shown in Fig. 4.4b, the punching capacity equation derived in Ref. 32 is reproduced here as shown below.

$$P_{YLP} = m(1+k_m)\frac{6\pi\rho\frac{A_{slab}}{A_{load}}}{3(\rho-1)\frac{A_{slab}}{A_{load}}-(\rho^3-1)} \qquad . \; . \; . \quad (4.4)$$

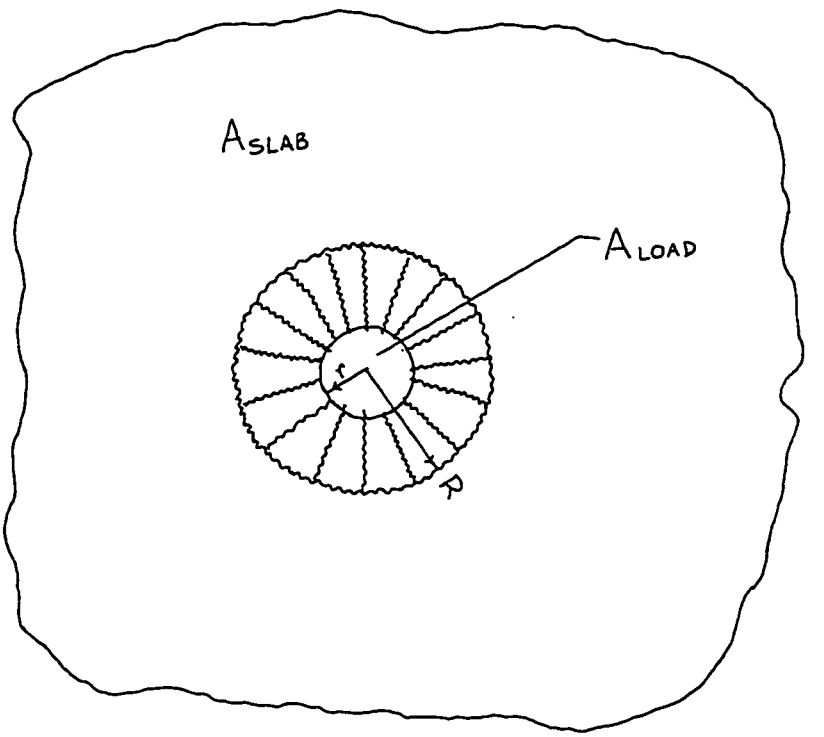

(a)

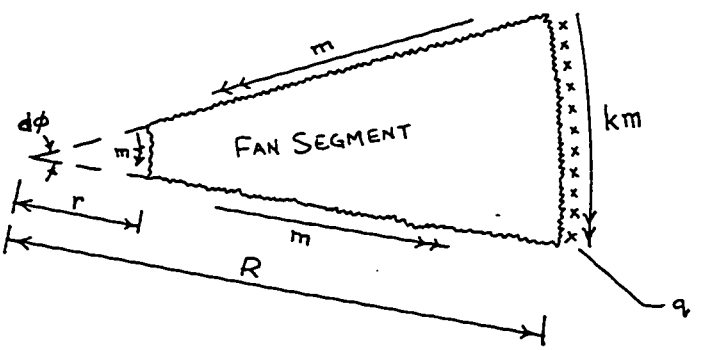

(b)

Fig. 4.4: Yield Line Pattern for Punching Failure.

where

$$\rho = \sqrt[3]{\left(\frac{3}{2}\frac{A_{slab}}{A_{load}} - \frac{1}{2}\right)} \qquad . \; . \; . \quad (4.4a)$$

and A_{slab} is slab area and A_{load} is load area.

Similar equation was also given for square loaded area, but were found to give a considerably higher punching load than that given for circular area. Thus in the above equation, to calculate punching capacity (P_{YLP}) inscribed circular area in a square of area equal to the area of rectangular plate was used.

The value of Q is less than 2 for this study and the value of k_m was equal to one for all the three sets of the A3-series panels, since the top and bottom reinforcements were equal. The value of m was equal to the value M_u used for flexural yield line analysis in Section 4.1.1, for each panel set. The area of slab was equal to 710 x 1450 mm . The values calculated by the above method are shown in Table 4.4.

4.2.4 ACI Code Formula

The ACI formula given by Eq. 11.36 in Ref. 38 and reproduced below was used for calculating the punching capacity of A3-series panels.

$$P_{ACI} = (2 + \frac{4}{\beta_c})\sqrt{f'_c}\, b_0\, d \qquad . \; . \; . \quad (4.5)$$

Table 4.4: Punching Capacity of A3-Series Panels by Yield Line Analysis of Punching [32].

PANEL SET	LOAD AREA (mm x mm)	EQUIVALENT CIRC. DIA. OF LOAD (mm)	P_{YLP} (kN)
A3-1	75 x 150	108	221
	100 x 200	144	239
	200 x 400	287	331
	200 x 500	321	359
A3-2	75 x 150	108	133
	100 x 200	144	144
	200 x 400	287	200
	200 x 500	321	216
A3-3	75 x 150	108	65
	100 x 200	144	71
	200 x 400	287	98
	200 x 500	321	107

β_c is the ratio of the long side to the short side of the concentrated load or reaction area and b_0 is the perimeter of the critical section. For rectangular area this critical section was defined by straight lines drawn parallel to and at a distance d/2 from the edges of the loaded area.

For the evaluation of punching capacity of A3-series panels, β_c was taken equal to the ratio of the long side to the short side of the load. The value of the f'_c is the same as used earlier for calculations of punching capacity by other models. The values of punching capacities calculated from Equation 4.5 are given in Table 4.5. The little difference in the values of P_{ACI} for panels of each set for identical load area is due to small change in the effective depth arising from different bar diameters of the tensile steel.

Table 4.5: Punching Capacity of A3-Series Panels by ACI Code Formula [38].

PANEL SET	LOAD AREA (mm x mm)	P_{ACI} (kN)
A3-1	75 x 150	60
	100 x 200	74
	200 x 400	130
	200 x 500	148
A3-2	75 x 150	62
	100 x 200	76
	200 x 400	133
	200 x 500	152
A3-3	75 x 150	64
	100 x 200	78
	200 x 400	136
	200 x 500	155

Chapter 5

DISCUSSION OF TEST RESULTS

In this Chapter, a detailed discussion of test data presented in Chapter 3, its comparison with some theoretical values wherever computed are provided. Discussion is provided separately for each test series.

5.1 A1-SERIES

In this series four types of panels A1/ISO, A1/H, A1/M and A1/S were cast with the same amount of main transverse steel but with decreasing amounts of the distribution steel. These panels were tested under a simulated moving load to study the effect of distribution steel on the amount and the pattern of cracking.

5.1.1 Cracking and Strains

The first crack appeared around load level of 25 kN to 30 kN as noted from the visual observations. This observation could also be confirmed from the plots of the load vs strain in steel (Figs. 3.1 and 3.5), which showed a change in the slope at about this load level. Prior to the cracking, the load vs strain plot was essentially linear, since upto this load level the tension was taken by

concrete, with slab behaving essentially as plain concrete. After cracking, the behavior of the slab transforms to that of reinforced concrete, with rebars providing most of the tensile strength. The strain in the main steel bar M1 which was immediately below the load point (Fig. 2.2), was around $125x10^{-6}$ mm/mm and the strain in the longitudinal steel bar L1 which was immediately below the load was around $100x10^{-6}$ mm/mm.These strains indicate stress levels of 25 MPa and 20 MPa respectively for the transverse and longitudinal bar.

The photograph of cracks induced by the load of 40 kN, 60 kN, 70 kN, and 80 kN are shown in Plates 3.1 to 3.4 for all the four panels (A1/S, A1/M, A1/H and A1/ISO). Photographs for all four panels are shown side by side collectively to depict the relative density of cracking and the crack orientation.

From Plates 3.1 to 3.4, it is observed that, at lower load level, such as for example at P equal to 40 kN or 60 kN, the panel A1/S shows the minimum amount of the transverse cracking. The amount of transverse cracking increased somewhat with higher amount of distribution (longitudinal) steel, with the panel A1/ISO which has identical transverse and longitudinal steel showing the maximum amount of transverse cracking. The longitudinal cracks caused by the moment in the main transverse steel were more well formed and were relatively wider in the A1/S panel than those in the other panels with higher amount of longitudinal steel. Thus it appears that, with more distribution steel, more finer cracks in the transverse direction are expected to occur. This is due to the fact that, once the slabs crack, the distribution steel tends to distribute the load or

moment on a larger area of slab, effectively bringing in more slab width in the structural action.

This observation is also true by noting the difference in the strains in the transverse bars at identical load level for all the panels. As seen from the plots in Figs. 3.1 to 3.12, the strains in the main transverse steel bars are slightly lower for the panels with higher amount of distribution steel at identical load levels. More amount of distribution steel makes the slab more stiffer in that direction and hence more moment is taken up in that direction. This would result in reduced stress level in the transverse bars for panels with higher amount of distribution steel.

Strains plot for longitudinal steel in Figs. 3.13 to 3.23 indicate that the strains in the longitudinal steel are lower for panels with higher distribution steel even though the longitudinal moment is expected to be higher with increased amount of distribution steel. This could be explained on the basis that the diameter and as well as the spacing of the bars differed and that the bigger diameter bars in the panels with higher distribution steel may show lower strains compared to that of the smaller diameter bars at a particular load level. However, at higher load levels when the cracking at the tension face of the slab is highly pronounced, the strains in the longitudinal bars appear to be higher for panels with higher longitudinal steel (Figs. 3.16 and 3.20). This would indicate that the ratio of transverse to longitudinal moment is not the same for all levels of the load. At subcritical load level, the longitudinal moment increment is higher which has resulted in higher strains in the longitudinal steel.

Also, as seen from the plots in Figs. 3.1 to 3.12, the strain in bar M1, which is immediately below the load are higher compared to that of the strains in bar M2 and M3 which are away from the loaded area (Fig. 2.2). Similar observation could also be seen for longitudinal bars where bar L1 showed higher strains (Figs. 3.13 to 3.23).

As the load increased, more longitudinal and transverse cracks appeared, with most of the earlier developed cracks extending and becoming wider. The transverse cracks appear to diverge from the loaded area, more radial in nature or fan shaped (Plates 3.2 to 3.4). The cracks generally develop in the direction perpendicular to that of the direction of steel. The longitudinal cracks or cracks parallel to the longitudinal steel develop due to the moment resisted by the main transverse steel and that the transverse cracks parallel to the main transverse steel are developed due the tensile stress in the longitudinal bars. However the cracks in the transverse direction are not truely transverse, they are generally inclined, fanning out from the loaded area. The development of this diverging or fan shaped cracks show that the load is taken up by both the transverse and longitudinal steel. The divergent cracks developed with nucleus at loaded points along the length of the panel portray the crack damage inflicted by the subcritical load levels.

At higher load level, the difference between the crack pattern for different panels appear to be lesser than that when compared in the early stage of loading. The cracks widened up and the width of the cracks observed was smaller for panels with higher amounts of distribution steel. At the load level

of 80 kN, some of the well formed longitudinal cracks exceeded 0.3 mm in width.

5.1.2 Failure Loads

After the marking of cracks for load cycle of 80 kN, the panel was loaded to failure by keeping the load in the central location of the panel. All the panels failed in punching shear failure, with top failure surface equal to the area of the loading plate and a much larger dislocated bottom surface area. Table 5.1 has been reproduced from Table 3.4, showing the test data and also the values of failure load adjusted to a common core strength of 27.1 MPa. This small adjustment for a better comparison of test results, was made by multiplying the failure loads by a correction factor. Since the punching capacity is a function of the square root of the concrete strength, the correction factor was taken as the square root of the ratio of the average core strength for the A1-series given in Table 3.1 to the core strength of that particular panel. These values clearly indicate that the punching failure load was highest for the panel A1/ISO which had isotropic steel at the bottom. As the amount of distribution steel was gradually reduced, the failure load showed a progressive decline in value. For panel A1/S which had the smallest amount of distribution steel (18% of the main steel), the value of failure load was 103.0 kN, being about 18% less than that for the panel A1/ISO. Fig. 5.1 shows the punching loads plotted against the amount of distribution steel as percentage of the main steel for different A1-series panels.

Table 5.1: Test Results of A1-Series Panels Adjusted to Average Core Strength of 27.1 MPa.

PANEL	AVERAGE CORE STRENGTH (MPa)	FAILURE LOAD (kN)	ADJUSTED FAILURE LOAD (kN)	DIMENSIONS OF BOTTOM FAILURE SURFACE (mm)	
				WIDTH	LENGTH
A1/ISO	27.9	127.0	125.0	600	800
A1/H	27.8	117.0	115.0	600	700
A1/M	26.5	105.0	106.0	560	600
A1/S	26.2	101.0	103.0	500	550

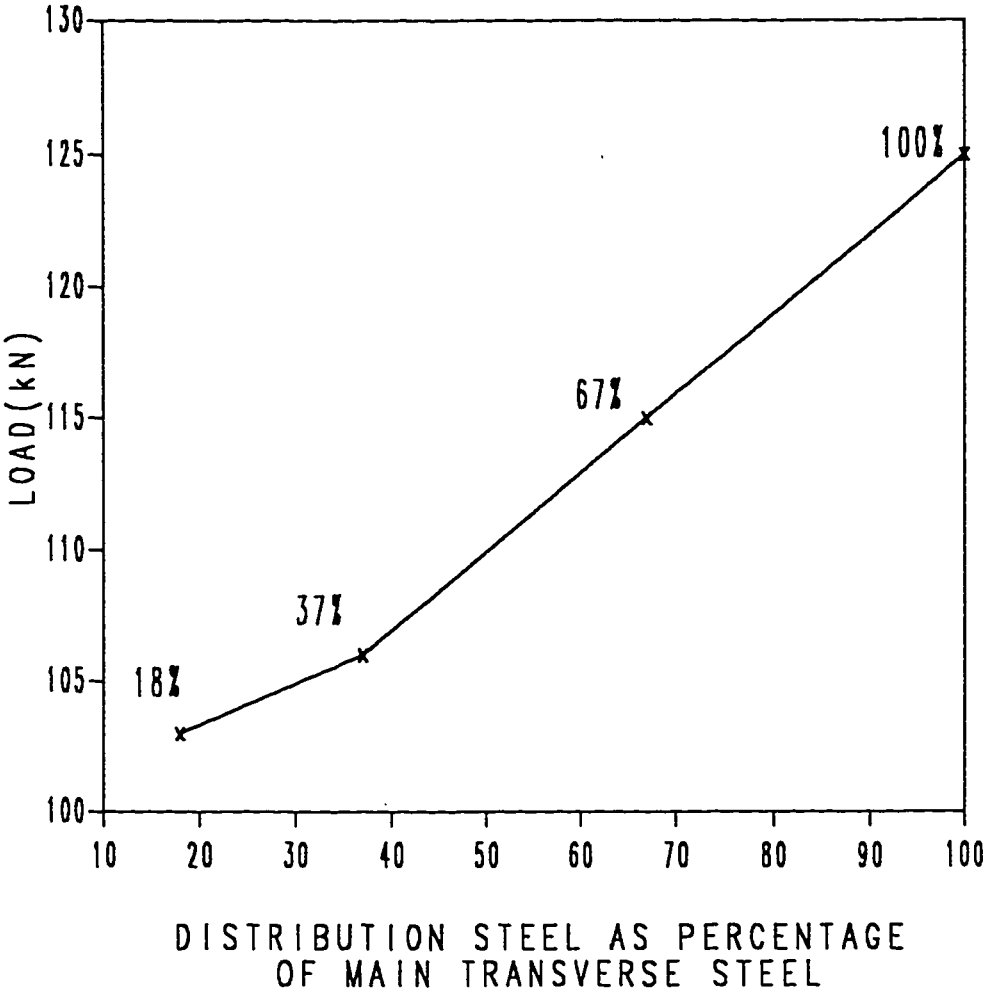

Fig. 5.1: Load Capacity-Distribution Steel Relationship of A1-Series Panels.

The increase in punching load for panels with higher distribution steel can be attributed to the increased dowel action provided by these longitudinal bars, in addition to the contribution made by the main transverse steel bars. The increase in the punching failure load from 103.0 kN for panel A1/S to 125.0 for A1/ISO was attained by an increase in the distribution steel from 18% to 100% of the main transverse tension steel. In view of the test data, one may conclude that an increase in distribution steel would enhance the punching capacity to some extent.

Plate 3.5 shows a typical top failure surface and Plate 3.6 shows the bottom failure surfaces of different panels. An attempt was made to compare approximately the sizes of the bottom failure zones, by taking measurements of the pot hole across its length and width. These measurements are also shown in Table 5.1.

As seen from Plate 3.6 the shape of the bottom failure surface was more circular for the panel A1/S than the others. The bottom surface became more elliptical or oval in shape for panels with increasing amount of distribution steel. For panel A1/ISO, the approximate area was 800 x 600 mm compared to that of 550 x 500 mm for panel A1/S. The relative sizes of the bottom failure surfaces provide further evidence of participation of a larger width of the slab for the panel with higher amount of distribution steel.

Figs. 3.4, 3.8 and 3.12 show that as the load on the panel approaches the failure load, the transverse bars M1 and M2 under the load (Fig. 2.2) approaches yielding, with bar M1 yielding first followed by the bar M2.

5.2 A3-SERIES

5.2.1 Static Load Tests

The A3-series panels which were cast with three different amounts of main transverse steel and longitudinal steel were tested under a single patch load, to study the static load carrying capacity. Four different load areas of 75 x 150 mm, 100 x 200 mm, 200 x 400 mm, and 200 x 500 mm were used to test these panels for the load carrying capacity and also to observe the transition, if any, from punching shear mode of failure to that due to flexure or edge shear failure.

5.2.1.1 Deflections

As seen in Figs. 3.24 to 3.27, the load-deflection relationship for the slabs is essentially linear only upto a load level of about 30 kN, which is approximately the cracking load i.e., the load at which the slab would crack, transforming its behavior to that of a reinforced concrete member.

As the load increases, the deflection progressively becomes non-linear with declining slope, indicating gradual degradation of the slab stiffness. This is due to the fact that as the load increases, new cracks are formed and some of the existing cracks advance deeper into the slab thickness, resulting in progressive increase in the compliance of the slab.

Figs. 3.24 to 3.27, also indicate that generally there is not much difference in the deflections for panels A3-1 to that of A3-3, indicating that the influence

of tension steel on deflection is marginal for restrained panels. All three panels of different amount of main tension steel depicted similar load-deflection behavior.

Figs. 3.28 to 3.30 show that for a particular load level the deflection corresponding to smaller loaded area is slightly greater than the value obtained under a larger load area. As a quantitative representation, a load of 60 kN produced a deflection of 2.1 mm and 1.35 mm deflection under a load area of 75 x 150 mm and 200 x 500 mm area respectively in the panels of set A3-1.

Table 5.2 shows the values of static deflection obtained from finite element analysis using STRUDL package for different load areas along with values obtained from the experiment. As seen from Table 5.2 the values given by STRUDL agrees very well with the experimental values at lower load level. The difference in the values increases as the load increases. This is because the deflection in the STRUDL package is a linear function of applied load and does not take into account the progressive cracking of the slab and the degradation of the slab stiffness with increasing load which results in increase of deflections.

5.2.1.2 Strains

As observed from Figs. 3.31 to 3.35, the strain versus load plots show linearity only upto a load level of about 25 to 30 kN, which is the first cracking load. Immediately after this cracking load, the rebars strains increased at a faster rate, indicating the transformation of the behavior of the slab from plain

Table 5.2: Deflections of A3-Series Panels by STRUDL.

LOAD (kN)	LOAD AREA (mm x mm)	DEFLECTIONS (mm)	
		STRUDL	EXPERIMENTAL
20	100 x 200	0.24	0.25
	200 x 400	0.23	0.20
	200 x 500	0.22	0.20
30	100 x 200	0.37	0.50
	200 x 400	0.35	0.40
	200 x 500	0.33	0.35
40	100 x 200	0.49	0.80
	200 x 400	0.46	0.55
	200 x 500	0.44	0.50
60	100 x 200	0.73	2.10
	200 x 400	0.70	1.40
	200 x 500	0.47	1.20

concrete to that of a cracked reinforced section, in which most of the tensile strength is provided by the steel.

In all panels, the measured strains at the level of first cracking load was around $200x10^{-6}$ mm/mm and the steel stress was 48 MPa. The steel bar which was immediately below the loaded area reached the yield stress first and with the increase of the load yielding spread to the other distant bars, which is evident from the load vs strain plots.

The higher amount of transverse reinforcement present in A3-1 panel set, stiffened the slab in that direction, compared to the that of the panels of the other sets. Thus, as seen from the Figs. 3.31 to 3.35, the steel strain values recorded for the A3-1 set had lower strain values compared to that of the steel strains in other panels at the same load level.

Also the strain values are higher for smaller load areas compared to the strains with larger load area. This is because when the load is spread over a larger area, the intensity of the applied load is lower on the slab.

The yielding of the bar M1, which is immediately below the load (Fig. 2.6) occured at a load level of around 80 kN in the panel A3-1 for the load area of 75 x 150 mm, which is around 83% of the ultimate failure capacity of the panel. For the panel A3-3, the bar M1, yielded around the load level of 65 kN which is about 67% of the ultimate failure capacity of the panel. Also for the load area of 100 x 200 mm the bar M1, yielded around load level of 61% of the ultimate failure capacity of the panel A3-1 and around 82 kN for the panel

A3-2, which is about 73% of the ultimate failure capacity of the panel. As seen from the above values the steel in the panels A3-3 is more efficiently used than the other panels and that the failure was more ductile for A3-3 panels than that of the others.

For larger load area the behavior of the strain plots for bar M1 and bar M2 are similar with very little difference in strain values (Fig. 3.35). This is because the bar M2 under a larger area would be under the load plate as the spacing of the bars was only 100 mm c/c. The bar M1 which was immediately below the load yielded first followed by the bar M2.

5.2.1.3 Failure Loads

Test data in Table 5.3 has been reproduced from Table 3.6 along with adjusted failure load values for the average core strength of the A3-series using the correction factor as mentioned for A1-series. For all load areas used in tests, the mode of failure was punching. Data in Table 5.3 shows that the punching capacity increases as the load area increases in conformity with the expectation. For example when the loaded area was increased from 75 x 150 mm to 200 x 500 mm for A3-1 panel, the increase in the ultimate capacity was about 96%.

Table 5.4 shows the test data of different panel sets for same load areas, which indicate that there is only a small difference in the value of punching capacity P_u for panels with different amount of steel. For an increase of about

Table 5.3: Test Results of A3-Series Panels Adjusted to Average Core Strength of 26.6 MPa.

PANEL SET	LOAD AREA (mm x mm)	AVERAGE CORE STRENGTH OF PANEL SET (MPa)	EXPERIMENTAL FAILURE LOAD (kN)	ADJUSTED FAILURE LOAD (kN)
A3-1	75 x 150	25.2	97.0	99.0
	100 x 200		113.0	116.0
	200 x 400		169.0	174.0
	200 x 500		189.0	192.0
A3-2	75 x 150	24.1	92.0	97.0
	100 x 200		102.0	107.0
	200 x 400		163.0	171.0
	200 x 500		179.0	188.0
A3-3	75 x 150	30.6	98.0	91.0
	100 x 200		113.0	105.0
	200 x 400		161.0	150.0
	200 x 500		168.0	157.0

Table 5.4: Test Results of Different A3-Series Panels for Same Load Area Adjusted to Average Core Strength of 26.6 MPa.

LOAD AREA (mm x mm)	PANEL SET	EXPERIMENTAL FAILURE LOAD (kN)	ADJUSTED FAILURE LOAD (kN)
75	A3-1	97.0	99.0
x	A3-2	92.0	97.0
150	A3-3	98.0	91.0
100	A3-1	113.0	116.0
x	A3-2	102.0	107.0
200	A3-3	113.0	105.0
200	A3-1	169.0	174.0
x	A3-2	163.0	171.0
400	A3-3	161.0	150.0
200	A3-1	189.0	194.0
x	A3-2	179.0	188.0
500	A3-3	168.0	157.0

of 300% of amount of main steel in A3-1 panel the punching capacity is only 9% higher than the punching capacity of A3-3 panel for the load area of 75 x 150 mm and about 23% higher for the load area of 200 x 500 mm. When compared to A3-2 panel, A3-1 panel has about 80% higher amount of steel but the punching capacity is only 3% higher for the load area of 200 x 500 mm. Thus there had been no appreciable gain in the ultimate load capacity by increasing the amount of steel in the panels. The increase in the load capacity of the panels with higer amount of steel was also confirmed by earlier studies [6,10,25]. The relatively larger difference in the load capacities of the panels of A3-1 set to that of A3-3 set could be that apart from the difference in the steel, the ultimate strength of 4 mm bars (Section 3.1) used in A3-3 set is relatively lower than that for bars of 6 mm and 8 mm used in A3-1 and A3-2 panels.

The first crack was observed around load level of 25 kN to 30 kN, which is around the capacity of the concrete in bending. This development of cracks can also be observed from the plots of load vs deflection (Figs. 3.24 to 3.30) and also the plots of load vs the strains (Figs. 3.31 to 3.35) in steel. As the load increased these longitudinal cracks became more predominant with larger widths and lengths and more new cracks developed radiating from the loaded zone. Prior to failure extensive cracking was observed with cracking diverging in all directions from the central loaded region. Plates 3.10 and 3.11 show that the top failure surfaces depict a hole of the size of the load area which is typical of all punching failures. The bottom large dislocated failure area increases with increasing load area.

For smaller loaded area of 75 x 150 mm and 100 x 200 mm, the failure was very much localized with no damage to the other span of the panel. This can also be confirmed from the strain reading taken for the span A when load was applied on span B. At failure load of span B, the maximum strain recorded from the strain gauges in the span A was only -115×10^{-6} mm/mm, which is much lower than the strain at the first cracking load of the panels. This shows that the effect of loading on the other span is very small, thus allowing the usage of the other span of the panel for other static or fatigue tests.

There were a few top cracks observed in the central negative moment region of the panel over the middle supporting I-beam, for larger load areas of 200 x 400 mm and 200 x 500 mm . Usually three cracks ran parallel to the middle I-beam and the number of the cracks increased for the load area of 200 x 500 mm.

Comparison of Failure Loads with Theoretical Flexural Capacity

The values of flexural capacity calculated by yield line analysis and punching capacity calculated by different models are reproduced from Tables 4.1 to 4.5 and summarised in Table 5.5.

As seen from Table 5.5 the values given for the flexural capacity based on yield line theory are lower than the punching failure loads recorded in the tests (except for A3-1 panels). As the flexural capacity of a panel is almost directly proportional to the tension steel, the flexural capacity decreased with decrease

Table 5.5: Flexural and Punching Capacity of A3-Series Panels Using Theoretical Models and Experimental Values.

LOAD AREA (mm x mm)	PANEL SET	P_{FLEX}	P^{*}_{PLAS}	$P_{K\text{-}N}$	P_{YLP}	P_{ACI}	P_{EXP}
75	A3-1	140	93	55	221	60	99
x	A3-2	76	93	44	133	62	97
150	A3-3	52	93	27	65	64	91
100	A3-1	146	114	71	239	74	116
x	A3-2	79	114	55	144	76	107
200	A3-3	53	114	31	71	78	105
200	A3-1	168	197	144	331	130	174
x	A3-2	92	197	87	200	133	171
400	A3-3	59	197	42	98	136	150
200	A3-1	179	217	163	359	148	194
x	A3-2	98	217	95	216	152	188
500	A3-3	62	217	46	107	155	157

P_{FLEX} – *Flexural Capacity*
P_{PLAS} – *Plasticity Approach*
$P_{K\text{-}N}$ – *Kinnunen* and *Nylander*
P_{YLP} – *Yielding Analysis of Punching*
P_{ACI} – *ACI Approach*
P_{EXP} – *Experimental*
* For an assumed $v_t = 0.3$

in the percentage of steel. For load area of 75 x 150 mm, the difference in the flexural capacity of panels of set A3-1 and panels of A3-2 is about 90%. The difference in the percentage of steel in these panels is about 81%. But when compared to the experimental results for panels of these two sets, there was no appreciable gain due to increase in the reinforcement.

By observing that the panels A3-2 and A3-3 had lower amount of tension steel and that their flexure capacities were substantially lower than the failure load, the effect of the favourable influence of the lateral restraints provided by the supports can be noted. The flexural capacity of panel of set A3-2 set for a load area of 75 x 150 mm was computed as 76 kN and the experimental punching load value for this panel was 97 kN. Even though the panel failed in punching the failure load was about 30% higher than the theoretical flexural capacity. This shows that there is a substantial increase in the flexural capacity of the restrained panels due to in-plane compressive membrane force (arch action).

For the panels of A3-1 set which had the highest amount of the tension steel (0.98%), the computed flexural load was higher than the experimental failure load, but the panel failed in punching. The true flexural capacity is expected to be higher than the computed value of 140.0 kN due to the prevailing arch action.

To examine the applicability of the procedure suggested by Tong and Batchelor [6] to estimate the compressive force enhancement in the flexural capacity, Fig. 12-10 from Ref. 6 is used here and shown in Fig. 5.2.

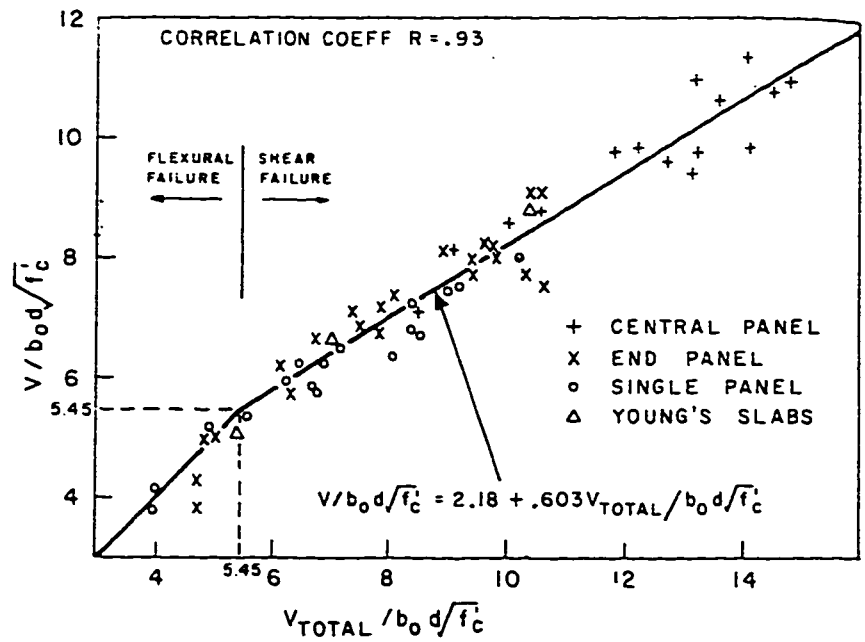

Fig. 5.2: Relationship between $V/b_o d\sqrt{(f'_c)}$ and $V_{TOTAL}/b_o d\sqrt{(f'_c)}$

Using the flexural capacity values P_{FLEX} (V in the Fig. 5.2), the values of V_{TOTAL} was calculated from Fig. 5.2 and are shown in Table 5.6. The variation of ratio V_{TOTAL}/V_{FLEX} (V_{TOTAL}/P_{FLEX}) from 1.00 to 1.35, shows the degree of enhancement in accordance with Ref. 6.

Comparison of Failure Loads with Theoretical Punching Capacity

Kinnunen and Nylander Model: The procedure for computation of punching load in this approach was originally developed from tests on axisymmetric circular panels. Thus the application of this approach to a bridge deck slab may not be accurate due to the geometric differences. However, disregarding this limitation, the method has been used to see the applicability to the bridge deck slabs. Though the Kinnunen and Nylander model is time consuming and complex, the realistic failure mechanism adopted in this approach encourages its adoption. It has been suggested [8] to increase the theoretical values by 15-20% to account for the dowel action of rebars.

As seen from Table 5.5, the values predicted by this model are consistently lower than the experimental values. The value of punching capacity decreases rapidly with decrease in the reinforcement ratio as the method accounts for the amount of tension steel. For small reinforcement ratio, the values predicted are much lower. For smaller load areas of 75 x 150 mm and 100 x 200 mm the values given by this model, even after increasing by 20% to account for dowel action are conservative. This conservativeness increases with decrease in the

Table 5.6: Flexural Capacity Enhancement Due to Support Restraint by Tong and Batchelor Equation [6].

PANEL SET	LOAD AREA (mm x mm)	$V\,(P_{FLEX})$ (kN)	V_{TOTAL} (kN)	$\frac{V_{TOTAL}}{V_{FLEX}}$
A3-1	75 x 150	140	189	1.35
	100 x 200	146	193	1.32
	200 x 400	168	176	1.05
	200 x 500	179	179	1.00
A3-2	75 x 150	76	84	1.10
	100 x 200	79	79	1.00
	200 x 400	92	92	1.00
	200 x 500	98	98	1.00
A3-3	75 x 150	52	52	1.00
	100 x 200	53	53	1.00
	200 x 400	59	59	1.00
	200 x 500	62	62	1.00

reinforcement ratio.

For a load area of 75 x 150 mm the values given by this model for A3-3 panel, which has the lowest amount of steel of 0.24% is about 27 kN. The experimental value for the same panel is about 91 kN, which shows an increase of 230%. Whereas the increase in the experimental values compared to that given by this model is about 80% for the panel of A3-1 set which has the highest amount of steel (0.98%). Table 5.7 gives the ratio of the experimental load values and values calculated by this model ($P_{EXP}/P_{K\text{-}N}$).

As the load area increases the conservativeness of this model decreases for A3-1 panel. For the load area of 200 x 400 mm or 200 x 500 mm, the difference in the value of punching capacity for panel A3-1 given by this model and the experimental values is about 20%, which is about the magnitude suggested for the dowel action. Even for higher load areas, the panels with lesser amount of tension steel (A3-2 and A3-3), the discrepancy between the experimental and the Kinnunen and Nylander model value is large with the latter values being smaller. It appears therefore that, for the Kinnunen and Nylander model to be more reliable, the load diameter should bear a minimum ratio with respect to the slab span and importantly the slab to be reinforced with a certain minimum amount of steel. The applicability of the formula appears to be sound for panels reinforced with steel amounting to about 1%.

Plasticity Approach: The plasticity approach to solve a punching shear failure

Table 5.7: Ratios of Experimental Load Values to Load Values Calculated Using Different Theoretical Models.

LOAD AREA mm x mm	PANEL SET	$\frac{P_{EXP}}{P^{*}_{PLAS}}$	$\frac{P_{EXP}}{P_{K\text{-}N}}$	$\frac{P_{EXP}}{P_{YLP}}$	$\frac{P_{EXP}}{P_{ACI}}$
75	A3-1	1.06	1.80	0.45	1.65
x	A3-2	1.04	2.20	0.73	1.56
150	A3-3	0.98	3.37	1.40	1.42
100	A3-1	1.02	1.63	0.49	1.57
x	A3-2	0.94	1.95	0.74	1.41
200	A3-3	0.92	3.39	1.48	1.35
200	A3-1	0.88	1.21	0.53	1.34
x	A3-2	0.87	1.97	0.86	1.29
400	A3-3	0.76	3.57	1.53	1.10
200	A3-1	0.89	1.19	0.54	1.31
x	A3-2	0.87	1.98	0.87	1.24
500	A3-3	0.72	3.41	1.47	1.01

P_{FLEX} – *Flexural Capacity*
P_{PLAS} – *Plasticity Approach*
$P_{K\text{-}N}$ – *Kinnunen* and *Nylander*
P_{YLP} – *Yielding Analysis of Punching*
P_{ACI} – *ACI Approach*
P_{EXP} – *Experimental*
* For an assumed $\nu_t = 0.3$

encounters difficulty, as the punching failure is essentially a brittle type failure. By introducing effectiveness factors v_t and v_c to the strength values f_t and f_c, plastic flow can be assumed to occur at stress levels of $v_t f_t$ and $v_c f_c$. The severe drawback in this model is the correct estimate of the values of v_t and v_c. The values shown in Table 5.5 are based on an assumed value of effectiveness factor v_t of tensile strength as 0.3, calculated from an assumed value of m = 11 and a value of v_c = 0.35 as suggested in Ref. 27. Based on this value of v_t, the values given by this approach are generally in good agreement with the experimental results. The maximum variation is 17% as seen from Table 5.7. As the load area increases this approach gives higher values. For a load area of 200 x 500 mm, this method overestimates punching capacity by 10% to 36% as seen from Table 5.7.

It should be noted that the plasticity approach does not take into account the effect of reinforcement. The dowel action can be taken approximately as 15% to 20% of the calculated load. From an observation of the relative values, it is apparent that this approach has potential for its direct application to deck slabs.

It is essential that a fair, safe estimate of v_t and v_c (plasticity effectiveness parameters) values must be made. In view of the value of v_c = 0.35 suggested in Ref. 27, it appears that a value of v_t should probably be in the range of 0.25 to 0.30. A lower value of v_t can be used, to a fair estimate of the predicted punching load.

Yield Line Analysis of Punching: The method assumes that yield line mechanism has developed fully and that steel yields along the yield lines. As seen from Table 5.5, the method yields much higher values of failure load than the experimental values for panels having higher amount of steel. For A3-1 set, which has the highest steel, the prediction is more than 120% higher than the punching load capacity. As the load capacity is directly related to the amount of steel in this method, the punching capacity of A3-3 panels which had lowest amount of steel, show values of failure loads lower than the experimental values. As seen, for load area of 75 x 150 mm the method predicts 30% lesser values for A3-3 panel than the experimental values.

This model tends to give very high values of punching capacity when the percentage of steel increases. This is due to the assumption in this method that a yield line mechanism would be developed fully with steel yielding along yield lines for a failure mechanism. But in actual case of failure as reported by Blakey [37] and Long [34] , the yield line mechanism does not form prior to punching or sudden displacement of the shear cone relative to the rest of the slab and also there is no evidence of full yielding of steel bars near the vicinity of the load area. This has also been clearly observed in this study. Only a few steel bars directly under the load area yield before the push out type failure is observed on punching.

It is apparent therefore that this model is not applicable generally for an estimation of the punching capacity in a bridge deck slab, as the proposed failure mechanism is somewhat incompatible with the actual failure. This

method however, would yield a resonable value of failure load, if the tension steel ratio is low.

ACI formula: ACI formula for the punching shear capacity disregards the influence of the dowel action of the reinforcement steel, thus the ACI punching value would be same for a given slab and load prints, regardless of the amount of steel in the slab.

As seen from Table 5.5, the values given by the ACI are conservative for the smaller load areas. For load area of 75 x 150 mm the difference is about 40% for the panel A3-1, which had the highest amount of steel. The minimum difference of about 30% for the panel A3-3 which had the lowest amount of steel. Part of conservativeness of the ACI formula is due to the neglect of the effect of reinforcement on punching capacity.

However as the load area increases, the difference between the ACI and the experimental values decreases. For the load area of 200 x 400 mm the difference in the values of ACI and experimental value is about 10% for the A3-3 panels. For the load area of 200 x 500 mm the difference in the values of the ACI and experimental value for the panel A3-3 is negligible. Table 5.7 shows the ratio P_{EXP}/P_{ACI} for all panels.

For a safe estimate of the punching value, the ACI formula can be used with confidence. Though the formula appears to yield highly conservative values for relatively smaller load perimeters, the nonavailability of a more reliable

easy-to-use method, ACI formula appears to be acceptable for the purpose of design.

5.2.2 Fatigue Tests

Limited fatigue tests conducted with R = 0.1, showed that panels did not fail in fatigue after one million cycles at a maximum load level of 60% of ultimate capacity of the panel ($P_{max} = 0.6\ P_u$). This value can be taken as the maximum safe value for punching under fatigue. The extension of test on panel A3-2 set confirms this, because this panel did not fail even after two million cycles. But since it is expected that moving wheel load would be more critical than the pulsating load at a fixed point, the maximum value of load of $P_{max} = 0.5\ P_u$ could be taken as a safe threshold value to inhibit punching failure of deck slab due to fatigue. Thus for the purpose of design of bridge deck slab, the maximum safe value of wheel load should not exceed 0.5 P_u, where P_u is the ultimate computed static failure load for the deck slab in punching.

5.3 A2-SERIES

All failure loads recorded in Table 3.5 are reproduced in Table 5.8 with an added column for the adjusted failure load corresponding to the average value of the core strength of all panels. These adjusted failure loads, P_u were calculated by multiplying the actual loads with the ratio of the square root of

Table 5.8: Test Results of A2-Series Panels Adjusted to Average Core Strength of 28.2 MPa.

PANEL		AVERAGE CORE STRENGTH OF PANEL (MPa)	EXPERIMENTAL FAILURE LOAD (kN)	ADJUSTED FAILURE LOAD (kN)
GROUP NO.	DESIGNATION			
1	A2C/P	25.2	30.0	32.0
	A2C/S	25.5	123.0	129.0
2	A2/20	27.4	71.0	72.0
	A2/30	30.6	74.0	71.0
	A2/45	32.8	106.0	99.0
	A2/60	30.6	128.0	123.0
	A2/90	27.9	124.0	125.0
3	A2/60/H	29.2	65.0	64.0
	A2/90/H	28.8	132.0	131.0
4	A2C/90/L	25.0	120.0	127.0
	A2C/90/H	24.4	50.0	54.0

the ratio of the core strength to the average core strength for the A2-series. This way the concrete strength variability on the failure load was removed to provide a better comparison.

The punching capacity of the panels of Group 2, which were cast with conical inserts of variable base diameter but of constant height of 44 mm, are plotted in Fig. 5.3 against the angle of inclination α of frustums to depict the influence of α on P_u. It is observed that the angle α has pronounced influence on the punching capacity of the panel. The punching capacity P_u equal to 125.0 kN for $\alpha = 90°$ (A2/90 panel) is about the same as the value of P_u (= 129 kN) for the panel A2C/S without any insert. A2C/S represent the panel without any flaw and its punching capacity should therefore be regarded as the maximum for the panels in consideration. Any substantive reduction in P_u value from this value for a panel in Group 2, would indicate the degree of damage induced by the embeded flaws.

As seen from Table 5.8 and Fig. 5.3, the value of P_u gradually declines as α decreases from 90°. When $\alpha = 30°$, the punching capacity for A2/30 was about 71 kN, being about 57% of the value for panel A2/90. The punching capacity is about the same for $\alpha = 30°$ and $\alpha = 20°$, with no large discrepancy, indicating that within this range of α ($\alpha = 20°$ to 30°), the minimum punching capacity is attained.

It should be recognized here that geometrics of the conical inserts were computed on the basis of Fig. 2.4, in which the design base diameters were of

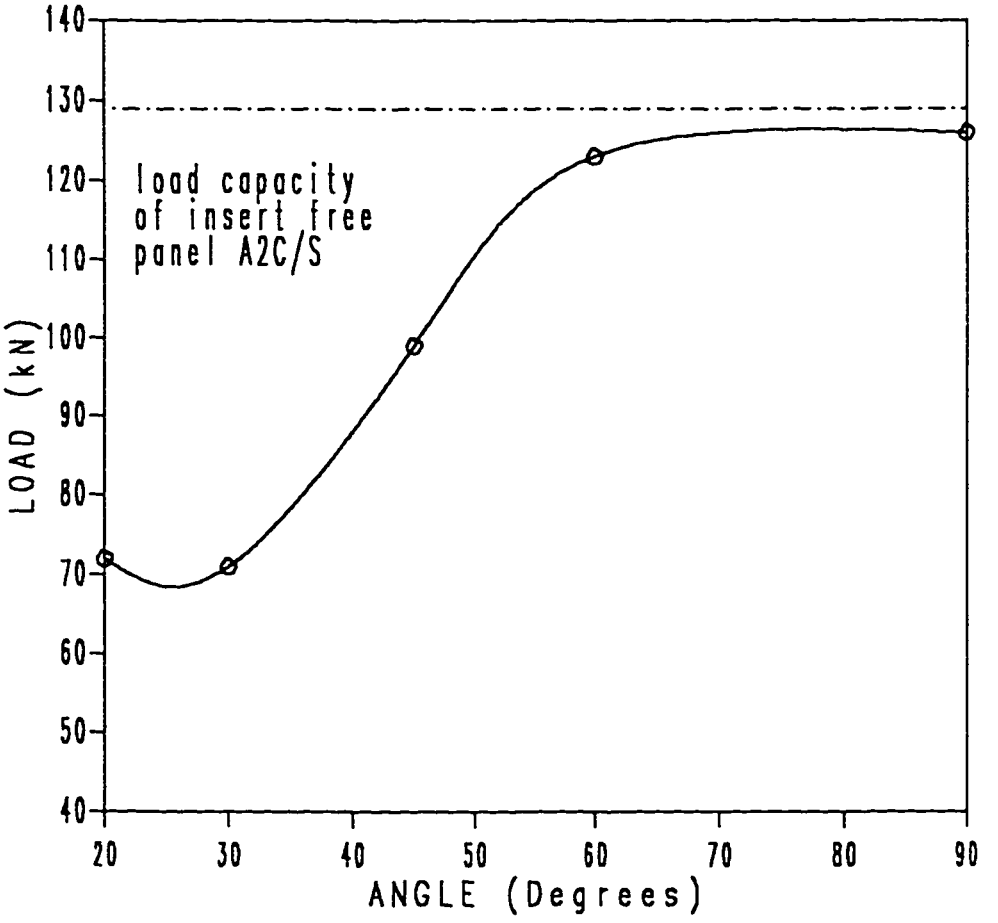

Fig. 5.3: Variation of Punching Load vs Angle (α) of Conical Insert for Group 2 Panels of A2-Series.

such values as to make the extended cone to meet the top loaded area. In other words, the diameter of load area (dia. = 88 mm) at top is the diameter of the frustum of the cone, if the cone is extended to the full depth of the slab. If we assume that punching takes place through sliding or slip along an axisymmetric inclined surface having an angle α with the horizontal, we can infer that there exists a critical orientation of the flaw which would impair the punching capacity to the largest degree. From the data recorded from tests of Group 2 panels (Table 5.8 and Fig. 5.3), it is apparent that critical angle of inserts is between 20° to 30° and therefore an orientation of the flaw within this range of angle can be viewed as the most detrimental from the viewpoint of punching.

In order to examine the effect of the height of inserts, Group 3 panels were tested. While the panels A2/60/H and A2/90/H both had heights of 64 mm, the former had a base diameter of 190 mm and α = 60°, whereas the latter had a base diameter of 88 mm and α = 90°. Test data in Table 5.8 shows that failure load for A2/60/H was only 64.0 kN whereas the panel A2/90/H yielded a punching load of 131 kN, being in the proximity of the failure load for A2/90 and for the insert free panel A2C/S.

A comparison of P_u values for A2/60 and A2/60/H shows the influence of the height of inserts. In both panels, the inserts had identical geometry, except the difference in the height. The failure load for A2/60/H (64 mm height of insert) was 64.0 kN, being 48% less from that of A2/60 (insert being 44 mm) of Group 2. Thus, it can be concluded that for a given angle flaw which is in the range of 20° to 90° the punching capacity would decrease with the increase in

the height of the flaw.

An interesting observation is made from the test of A2/90/H panel. Even with the increased height of 64 mm, the punching capacity was almost similar to that observed for A2/90, which had identical insert, but with a smaller insert height of 44 mm. This apparent independency on the height of insert with α less than 90° is well explained by the fact that punching shear failure plane is an inclined plane ($\alpha < 90°$) and that the embedded flaw which is remotely located from the failure surface will not influence adversely the punching capacity.

The bottom diameters for both A2/90/H and A2/90 were 88 mm which was the same as the load diameter on the top (Fig. 5.4). From the test data, it is clearly evident that for a flaw to have a damaging influence on punching capacity, the flaw at the bottom of the slab must be outside the load area so that an angle of inclination α less than 90° with respect to the load area (Fig. 5.4) exists. This observation is important, as it sets a condition for flaw (crack nucleation and orientation) to become detrimental from the viewpoint of punching.

As further evidence, Group 4 panels were cast and tested. Two types of panels, A2C/90/L and A2C/90/H had identical cylindrical ($\alpha = 90°$) inserts except that A2C/90/L had a height of 30 mm for the insert, whereas panel A2C/90/H had a height of 64 mm. The base diameter for insert was increased to 250 mm for both types. Test data show that the panel A2C/90/H in which the insert had crossed the failure plane (of $\alpha = 20°$ to 30°, Fig. 5.4), showed a decline

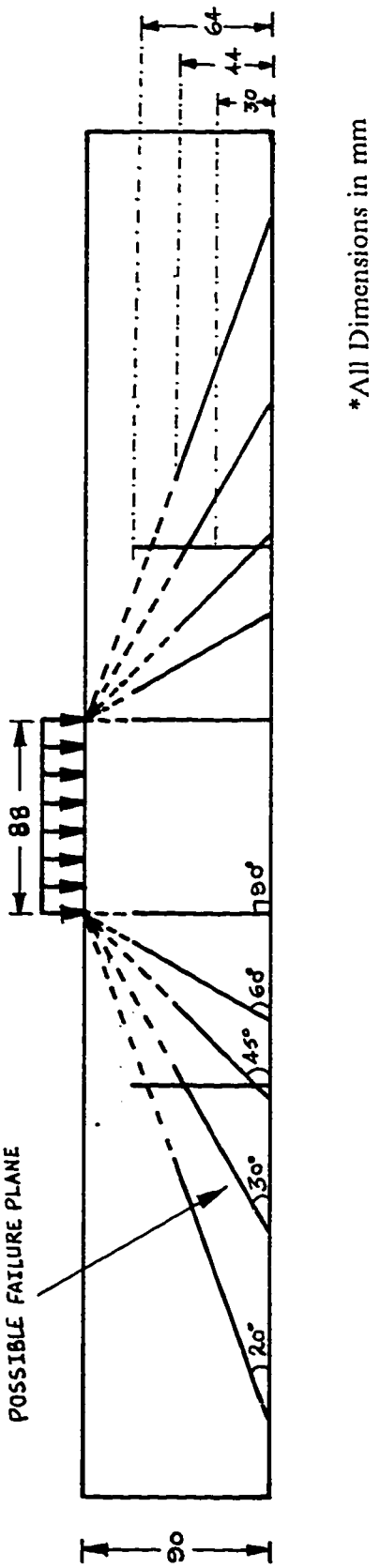

*All Dimensions in mm

Fig. 5.4: Proximity of Precast Notches to the Failure Plane (α = 20° - 30°) in A2-Series Panels.

in the punching capacity compared to the panel A2C/90/L which showed only a slight decline in the punching resistance. When compared to the P_u value for A2C/S (insert free), the decline in A2C/90/H was about 60%. Because of the shallower height of A2C/90/L, the top of the insert was somewhat remote from the critical failure plane and therefore the orientation of this flaw did not constitute a potentially damaging one. Clearly this was not the case with A2C/90/H, as seen from Fig. 5.4. The top of the embedded flaw (64 mm height) has dangerously crossed the failure plane, and in confirmity of the expectation, the punching capacity has been drastically reduced, as the slip plane is modified by joining of the flaw with the failure plane.

Panel A2C/P, cast without any reinforcement and without any conical insert failed at a load of 32 kN in flexure mode. The failure was sudden with the crack pattern as shown in Plate 3.7. The failure of the panel depicts typical yield lines extending from the four corners of the slab to the central load area, commonly seen in simply supported rectangular slabs.

Plate 3.8 shows view of the top and bottom failure surfaces of the panel A2/30. The top view shows that the failure surface is limited to the area of the loading plate which is typical of all punching failures. The bottom view indicates that the failure plane passes through the conical insert, with virtually no concrete outside the conical insert being mobilized. Plate 3.9 shows the view of the top and bottom failure surfaces of the panel A2/90 (labelled in photograph as A2/90/L/2 following the labelling system of the project [24]). The bottom view shows a significantly larger participation area of concrete in

resisting the loading, outside the insert, with significant cracking between the base of the insert and the base of actual failure zone. All panels which showed a reduction in punching capacity (A2/20, A2/30, A2C/60/H and A2C/90/H) had failure planes passing through the inserts. Panels showing minimum or no influence of inserts (A2/60, A2/90, A2/90/H, A2C/90/L) had a much larger base of failure zone, with significant cracking outside the insert base.

The first crack was observed around a load level of 30 kN in all these panels, which also is the capacity of plain concrete in bending as seen from tests on A2C/P. The failure was more brittle and explosive for panels without any conical insert and the failure was less explosive and more ductile with visual sign of failure for panels with conical inserts. The failure became more ductile as the depth of the conical inserts increased.

On the basis of test data from A2-series, it is seemingly appropriate to put forward the following hypothesis. For a flaw of the geometrical shape considered in this study to become damagingly effective in impairing punching capacity, the flaw must be located outside the load area with an angle of orientation of $20° \leq \alpha \leq 90°$ with respect to the load, as demonstrated in Fig. 5.4, and the possible damage (reduction in punching capacity) is dependent on the height of the flaw extending from the bottom. For a given angle of inclination of the flaw ($20° \leq \alpha \leq 90°$), the punching capacity decreases with increase in the height of the flaw.

The flaws introduced into the test panels were modelled from the existing random crack patterns in actual bridge deck slabs subjected to heavy vehicles.

The development of numerous transverse and longitudinal cracks under subcritical load level may result in successive crack nucleation leading to potentially weakened zone (flaws) of some height. The existence of such a weakened zone of a critical height may drastically reduce the punching resistance under a wheel load.

5.4 AN EPITOME OF FAILURE OF DECK SLABS

By virtue of the lateral restraints provided by the girders to the deck slab in a girder-slab bridge, the flexural capacity of the slab is enhanced to an appreciable extent due to the favourable influence of the inplane compressive force, often referred to as the arch action. Past studies [6,14,25] as well as the present one have endorsed this view point.

In view of the enhancement of flexural capacity to a large degree, a deck slab reinforced with tension steel, computed on the basis of an acceptable analysis, will not therefore fail in flexure under a heavy wheel load. Thus for a deck slab of normal proportions in girder-slab type bridge decks, punching failure is the only expected mode of failure. Following a recognized method or the design approach, such as, for example, ACI [38] or AASHTO [2], the deck slab thickness can be selected to avoid punching. Factor of safety introduced or inherent in the design will ensure safety of slab against occasional overloading from overweight vehicles.

However, it has been shown in this study that the punching capacity can be

impaired by the existance of a flaw within the slab intricately developed by the active process of crack growth and crack nucleation. A deck slab will normally be subject to two types of cracking: (i) non-structural cracking related to environmental factors such as plastic settlement, shrinkage and thermal effects and (ii) structural cracking caused by the tensile stresses from the load action. Superimposed crack prints of these two represent the current state of cracking in concrete bridges in Saudi Arabia, which is continually being altered by the progressive crack growth, nucleation and emergence of new cracks due to dynamic effects, overloading and thermal effects. This may lead to the formation of concrete zone which is separated from the surrounding body along an enclosed perimeter of the nucleated crack surface (Fig. 5.5). The height of this separation depends upon the depth of the nucleated crack surface. This separation along a closed perimeter constitute in effect a flaw, technically, but not necessarily geometrically similar to the flaw introduced by the conical frustums in A2-series panels.

Existence of random cracking at the slab soffit corresponding to subcritical cracking state (as witnessed in A1-series, Plates 3.1 to 3.4) is conducive to the formation of such a flawed zone, which may be dangerous from the punching view point. Test results from A2-series have emphatically shown that a critically placed flaw with regard to the shear plane (Fig. 5.4) and having a certain depth would reduce the punching capacity of a slab.

Generally, the boundary of the nucleated crack on the slab bottom should be larger or atleast equal to the foot print of the vehicular wheel load.

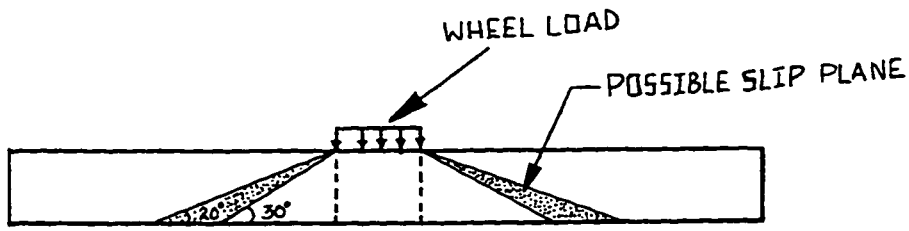

Sectional View

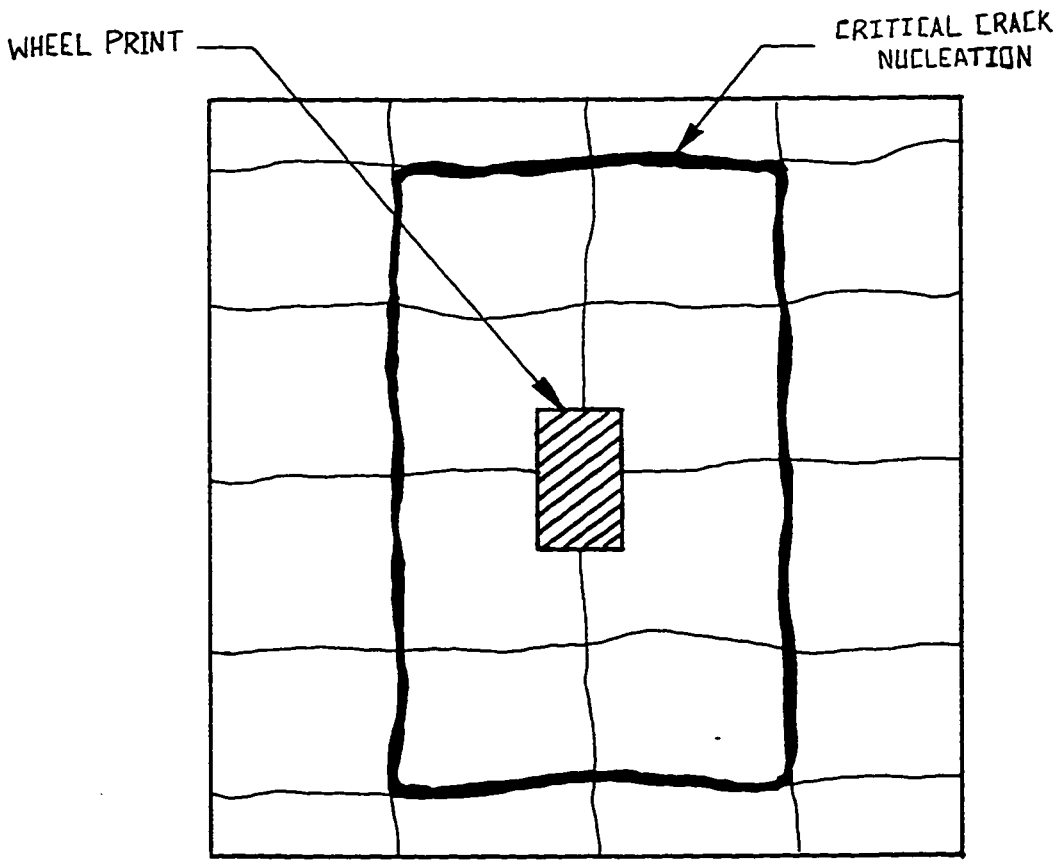

Plan

Fig. 5.5: Punching Failure Hypothesis.

Furthermore, the height of the enclosed crack surface should reach a level higher than the bottom rebar cover so as to make the flaw damaging. Tests of A2-series have clearly shown that with increasing height of the flaw, the punching capacity progressively diminishes.

In compliance with the test findings and the explanation put forward, an occurrence of unexpected punching failure under a lesser load level can be explained by the following hypothesis: ***punching capacity can be impaired by the development of a weakened zone in the deck slab, that may result from progressive crack nucleation and crack growth along a closed perimeter, creating in effect, a surface of separation. Impairment of punching capacity due to this flawed zone, occurs only when the crack surface geometry bears a critical orientation with regard to wheel load and has reached a critical height through the slab thickness.***

This hypothesis well explains the pot hole type failures witnessed in the deck slabs of girder-slab type bridges in Saudi Arabia (Plate 1.2). Existence of rectangular grid type crack patterns at soffit of slab is very common in these decks (Plate 1.1). These grids are formed by joining of the transverse and longitudinal cracks. Evidence of large crack depths through the slab thickness (reaching in some cases over 70% of the slab depth) was not uncommon. Ref. 24 has documented existence of such cracks by taking cores through the cracks. These cracks may have been driven up so high by the combined effect of thermal and excessively high loading which was known to exist at an alarming level in the past. The likely development of such a flawed concrete zone in the deck has caused an eventual pot-hole type punching failure.

It may be of interest to note here that the punching failures were witnessed only in the girder-slab type bridge decks. This can be explained by the fact that the slab thickness is relatively smaller in girder-slab decks by virtue of the shorter slab span between the girders. Comparatively a slab-type bridge deck will have a much bigger slab thickness. Even with the development of a flaw reaching a high depth, the residual punching capacity of the slab will still be sufficient to sustain the wheel load. Thus punching failure is expected only in slabs which are relatively thin such as those commonly used in girder-slab type bridge decks.

5.5 PREVENTIVE MEASURES AGAINST PUNCHING FAILURE

Punching failure can be effectively prevented by exercising rigid control on the weight of trucks using the highway system. Under occasional slight overloads, the deck slab will not suffer serious damage. In situations, where overloading is not effectively controlled, the design should implicitly recognize the need of provisional measures to avert punching failures and may consider the following:

(1) The slab should have a minimum thickness, regardless of the amount of reinforcing steel. This value should be decided from the anticipated heavy wheel loads that may cross bridge.

(2) Development of excessive flexure cracks and thermal cracks should be controlled by closely spaced steel in both transverse and longitudinal

directions at both faces.

(3) Slab construction should conform to good construction practice to prevent development of non-structural cracks.

Chapter 6

SUMMARY AND CONCLUSIONS

6.1 SUMMARY

An experimental program was planned to study the cracking and failure of concrete bridge deck slabs in girder-slab type bridge decks, by undertaking tests on a number of panels. Three different types of panels were used in this study: (i) A1-series panels cast with same amount of main transverse steel but with varying amounts of distribution steel, were tested under a simulated moving wheel load, to determine the influence of distribution steel on the crack pattern and density of cracking. The distribution steel used amounted to 100%, 67%, 37% and 18% of the main tension steel in different panels, (ii) A2-series panels cast with initial flaw in the form of conical frustum with different inclinations, height and base diameters, were tested under a circular patch load to determine the critical orientation and nucleation of cracks which impair punching capacity, and (iii) Static tests on A3-series panels cast with three different amounts of both transverse and longitudinal steel to evaluate the ultimate load carrying capacity P_u, using four different load areas (75 x 150 mm, 100 x 200 mm, 200 x 400 mm and 200 x 500 mm). Limited fatigue tests on A3-series panels with maximum load level of 60% of ultimate static load capacity P_u. The load ratio R was kept about 0.1 and a load area of 75 x 150 mm was used for

all fatigue tests.

The significant aspects of this study were to determine the mode of failure of a deck slab in girder-slab type bridge decks, to observe the reduction of punching capacity of the slabs in presence of flaws ensuing from the cracking of slab and to observe influence of distribution steel on the crack pattern and distribution of cracks induced by wheel load.

All tests were conducted on girder-slab type bridge deck models in which a thin reinforced concrete slab was supported by steel I-beams. For all tests, a single load was applied by an MTS actuator to the deck slab, distributing the load on an area to simulate the action of a wheel. Test measurements included record of failure of load, mode of failure, crack mapping, measurement of deflection and measurement of strain in a selected number of rebars.

6.2 CONCLUSIONS

Based on the findings of this study the following conclusion are drawn:

1) Lesser amount of distribution steel tends to produce lesser amount of transverse or radial cracks in the early stage of cracking, though no sharp difference in the crack pattern is noticeable at subcritical load levels for different amounts of distribution steel. However, the flexure cracks in panels with the lesser distribution steel are relatively wider than those with higher amount of distribution steel. When the percentage of distribution steel was increased finer cracks spread over a larger were observed.

2) Larger width of slab participates in resisting the transverse moment due to loads with increasing amount of distribution steel, as evidenced from measurement of rebar strain.

3) Punching capacity of a deck slab is enhanced to some extent, by increasing the amount of distribution steel, presumably by the increased dowel action.

4) The flexure capacity of a deck slab on girder-slab bridge type decks is enhanced to an appreciable degree by the favorable influence of the lateral restraint provided by supports resulting in the development of in-plane compressive membrane forces (arch action).

5) In view of the prevailing arch action, the mode of failure of a deck slab of normal design in a typical girder-slab type bridge deck, is essentially by punching.

6) Although punching capacity is enhanced to a small degree by the increase in amount of tension steel, in view of the enhancement of flexural capacity due to prevailing arch action, no significant advantage is gained in design by increasing the amount of steel in the deck slab of a girder-slab bridge.

7) Load-deflection response of restrained panels is approximately linear up to first cracking load and thereafter the response is nonlinear. The deflection is not greatly influenced by the amount of steel reinforcement in the slab.

8) Prior to the failure of a slab under a patch load, the tension steel in the vicinity of the load area yields. The rebar under the load is subjected to

highest level of stress and the stress in bars away from load area diminishes with distance.

9) A typical punching failure under a monotonically applied load is characterized by a push through failure of a concrete mass under the load area, whose top matches exactly with the load area and the bottom encompasses a relatively large area. Prior to failure, extensive cracking in the form of radial or fan-shape, is notable visual distressed condition of the slab.

10) Approximate failure or slip plane of punching appears to be in between 20° to 30°, with respect to the horizontal plane. Lower range of the angle is applicable to a slab with higher amount of steel.

11) None of the theoretical models developed thus far for punching capacity are truely applicable to a deck slab, not only from the view point of geometrical differences, but also from the results, which are not consistent with test data for all types of panels. Kinnunen and Nylander model appears to be reasonably accurate for slabs with moderate amount of steel. Also the plasticity model appears to be appealing, but is hindered by the requirement of an appropriate value of the effectiveness factor v_t in tension.

12) Based on the tests results, a hypothesis has been advocated that, punching capacity can be impaired by the development of a weakened zone in the deck slab, that may result from progressive crack nucleation and crack growth forming a closed envelop, creating in effect a surface of separation.

Impairment of punching capacity due to this flawed zone occurs only when the crack surface geometry bears a critical orientation with regard to wheel load and has reached a critical height through the slab thickness. The closed boundary of this weakened zone at the slab bottom should be greater than the wheel print.

13) Limited fatigue tests show that punching failure under cyclic loading can be averted by restricting the maximum load level to 50% of the maximum static capacity.

6.3 FUTURE RECOMMENDATIONS

The restrained panels, even with a low reinforcement ratio of 0.24% and a large load area covering about 10% of slab area failed in punching failure. It would be of interest to obtain the ultimate flexural capacity of such slabs by further reducing the reinforcement ratio and / or increasing load area.

Also of interest, is the development of a refined analytical model, which would reliably predict the influence of support restraint on the flexure capacity.

No theoretical model exists which can be routinely applied to a bridge deck slab to calculate the punching capacity. Efforts should be made in this direction for the development of an analytical approach. The enhancement of punching capacity due to support restraint and also due to the dowel action of the rebars need to be established.

REFERENCES

1. Johansen, K. W., *"Yield Line Theory,"* Cement and Concrete Association, London, England, 1962.

2. *Standard Specifications for Highway Bridges* , 13th edition, 1983, American Association of State Highway and Transportation Officials (AASHTO).

3. *Ontario Highway Bridge Design Code*, 2nd edition, Ministry of Transportation and Communications, Highway Engineering Division, Ontario Canada, 1983.

4. Okleston A. J., *"Load Tests of Three Storey Reinforced Concrete Building in Johannesberg,"* The Structural Engineer, London, England, Vol. 33, October, 1955, pp. 304-22.

5. Okleston A. J., *"Arching Action in Reinforced Concrete Slabs,"* The Structural Engineer, London, England, Vol. 36, June, 1958, pp. 197-201.

6. Tong P.Y., and Batchelor B.dev., *"Compressive Membrane Enhancement in Two Way Bridge Slabs,"* ACI Journal Vol-69, No. 1 January, 1972 and SP-30, ACI, 1971 pp. 271-86.

7. Brotchie J.F., and Holley M.H., *"Membrane Action in Slabs,"* ACI SP-30, 1971, 345-77.

8. Kinnunen, S., and Nylander H., *"Punching of Concrete Slabs Without Shear Reinforcement,"* Transactions of the Royal Institute of Technology, No. 158 Stockholm, Sweden, 1960.

9. Kinnunen, S., *"Punching of Concrete Slabs With Two-Way Reinforcement,"* Transactions of the Royal Institute of Technology, No. 198 Stockholm, Sweden, 1963.

10. Taylor, R., and Hayes, B., *"Some Tests on the Effect of Edge Restraint on Punching Shear in Reinforced Concrete Slabs,"* Magazine of Concrete Research, Vol. 17, March, 1965, pp. 39-44.

11. ASCE-ACI Committee 426, *"The Shear Strength of Reinforced Concrete Members-Slabs,"* Journal of the Structural Division, ASCE, Vol. 100, No. ST 8, Proc. paper 10733, August, 1974, pp. 1543-91.

12. Hewitt B. E., *"An Investigation of the Punching Shear Strength of Restrained Slabs with Particular Reference to Deck Slabs of Composite I-Beam Bridges,"* dissertation presented to the Dept. of Civil Engineering, Queens University, Kingston, Ontario, Canada, in March 1972 in partial

fulfillment of the requirements for the degree of Ph. D.

13. Hewitt B. E., and Batchelor B.dev., ***"Punching Shear Strength of Restrained Slabs,"*** Journal of the Structural Division, ASCE, Vol. 101, No. ST 9, September, 1975, pp. 1837-53.

14. Csagloy P.F., ***"Design of Thin Concrete Deck Slabs by the Ontario Highway Bridge Design,"*** May, 1979, report SRR79-11, submitted to the Ministry of Transportation and Communications, Canada.

15. Beal D. B., ***"Load Capacity of Concrete Bridge Decks,"*** Journal of the Structural Division, ASCE, Vol. 108, April, 1982, pp. 814-32.

16. Fang I. K., ***"Behavior of Ontario-type Bridge Decks on Steel Girders,"*** dissertation presented to the Dept. of Civil Engineering, The University of Texas at Austin, Austin, Texas in December, 1985, in partial fulfillment of the requirement for degree of Ph.D.

17. Sanoda K., and Horikawa T., ***"Fatigue Strength of Reinforced Concrete Slabs under Moving Loads,"*** Proceeding of the ABSE colloquium, Fatigue of steel and concrete structures, Vol. 37, Lausanne, Switzerland, 1982, pp. 455-62.

18. Perdikaris P. C., and Sergio Beim, ***"RC Bridge Decks under Pulsating and Moving Load,"*** Journal of the Structural Division, ASCE, Vol. 114, No. 3, March, 1988, pp. 591-607

19. Azad, A. K., Baluch, M. H., Al-Mandil, M. Y., and Al-Suwaiyan M. S., ***"Static and Fatigue Tests of Simulated Bridge Decks,"*** Experimental Assessment of Performances of Bridges, proceeding of a session at ASCE convention, Boston, Oct. 27 1986.

20. Ingerslev, A., ***"The Strength of Rectangular Slabs,"*** Journal of the Structural Engineer, Vol. 1, No. 1, January 1923, 1974, pp. 677-720.

21. Aoki Y., and Seki H., ***"Shearing Strength and Flexural Cracking and Capacity of Two-Way Slabs Subjected to Concentrated Loads,"*** ACI SP-30, 1971, pp. 103-26

22. Batchelor, B. dev, ***"Are Composite Bridge Slabs Too Conservatively Designed - Fatigue Studies,"*** Fatigue of Concrete (SP-41) Detriot, ACI, 1974, pp. 331-346.

23. Okada, Okamura and Sonoda, Transportation Research Record No. 664. ***"Bridge Engineering,"*** Vol. 1, Proceeding of a Conference conducted by the Transportation Research Board, September 25-27, 1978.

24. Al-Mandil, M. Y., Azad, A. K., Baluch, M. H., Pearson-kirk, D., Al-

farabi Sharif and Al-Dhalaan, M.A., *"A Study Of Cracking Of Concrete Bridge Decks in Saudi Arabia,"* Progress reports 4-6, report to KACST, Saudi Arabia.

25. Al-Suwaiyan M. S., *"Progressive Fracture of Reinforced Deck Slab in Girder-Slab Type Bridge Deck,"* dissertation presented to the Dept. of Civil Engineering, King Fahd University of Petroleum and Minerals, Saudi Arabia, in partial fulfillment of requiremen: of degree of Master of Sciences, January 1987.

26. Nielson, M. P., *"Limit Analysis and Concrete Plasticity,"* Prentince-Hall, Inc., Englewood Cliffs, New Jersey, 1984.

27. Jiang Da-Hua and Shen Jing-Hua, *"Strength of Concrete Slabs in Punching Shear,"* Journal of Structural Enginering, Vol. 112, No. 12, December, 1986, 2578-91.

28. Withney, C. S., *"Ultimate Shear Strength of Reinforced Concrete Flat Slabs, Footing, Beams, and Frame Members Without Shear Reinforcement,"* Journal of American Concrete Institute, Vol. 29, No. 4, October, 1957, 265-98.

29. Hognestad, E., *"Shearing Strength of Reinforced Concrete Column Footings,"* ACI Journal, Vol. 50, November, 1953, pp. 189-208.

30. Elstner, R. C. and Hognestad, E., *"Shearing Strength of Reinforced Concrete Slabs,"* ACI Journal, Vol. 28, July 1956, No. 1, pp. 29-58.

31. Yitzhaki, D., *"Punching Strength of Reinforced Concrete Slabs,"* ACI Journal, Vol. 63, No. 5, May, 1966, pp. 527-540.

32. Gesund, H. and Dikshit, O. P., *"Yield Line Analysis of the Punching Problem at Slab/Column Intersections,"* ACI, SP-30, 1971, pp. 177-201.

33. Herzog, M., *"A New Evaluation of Earlier Punching Shear Tests,"* Concrete (London), Vol. 4, No. 12, December, 1970, pp. 448-450.

34. Long, A. E., *"A Two-Phase Approach to the Prediction of the Punching Strength of Slabs,"* ACI Journal, February, 1975, pp. 37-45.

35. American Society for Testing and Materials, *"Standard Method for Obtaining and Testing Drilled Cores and* Sawed Beams of Concrete," C42-87, pp. 26-28.

36. Sayed, M. H., *"Estimation of In-Situ Concrete Strength by Combined Non-Destructive Method in Eastern Province of Saudi Arabia,"* dissertation presented to the Dept. of Civil Engineering, King Fahd University of Petroleum and Minerals, Saudi Arabia, in partial fulfillment of

requirement for degree of Master of Sciences, Febraury 1987.

37. Blakey, F. A., *"A Review of Some Experimental Studies of Slab-Column Junctions,"* Bulletin d'Information No. 58, Comite Europeen du Bocon, Paris, Oct., 1966 pp. 51-66.

38. *"Building Code Requirements for Reinforced Concrete', ACI 318-83, Detriot, 1983.*

39. Gesund, H and Kausik, Y. P., *"Yield Line Analysis of Punching Failures in Slabs,"* Publications, International Association for Bridge and Structural Engineering, Zurich, V. 30-I, 1970, pp. 41-60.

VITA

KAISER KAREEM was born in Hyderabad, India, in October 1962. He finished his schooling in 1980.

He joined Osmania University in 1980 and completed his B.E., in Civil Engineering in 1984.

He joined King Fahd University of Petroleum and Minerals as a Research Assistant in the Department of Civil Engineering in 1984, where he did his M.S. in the field of Structures.

He hopes that this small work of his thesis be of some benefit in the field of bridges.